

**RELATIVE RATES OF SULPHIDE OXIDATION BY CHEMICAL AND MICROBIAL  
MEANS: THE ROLE OF MINERALOGY AND TEXTURE IN ACID ROCK DRAINAGE  
(ARD) FROM THE MEGUMA SUPERGROUP, NOVA SCOTIA**

Rachel A. Jones

Submitted in Partial Fulfilment of the Requirements  
for the Degree of Bachelor of Science, Honours  
Department of Earth Sciences  
Dalhousie University, Halifax, Nova Scotia  
March, 1997

## Distribution License

DalSpace requires agreement to this non-exclusive distribution license before your item can appear on DalSpace.

### NON-EXCLUSIVE DISTRIBUTION LICENSE

You (the author(s) or copyright owner) grant to Dalhousie University the non-exclusive right to reproduce and distribute your submission worldwide in any medium.

You agree that Dalhousie University may, without changing the content, reformat the submission for the purpose of preservation.

You also agree that Dalhousie University may keep more than one copy of this submission for purposes of security, back-up and preservation.

You agree that the submission is your original work, and that you have the right to grant the rights contained in this license. You also agree that your submission does not, to the best of your knowledge, infringe upon anyone's copyright.

If the submission contains material for which you do not hold copyright, you agree that you have obtained the unrestricted permission of the copyright owner to grant Dalhousie University the rights required by this license, and that such third-party owned material is clearly identified and acknowledged within the text or content of the submission.

If the submission is based upon work that has been sponsored or supported by an agency or organization other than Dalhousie University, you assert that you have fulfilled any right of review or other obligations required by such contract or agreement.

Dalhousie University will clearly identify your name(s) as the author(s) or owner(s) of the submission, and will not make any alteration to the content of the files that you have submitted.

If you have questions regarding this license please contact the repository manager at [dalspace@dal.ca](mailto:dalspace@dal.ca).

Grant the distribution license by signing and dating below.

---

Name of signatory

---

Date



## ABSTRACT

The Meguma Supergroup in Nova Scotia contains abundant sulphide minerals that potentially can cause acid rock drainage (ARD), which is environmentally damaging and expensive to ameliorate. The problem is most intense in the basal Halifax Group where a well-defined suite of sulphide minerals is dominated by monoclinic pyrrhotite and lesser pyrite. Meguma rocks also contain hexagonal pyrrhotite, arsenopyrite, chalcopyrite, galena, and sphalerite. These occur in different textures, sizes, orientations, or mineral associations, depending on such factors as rock type, stratigraphy, composition, structure, and metamorphism.

This project investigated the relative rate of chemical and microbially assisted oxidation of a selected suite of sulphide minerals. Six pairs of polished thin sections containing a wide selection of sulphide minerals and textures were oxidized in a controlled laboratory experiment with two treatments. One thin section of each pair was placed in a natural uncultured sample of ARD collected from a quarry near the Halifax International Airport (pH between 3.62 and 3.76). The matching thin section of the pair was placed in ARD (pH = 3.16) from the same source but double filtered at 0.2 microns to remove bacteria. Surface changes were monitored regularly and documented with photomicrography, and final surface characteristics were documented in detail with the SEM. Tarnish (colour changes) and etching of pits, cracks and polishing scratches were interpreted as oxidation. Photomicrographic evidence indicates a significant difference between the treatments. In general, sulphide minerals exposed to unfiltered, biologically active ARD oxidize faster than in filtered ARD. In the microbial treatment, the relative degree of oxidation among sulphides was galena > hexagonal pyrrhotite > monoclinic pyrrhotite > anhedral pyrite >> arsenopyrite, sphalerite > euhedral pyrite > chalcopyrite. In the sterile treatment, the relative degree of oxidation was galena > anhedral pyrite > monoclinic pyrrhotite >> hexagonal pyrrhotite, sphalerite, arsenopyrite > euhedral pyrite > chalcopyrite.

This study confirms the essential role played by biological agents in ARD, but also shows that sulphide mineralogy, texture, grain orientation and geology must be considered in the evaluation of ARD potential in Meguma rocks.

<b>TABLE OF CONTENTS</b>	<b>page</b>
Abstract	i
Table of Contents	ii
Table of Figures	iv
Table of Tables	v
Acknowledgements	vi
<b>Chapter 1: Introduction</b>	<b>1</b>
1.1 Thesis Statement And Scope	1
1.2 Introduction To Acid Rock Drainage (ARD) With Examples In Nova Scotia	1
1.3 Introduction To The Meguma Supergroup With Respect To Sulphide Occurrence	4
1.3.1 The Goldenville and Halifax Groups	4
1.3.2 The Goldenville-Halifax Transition Zone (GHT)	7
1.3.3 Mineralogy and Geochemistry	7
1.3.4 Structure and Metamorphism	8
1.4 Sample Localities	9
1.5 Methodology	9
1.6 Organization	11
<b>Chapter 2: The Role of Bacteria in the Oxidation of Sulphide Minerals</b>	<b>12</b>
2.1 Brief Introduction To Microbiology	12
2.2 Types Of Bacteria Associated With ARD	14
2.2.1 Metabolism	14
2.2.2 Species Potentially Present in ARD Environments	18
2.3 Reactions Of ARD Production: Biological And Chemical	20
2.4 Are Bacteria A Major Cause Of ARD?	22
<b>Chapter 3: Design of the Oxidation Experiment</b>	<b>26</b>
3.1 Background	26
3.2 Experimental Setup and Procedure	26
3.2.1 Rock Sample Descriptions	26
3.2.2 Preparation of Rock Samples	38
3.2.3 Preparation of ARD Samples	40
3.2.4 Apparatus	42
3.2.5 Procedure	43

<b>Chapter 4: Results and Discussion</b>	47
4.1 Results	47
4.1.1 Electron Microprobe Results	47
4.1.2 Relative Rates of Oxidation by Image Analysis	49
4.1.3 Preliminary Analyses of Secondary Precipitates: XRD and SEM	75
4.1.4 Evidence for Microbial Activity	79
4.2 Discussion	81
4.2.1 Factors Affecting Oxidation Sensitivity among Sulphides	81
4.2.2 Why were the Oxidation Rates Different Between Treatments?	91
4.2.3 Experimentation with Mixed Microbial Species	92
<b>Chapter 5: Conclusions, Recommendations and Future Work</b>	94
5.1 Conclusions	94
5.2 Recommendations	94
5.3 Future Work	95
<b>References</b>	97
<b>Appendix A: Microprobe Data</b>	A1
<b>Appendix B: Water Chemistry of ARD Sample: Before Oxidation, After Oxidation in the Microbial Treatment, and After Oxidation in the Sterile Treatment</b>	B1
<b>Appendix C: Hexagonal Pyrrhotite XRD Analysis</b>	C1

## TABLE OF FIGURES

		<b>Page</b>
1.1	Sample location map	6
2.1	A generalized bacterium	15
2.2	A phylogenetic tree based on rRNA	15
2.3	Plot of Eh/pH preferred environments of some iron-oxidizing bacteria	21
2.4	Reactions involved in pyrite oxidation, and the relationships between oxidizing agents, secondary minerals and catalysts	21
3.1	Thin section of RJ-96-001	27
3.2	RJ-96-001, anhedral pyrite with grey lamellae, an oxide rim, and minor chalcopyrite	29
3.3	Thin section of RJ-96-002	30
3.4	Thin section of RJ-96-003	31
3.5	RJ-96-003, hexagonal pyrrhotite rimmed with chalcopyrite	32
3.6	RJ-96-003, subgrains of hexagonal pyrrhotite	32
3.7	Thin section of BH-20-I	33
3.8	BH-20-I, subgrains of monoclinic pyrrhotite	34
3.9	Thin section of CR-95-002	35
3.10	CR-95-002, fine grains of monoclinic pyrrhotite associated with oxides	36
3.11	Thin section of CR-95-016	37
3.12	CR-95-016, two pyrrhotite textures	41
3.13	Quarry near the Halifax International Airport	41
3.14	Experimental setup design	44
3.15	Sulphide minerals (BH-20-I, microbial treatment) before and after brushing	46
4.1	Plot of atomic % S versus atomic % Fe for pyrrhotite compositions	48
4.2	BH-20-I, microbial treatment, monoclinic pyrrhotite, pyrite, chalcopyrite, and sphalerite	50
4.3	SEM image of BH-20-I, microbial treatment, monoclinic pyrrhotite, chalcopyrite and sphalerite	52
4.4	SEM image of BH-20-I, microbial treatment, pyrite	52
4.5	BH-20-I, sterile treatment, monoclinic pyrrhotite, chalcopyrite	53
4.6	SEM image of BH-20-I, sterile treatment, monoclinic pyrrhotite and chalcopyrite	54
4.7	SEM image of BH-20-I, sterile treatment, pyrite	54
4.8	RJ-96-003, microbial treatment, hexagonal pyrrhotite, chalcopyrite, and galena	55
4.9	SEM image of RJ-96-003, microbial treatment, hexagonal pyrrhotite, chalcopyrite	57
4.10	SEM image of RJ-96-003, microbial treatment, hexagonal pyrrhotite, galena	57
4.11	RJ-96-003, sterile treatment, hexagonal pyrrhotite and galena	58
4.12	SEM image of RJ-96-003, sterile treatment, hexagonal pyrrhotite and galena	59
4.13	SEM image of RJ-96-003, sterile treatment, hexagonal pyrrhotite and galena, higher power	59
4.14	RJ-96-001, microbial treatment, euhedral pyrite	60

4.15	RJ-96-001, sterile treatment, euhedral pyrite	61
4.16	SEM image of RJ-96-001, microbial treatment, euhedral pyrite	62
4.17	RJ-96-001, sterile treatment, anhedral pyrite	64
4.18	SEM image of RJ-96-001, microbial treatment, anhedral pyrite	65
4.19	SEM image of RJ-96-001, sterile treatment, anhedral pyrite	66
4.20	SEM image of RJ-96-001, microbial treatment, secondary precipitate	67
4.21	RJ-96-002, sterile and microbial treatments, arsenopyrite	68
4.22	CR-95-016, microbial treatment, pyrrhotite subgrains	70
4.23	CR-95-016, microbial treatment, two pyrrhotite grains	71
4.24	CR-95-002, sterile treatment, pyrrhotite lamellae	73
4.25	SEM images of CR-95-002, sterile treatment, pyrrhotite lamellae	74
4.26	XRD analysis of amorphous iron precipitate	77
4.27	(a) Rust-coloured precipitate in the microbial treatment	78
	(b) No precipitate in the sterile treatment	78
4.28	Images taken with the ESEM as evidence for microbial activity	80
4.29	An example of an Eh/pH plot that shows the stability fields of iron oxides and iron sulphides in water at 25°C, 1atm total pressure, with an activity of dissolved sulphur of 10 <sup>-1</sup>	82
4.30	An Eh versus pH plot showing stability fields for various types of water environments	83
4.31	A possible example of galvanic interactions (sample BH-20-I)	86
4.32	Another possible example of galvanic interactions (sample RJ-96-003)	87
4.33	Structure of sub-grain boundaries, showing interrupted lattice structure causing unsatisfied bond locations	89
4.34	SEM image of monoclinic pyrrhotite (BH-20-I, sterile treatment) showing subgrain boundaries that have been etched preferentially into grooves	89
4.35	Monoclinic pyrrhotite subgrains from BH-20-I (sterile treatment)	90
4.36	An illustration of how different crystallographic orientations are etched to create different surface patterns that reflect light in various directions	90

### TABLE OF TABLES

1.1	Chemistry of ARD from the waste rock pile at the Halifax International Airport	3
1.2	Stratigraphic nomenclature of Meguma lithologies	5
1.3	Sample locations	10
2.1	Main differences between prokaryotes and eukaryotes	13
2.2	Reactions that produce energy for chemolithoautotrophs	17
2.3	Bacteria potentially involved in acid rock drainage and their conditions of growth	19
4.1	Relative order of oxidation among sulphide minerals for each sample	76
4.2	List of rest potentials of some common sulphide minerals	85



### **Acknowledgements**

I wish to thank my supervisor, Dr. Marcos Zentilli, whose constant support, enthusiasm, and guidance have helped me immensely, and Don Fox, whose patience, laughter, attention to detail, friendship, and all-around helpfulness have made this year so much easier and fun. I also wish to thank Milton Graves, the king of probe data, whose clear-headed advice has saved me on a number of meltingly stressful occasions.

I thank Dr. Gibling for expert thesis class coordination and helpfulness, Sandy Grist for suggestions and help with experimental apparatus, Gordon Brown for thin section preparation, Bob MacKay for help with the microprobe, Lynne Maillet-Frotten for help with the SEM, Frank Thomas for help with the ESEM, and Dr. Silver and Dr. Mann for microbial advice.

Finally, I thank my family and friends for their love and support.

## CHAPTER 1: INTRODUCTION

### 1.1 Thesis Statement and Scope

Two questions are explored in this thesis. Firstly, do bacteria in acid rock drainage (ARD) substantially increase the rate of oxidation of sulphide minerals in the Meguma Supergroup, Nova Scotia, or are they simply opportunistic of the extreme geochemistry? Secondly, what is the relative order of oxidation among the following sulphide minerals: monoclinic pyrrhotite ( $\text{Fe}_7\text{S}_8$ ), hexagonal pyrrhotite ( $\text{Fe}_9\text{S}_{10}$ ), pyrite ( $\text{FeS}_2$ ), arsenopyrite ( $\text{FeAsS}$ ), chalcopyrite ( $\text{CuFeS}_2$ ), galena ( $\text{PbS}$ ) and sphalerite ( $\text{ZnS}$ )?

This study is significant because there are no previous studies on the role of a natural sample of microorganisms in sulphide oxidation in rocks of the Meguma Supergroup, Nova Scotia. The use of a natural uncultured sample of organisms associated with ARD is unusual because most previous studies use cultured, isolated strains such as *Thiobacillus ferrooxidans*, *T. thiooxidans*, or *T. thioparus*, etc. (see Table 2.3 for more bacterial species studied). Therefore, results of these previous studies may not be applicable to oxidative behaviour in a more complex microbial environment. The conditions chosen in this experiment are intended to approximate reality, so that as much as possible the sulphide minerals and organisms behave as they would in "nature." The results provide new insights into the oxidation process of sulphide minerals in Nova Scotian rock, and hopefully will help in preventing ARD.

### 1.2 Introduction to Acid Rock Drainage (ARD) with Examples in Nova Scotia

When a metallic sulphide mineral (especially with iron; Strumm and Morgan, 1970) oxidizes in the presence of oxygen and water, it produces sulphuric acid and releases a metallic

ion into solution (section 2.3). In nature, this reaction produces acid rock drainage (ARD), also called acid mine drainage (AMD) because it is commonly associated with sulphide-bearing mine waste. Because weathering generally outpaces erosion, the acid production is not a problem unless the fresh rock is disturbed by human influence, rapidly exposing sulphides to an oxidizing environment (the Earth's surface). In Nova Scotia, the problem is exacerbated by the slow development of soil and the deep abrasion caused by the last glaciation. Common disturbance of sulphide-bearing material includes mining, highway and road construction, quarrying, and industrial or urban development such as the digging of trenches and foundations (Hennigar and Gibb, 1987). All have created ARD in southern Nova Scotia. In the past, slate has been used in many construction activities because it is cheaper to excavate than quartzite, due to its easy fracture along cleavage planes, and because it is widespread in southern Nova Scotia, close to many areas of rapid development. A few examples of human activities that have triggered severe ARD in Nova Scotia include: (1) construction of and improvements to the Halifax International Airport, located on sulphide-rich black slate at the headwaters of three major drainage basins (Lund et al., 1987; King and Hart, 1987; Pašava et al., 1995); (2) mine tailing sites (Lund et al., 1987); (3) highway construction near Petpeswick Lake, Halifax County, which disrupted black slates (Jacques, Whitford and Associates Ltd., 1990); and (4) disposal of foundation excavations from Park Lane Mall in Bayers Lake Industrial Park, Halifax (Sadler, 1991).

Not only are rivers and lakes contaminated with sulphuric acid ( $H_2SO_4$ ), but the acid leaches major elements (e.g. Fe, Mn, Al, As) and toxic metals (e.g. Pb, Cu and Zn) from the rocks, producing a toxic leachate (Nordstrom, 1982). After a rain, the pH in a stream draining an acid drainage site can drop rapidly and dramatically (e.g. through a range of 2.5 pH units in

Biscuit Brook, Nova Scotia; Pettipas, 1979), surpassing the tolerance of much aquatic life of approximately 0.2 pH units per day (Pettipas, 1979). Table 1.1 compares some chemical concentrations found in ARD from the waste rock pile at the Halifax International Airport (HIA) to the maximum tolerance for fresh water aquatic life, of which some species are economically significant (eg. fish hatcheries; Thompson, 1978). Other problems with ARD include public water supply contamination resulting in closures, private well contamination, and damage to engineering works (Hennigar and Gibb, 1987). An aquatic ecosystem may take months to recover, even if the pulse of acid runoff passes fairly quickly. The damage has already been done, and some rivers and lakes may only recover in years. In addition, sulphide-containing rocks can continue to produce ARD for tens to hundreds of years (Ritchie, 1994; Gould *et al.*, 1994) once the oxidation process has begun. This is a tremendous length of time in terms of the effort and cost of remediation.

Interest in ARD research is most often driven by environmental damage and the expense of remediation, especially at mine sites (Alpers and Blowes (eds.), 1992; Jambor and Blowes (eds.), 1994). In Nova Scotia, various remediation techniques have been tried with only partial

**Table 1.1:** A chemical comparison of fresh ARD from the HIA (Lund, 1987) with tolerance limits of freshwater aquatic life (Canadian Water Quality Guidelines, 1987). Compiled by Robinson (1996).

HALIFAX INTERNATIONAL AIRPORT	LIMITS FOR FRESHWATER AQUATIC LIFE
Fe = 3 800 mg/L	Fe = 0.3 mg/L
Al = 3 247 mg/L	Al = 0.005 - 0.1 mg/L
SO <sub>4</sub> = 27 000 mg/L	SO <sub>4</sub> = (?)
pH 2.4 - 3.2	pH 6.5 - 9.0

success, including settling ponds (Lund, 1987), lime dumping (Worgan, 1987), fertilization (Kerekes et al., 1984), addition of peat (Roberts, 1986), construction of a wetland vegetated system (Silver, 1988), sealing exposed rock surfaces with clay or asphalt to remove the source of oxygen (air) and discourage aerobic organisms (Thompson, 1978), or capping the rock with shotcrete as at Petpeswick Lake (Jacques, Whitford and Associates Ltd., 1990). None of these is as satisfactory a solution as prediction and prevention.

### **1.3 Introduction to the Meguma Supergroup with Respect to Sulphide Occurrence**

Southern Nova Scotia is underlain by a very thick Cambro-Ordovician siliciclastic sequence known as the Meguma Supergroup (Schenk, 1995). This body of rock covers approximately 200 000 km<sup>2</sup>, extending beneath the Scotian Shelf to the south, and underlying parts of the continental shelf in addition to subaerial southern Nova Scotia (Schenk, 1995). The unit has been studied by several workers and the stratigraphic nomenclature is controversial. Table 1.2 lists the nomenclature favoured by various authors. This thesis uses the terminology proposed by Schenk (1995): the Meguma Supergroup. Figure 1.1 is a map of southwestern Nova Scotia showing the distribution of the Meguma Supergroup.

#### *1.3.1 The Goldenville and Halifax Groups*

The Goldenville Group was deposited as a sand-dominated, thickly stratified flysch (Schenk, 1970). The overlying Halifax Group was deposited as a shale-dominated, thinly stratified flysch (Schenk, 1970). Both groups contain evidence of turbidites, but the Goldenville appears proximal and the Halifax distal (Walker, 1967, cited in Schenk, 1970). The minimum thickness of the Meguma Supergroup has been estimated by Schenk (1970) to be approximately

**Table 1.2: Nomenclature of the Meguma Lithologies**

Southern NS	Southern NS	Tancook Island area of Mahone Bay	Beaverbank Highway	Southern NS
Ami (1900, cited in Schenk, 1995)	Woodman (1904, cited in Schenk, 1995)	O'Brien (1986)	Ryan <i>et al.</i> (1995)	Schenk (1995)
Halifax Formation	Meguma Series  Goldenville Formation	Meguma Group Halifax Formation Feltzen Member Cunard Member Green Bay Formation Mosher's Island Member Tancook Member Goldenville Formation New Harbour Member	Meguma Group Halifax Formation Glen Brook Unit Rawdon Unit Beaverbank Unit Goldenville Formation Steve's Road Unit Lewis Lake Unit Long Lake Unit Mt. Uniacke Unit Undivided Goldenville	Meguma Supergroup Halifax Group Rockville Notch Formation Delanceys Formation Feltzen Formation Cunard Formation Mosher's Island Formation Goldenville Group West Dublin and Tancook Formations Risser's Beach Formation New Harbour Formation

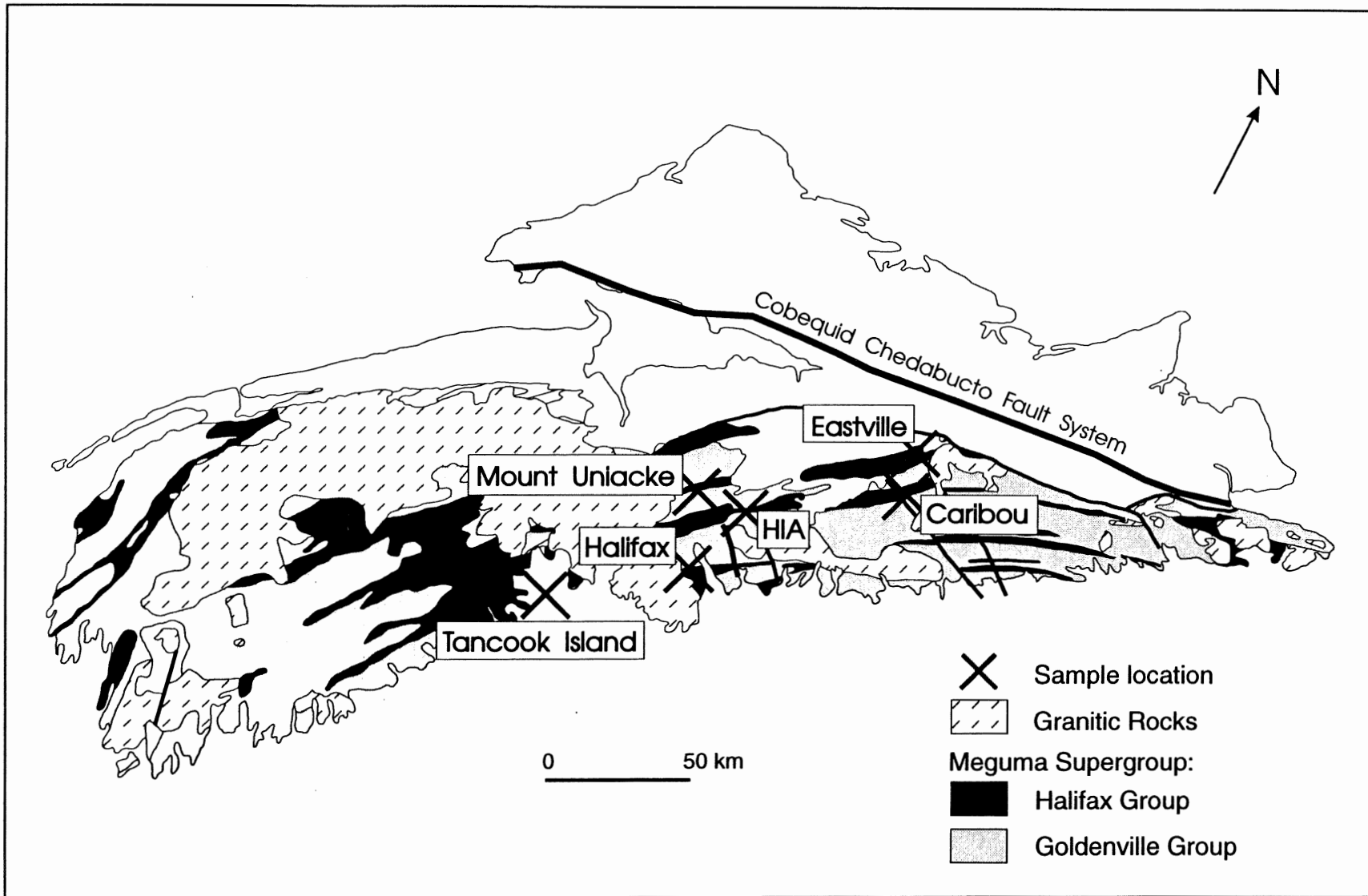


Figure 1.1: Geological map of the Meguma Supergroup in Nova Scotia (modified from the Geological Map of Nova Scotia (1979), NS Department of Mines and Energy).

14 km, 7 km each for the Goldenville and Halifax Groups.

### *1.3.2 The Goldenville-Halifax Transition Zone*

At the contact between the Goldenville and Halifax Groups there is a characteristic lithology that has been referred to as Goldenville-Halifax transition zone, or GHT, by Zentilli et al. (1986). This zone includes a calcareous argillite unit enriched in metals, "spessartine quartzites," (formed from Mn carbonate during regional metamorphism), and sulphide minerals (Graves and Zentilli, 1988). The upper levels of the GHT are characterized by black carbonaceous slate rich in sulphide minerals (Graves and Zentilli, 1988; Waldron, 1992). In the Mahone Bay area, the calcareous argillite unit has been named the Mosher's Island Formation and the black slate the Cunard Formation (O'Brien, 1986, modified by Schenk, 1995). The GHT varies widely in thickness, from approximately 35 to 45 m at Eastville (Binney et al., 1986) to 2 km at Mahone Bay (O'Brien, 1986).

### *1.3.3 Mineralogy and Geochemistry*

Sulphide minerals vary substantially in concentration throughout the Meguma Supergroup, with the main phases consisting of pyrite and/or pyrrhotite, with minor amounts of other sulphides (mainly chalcopyrite and arsenopyrite). At Eastville, the sulphides present (in decreasing abundance) are pyrrhotite, pyrite, sphalerite, galena, chalcopyrite and arsenopyrite (Binney et al., 1986). At the Halifax International Airport (HIA) 4-C monoclinic pyrrhotite, pyrite, marcasite, arsenopyrite and chalcopyrite are the major sulphides (Pašava et al., 1995). A third example is the Cunard Formation in the Mahone Bay area described by O'Brien (1986) to be "pyritiferous." Overall, pyrrhotite abundance in the Halifax Group has been shown to correlate with large-scale



aero-magnetic anomalies (McGrath, 1969; Cameron and Hood, 1975; Schwarz and Broome, 1994).

Geochemical studies (Zentilli et al., 1986; MacInnis, 1986) have shown that lithological divisions in the Meguma Supergroup have characteristic whole rock chemistries. The GHT, for example, is recognizable by its anomalous enrichment in S, Mn, C, Ba, Pb, Zn, Cu, Mo, W, and Au in comparison to the surrounding Meguma rocks and other units within the GHT (Graves and Zentilli, 1988).

#### *1.3.4 Structure and Metamorphism*

Exposure of the sulphide-rich GHT is increased by folding of the Meguma Supergroup into tight anticlines and synclines, as seen on a geologic map (e.g. Keppie, 1979). These large-scale folds are parallel to the length of Nova Scotia (roughly NE-SW) with continuous axial traces 100 km or more in length. The repetitive outcrop pattern exposes a very large area of sulphide-bearing rocks throughout the province that make ARD a generalized problem.

Although pyrrhotite is distributed mainly in bedding planes, in many areas regional deformation has mobilized it and transposed its orientation into the slaty cleavage (Binney *et al.*, 1986; MacInnis, 1986; Pašava *et al.*, 1995; Robinson, 1996). This means that when the rock is blasted, it may break along the cleavage plane, exposing sulphides preferentially. This fact makes sulphides particularly vulnerable to oxidation.

Metamorphism is another factor affecting sulphide minerals. Regional metamorphism at greenschist facies, the prevalent grade throughout south-central Nova Scotia (Keppie and Muecke, 1979), caused replacement of pyrite with pyrrhotite in elongate 1-10 mm sulphide blebs

at Eastville (Binney et al., 1986), increasing the relative abundance of pyrrhotite. Also, hydrothermal sulphide-rich quartz veins in the Meguma Supergroup (O'Brien, 1985) provide an additional source for sulphide exposures. Late Devonian and Early Carboniferous contact metamorphism in the hornblende hornfels facies (Keppie and Muecke, 1979) also affects sulphide mineralogy and texture; ARD problems do exist within Halifax Group rocks of the contact aureole (Robinson, 1996; Robinson and Fox, 1996).

#### **1.4 Sample Localities**

Six samples were selected from throughout the Meguma Supergroup (Fig. 1.1, Table 1.3) to represent most of the common sulphide minerals that occur, with a variety of textures. Sample descriptions are presented in Section 3.2.1.

#### **1.5 Methodology**

The thesis work was developed in two main inter-related parts. 1) A review and critical analysis of previous studies of acidophilic bacteria associated with ARD. This review gives the identification and metabolism of many species potentially present in ARD, some chemical reactions involved, and a discussion considering the possible causal effect of bacteria in ARD formation. 2) An oxidation experiment that compared the relative oxidation rates of sulphide minerals in polished thin sections between two ARD samples from the same source, one with a natural sample of bacteria, and the other sterile. The progress of oxidation was monitored visually and documented with photomicrographs taken in reflected light. The final surface appearance was also documented with the SEM.

**Table 1.3: Sample localities**

Sample #	Stratigraphic Position	Location	UTM Coordinates (Easting, Northing)	collected by
RJ-96-001	Halifax Group (Cunard Formation)	Tancook Island	(406 900, 4 924 200) grid zone 20	Don Fox
RJ-96-002	Goldenville Group (Montreal Slate Belt)	Mt. Uniacke slate pile	(436 200, 4 974 950) grid zone 20	Don Fox
RJ-96-003	Goldenville Group	Caribou Drill Core: Sherritt Gordon Bruckner Lake 89-5A (core box 103, 587.2m depth)		Don Fox
CR-95-002	Halifax Group	near the Bayers Lake Industrial Park (along the Bicentennial Highway)	(447 850, 4 943 400) grid zone 20	Don Fox
CR-95-016	GHT (Black Slate)	Eastville core (Drill Hole 18)		Clare Robinson
BH-20-I	Halifax Group	HIA drill core	(459 000, 4 969 500) grid zone 20	Rachel Jones

UTM coordinates estimated from 1:50 000 scale NTS sheets of the Dept. of Energy, Mines, and Resources.

## **1.6 Organization**

Following this introduction, Chapter 2 contains a comprehensive review of previous studies of acidophilic bacteria associated with ARD with special consideration given to their possible causal effect. Chapter 3 discusses the design of the oxidation test, including previous work, sulphide sample preparation, bacteria sample preparation, laboratory setup and procedure. Chapter 4 gives the results and discussion sections. Chapter 5 gives conclusions, recommendations and future work. Appendix A contains data from the microprobe, Appendix B contains three water chemistry analyses: ARD before the experiment, ARD after oxidation of sample CR-95-016 in the microbial treatment, and ARD after oxidation of the same sample in the sterile treatment, and Appendix C contains an XRD pattern of hexagonal pyrrhotite from sample RJ-96-003.

## CHAPTER 2: THE ROLE OF BACTERIA IN THE OXIDATION OF SULPHIDE MINERALS

### 2.1 Brief Introduction to Microbiology

The field of microbiology is extremely broad, and a complete introduction is far beyond the scope of this thesis. The reader should refer to an introductory text such as Microbiology (Prescott *et al.*, 1996) for further information. However, this being an Earth Science thesis, it is appropriate to offer a brief introduction to this complex field.

Microbiology is a relatively new discipline which developed with the invention of the microscope. Any organisms that are small enough to require a microscope for viewing are considered "microbes" or "microorganisms." Thus a tremendous biological diversity is represented by these terms.

Before giving an overview of this diversity, a few terms are defined. "Bacteria" is the common name for organisms in the Kingdom Monera. These organisms are single cells with no nucleus (see Fig. 2.1: a generalized bacterium). All cells with nuclei are classified within the four other kingdoms listed below. Nucleated cells are called 'eukaryotes' (Gr. prep. *eu* true, nice, beautiful; n. *karyon* kernel (Raven and Johnson, 1992)), and non-nucleated cells are called 'prokaryotes' (Gr. *pro* before (Raven and Johnson, 1992)). Table 2.1 gives the distinguishing characteristics of prokaryotes and eukaryotes, as explained by Raven and Johnson (1992).

The currently accepted classification of all organisms (except viruses) consists of five kingdoms: Monera or Procaryotae (unicellular prokaryotes), Protista (unicellular or colonial eukaryotes), Fungi (mainly multinucleate eukaryotes), Plantae (multicellular autotrophic eukaryotes), and Animalia (multicellular heterotrophic eukaryotes) (Raven and Johnson, 1992).

**Table 2.1: Prokaryotes vs. Eukaryotes**  
(modified from Raven and Johnson, 1992)

<b>FEATURE</b>	<b>PROKARYOTES</b>	<b>EUKARYOTES</b>
nucleus	no	true, membrane bound
membrane-bound organelles	no	yes
microtubules	no	yes
flagella	simple, rigid	complex, flexible
DNA	1) does not bind with proteins 2) in a single ring	1) binds with proteins 2) in multiple chromosomes
cell wall	almost always present, contains muramic acid	sometimes present, muramic acid never present, walls made of cellulose fibres, polysaccharides and protein
genetic recombination	via plasmids or transposons	meiosis
duplication	binary fission	mitosis
size	approximately 2 $\mu\text{m}$	5 to 10 $\mu\text{m}$ , some much larger

Microbiology covers the study of Monera, most members of Protista, and some members of Fungi. A number of other classifications have been proposed involving six or eight kingdoms, but the newest proposal by Woese *et al.* (1990, cited in Raven and Johnson, 1992) consists of only three domains: archaee (archaeobacteria), bacteria (eubacteria) and eucarya (eukaryotes), where the first two contain organisms previously classified as Kingdom Monera, and the last one groups the other four kingdoms together. This classification is based on rRNA sequence comparisons to create a phylogenetic tree (Fig. 2.2) where the length of a line represents the number of differences between groups of organisms and branches represent diversification from a common ancestor. This approach shows that there is a greater difference between archaeobacteria and eubacteria than between archaeobacteria and eukaryotes, or between plants and animals.

Despite common misconceptions, sulphur- and iron-oxidizing bacteria are not groupings based on phylogeny, but on similarities in living conditions and metabolism. There are sulphur- and iron-oxidizing bacteria among both eubacteria and archaeobacteria.

## 2.2 Types of Bacteria Associated with ARD

### 2.2.1 Metabolism

Metabolism is a word that encompasses all the chemical reactions (organic and inorganic) in an organism involved in the gathering of energy and building blocks needed for maintenance, growth and reproduction. The energy collection process is described in great detail in Prescott *et al.* (1996). Summarizing briefly, an energy source donates an electron with a certain amount of energy. This electron follows a series of proteins called the "electron transport chain," losing a little energy at each step, and is finally deposited on an electron acceptor (such as O<sub>2</sub> or Fe<sup>3+</sup>).

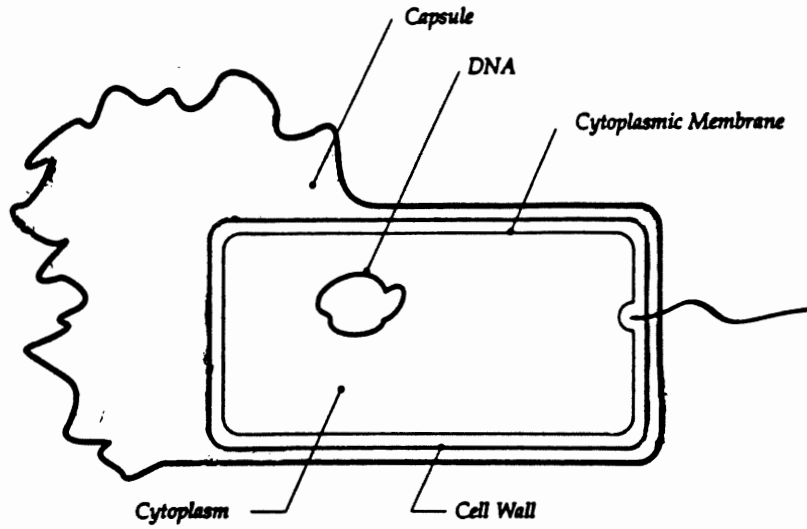


Figure 2.1: A generalized bacterium (from Gould *et al.*, 1994).

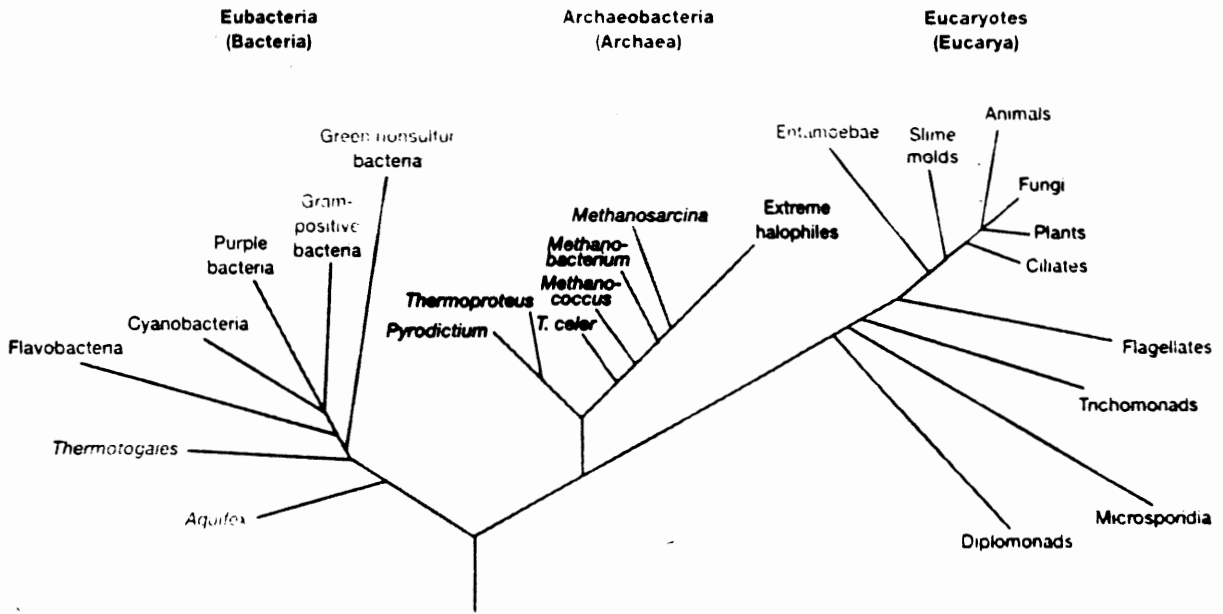


Figure 2.2: Phylogenetic tree of life based on rRNA sequence comparisons (Olsen and Woese, 1993, cited in Prescott *et al.*, 1996)



Some of these proteins in the chain use the electron's energy to pump protons from one side of a membrane to another, setting up a proton gradient. The gradient passively drives the formation of chemical bonds (connecting phosphate groups to adenosine triphosphate) that can be broken later, releasing the stored energy to drive normal cellular reactions. This is common to all organisms, but the initial source of energy varies, as does the reductant and carbon source. The metabolism (abbreviated as the suffix "-troph") of sulphur- and iron-oxidizing bacteria involves a chemical energy source (abbreviated as the prefix "chemo-") instead of light energy ("photo-"), they use inorganic electron donors ("litho-") instead of organic ("organo-") and they reduce their own carbon from  $\text{CO}_2$  ("auto-") instead of assimilating carbon from other organisms ("hetero-"). Therefore, sulphur- and iron-oxidizing bacteria are said to be "chemolithoautotrophic" (in comparison, humans are "chemoorganoheterotrophic"). Specifically, these bacteria can oxidize (remove electrons from) reduced sulphur compounds or ferrous iron, and reduce (add electrons to) molecular oxygen. Also, the bacteria *Thiobacillus ferrooxidans* (Nordstrom, 1982), *T. thiooxidans* and *Sulfolobus acidocaldarius* (Brock and Gustafson, 1976, cited in Nordstrom, 1982) can use ferric iron as an electron acceptor in the absence of oxygen. If the replacement of  $\text{O}_2$  with  $\text{Fe}^{3+}$  does not affect the catalytic effect of the bacteria in the oxidation of sulphides, this could have major implications for remediation techniques that involve anoxic conditions (Nordstrom, 1982).

Due to the small amounts of energy available from inorganic sources such as reduced sulphur compounds or ferrous iron (Table 2.2), bacteria need to process large amounts of material. This means that ferric iron precipitates and oxidized sulphur are produced far in excess of cellular substance (Lundgren and Dean, 1979). This has implications for the rate of sulphide

group	ATP-yielding reaction	$\Delta G^{0'}$	
		kJ/reaction	kJ/ $2e^-$
hydrogen bacteria	$H_2 + \frac{1}{2}O_2 \rightarrow H_2O$	-237.2 (-56.7)	-237.2 (-56.7)
carboxydobacteria	$CO + \frac{1}{2}O_2 \rightarrow CO_2$	-257.1 (-61.5)	-257.1 (-61.5)
sulfur bacteria	$S^2 + 2O_2 \rightarrow SO_4^{2-}$	-794.5 (-189.9)	-198.6 (-47.5)
	$S^0 + 1\frac{1}{2}O_2 + H_2O \rightarrow SO_4^{2-} + 2H^+$	-584.9 (-139.8)	-195.0 (-46.6)
iron bacteria	$Fe^{2+} + \frac{1}{4}O_2 + H^+ \rightarrow Fe^{3+} + \frac{1}{2}H_2O$	-44.4 (-10.6) <sup>a</sup>	-88.8 (-21.2) <sup>a</sup>
ammonia oxidizers	$NH_4^+ + 1\frac{1}{2}O_2 \rightarrow NO_2^- + 2H^+ + H_2O$	-270.7 (-64.7)	-90.2 (-21.6)
nitrite oxidizers	$NO_2^- + \frac{1}{2}O_2 \rightarrow NO_3^-$	-77.4 (-18.5)	-77.4 (-18.5)

<sup>a</sup>  $\Delta G^{0'}$  values for pH 0 are given; iron bacteria can grow at acidic pH values only; the  $\Delta G^{0'}$  value for pH 7 would be -4 kJ/reaction. Kcal values in parentheses.

**Table 2.2:** Reactions that produce energy for chemolithoautotrophs (from Gottschalk, 1986).

oxidation and detection of the presence of bacteria (see Sections 2.4 and 4.1.4).

### 2.2.2 *Species Potentially Present in ARD Environments*

Table 2.3 lists a number of types of acidophilic bacteria found in ARD and their specific growth conditions. *Thiobacillus ferrooxidans* is the one most studied, but that does not necessarily mean it is the most important in every situation. For example, *T. prosperus* has almost exactly the same general requirements as *T. ferrooxidans*, but is extremely halotolerant. It can thrive in salt concentrations up to 3.5% (Holt *et al.*, 1994). Some ARD remediation techniques involve the addition of salt with the intention of thwarting the growth of *T. ferrooxidans* (McCready, 1987), but this salt would have much less effect on *T. prosperus*.

A given site is neither limited to nor must include all the bacteria types listed here. ARD ecosystems vary substantially from site to site, depending on such factors as climate (e.g. temperature and rainfall), sulphide and matrix characteristics, elapsed time since first sulphide exposure, identity and activity of coexisting organisms (including interdependence or predator-prey relations), pH, Eh, or water chemistry (e.g. Ralph, 1979; Nordstrom, 1982; Evangelou and Zhang, 1995; Leduc and Ferroni, 1993; Gould *et al.*, 1994). Figure 2.3 shows the optimal pH and Eh conditions of a number of genera of iron-oxidizing bacteria. In addition to any of the sulphur or iron oxidizing bacteria in Table 2.3, it is well established that an ARD ecosystem may include acid- and metal-tolerant heterotrophic bacteria, fungi, yeasts, algae, and protozoa (Ralph, 1979, and references therein). Each bacterium has specific nutritional and habitat needs that vary between species, and even between different strains within a species (Leduc and Ferroni, 1993). Given this biotic complexity and the infinite combinations of conditions, it is clear that each ARD site will likely host a different set of microorganisms that are best suited to those conditions

**Table 2.3:** Bacteria Potentially involved in Acid Rock Drainage (references below) and their conditions of growth (Holt *et al.*, 1994)

Name and reference	trophy	electron donor > electron acceptor	pH range	T range °C	NaCl tolerance
<i>Thiobacillus ferrooxidans</i> (1,2,3,4,5,6)	obligately chemolithoautotrophic	reduced S compounds or ferrous iron > O <sub>2</sub> or Fe <sup>3+</sup> (4)	2-4	30-35	<1%
<i>T. cuprinus</i> (7)	facultatively chemolithoautotrophic	reduced S compounds or organic or sulphides > O <sub>2</sub>	3-4	30-36	?
<i>T. thiooxidans</i> (1,2,4)	obligately chemolithoautotrophic	sulphur > O <sub>2</sub> or Fe <sup>3+</sup> (4)	2-4	25-30	?
<i>T. acidophilus</i> (4)	facultatively chemolithoautotrophic	reduced S and organic compounds > O <sub>2</sub>	2-4	25-30	?
<i>T. prosperus</i> (6)	obligately chemolithoautotrophic	reduced S compounds > O <sub>2</sub>	1-4	30-35	<3.5%
<i>T. albertis</i> (7)	obligately chemolithoautotrophic	reduced S compounds > O <sub>2</sub>	2-4	25-30	?
<i>Leptospirillum ferrooxidans</i> (1, 6)	obligately chemolithoautotrophic	ferrous iron, sulphides > O <sub>2</sub>	1.5-4.0	moderately thermophilic	?
<i>Metallogenium spp.</i> (8,9)	chemoorganotrophic or parasitic on fungus	manganous compounds leached from Mn(II) minerals > O <sub>2</sub>	6-8	up to 80	?
<i>Sulfolobus spp.</i> (9, 10)	lithotrophic and organotrophic	sulphide, possibly S <sup>0</sup> > O <sub>2</sub> , Fe <sup>3+</sup>	1-6	55-87	?
<i>Sulfobacillus thermosulfidooxidans</i> (10)	facultatively chemolithoautotrophic	Fe <sup>2+</sup> , sulphides, or S > O <sub>2</sub>	1.1-5.0	20-60	?
<i>Acidianus spp.</i> (10)	chemolithotrophic	S <sup>0</sup> > O <sub>2</sub> (in presence of O <sub>2</sub> ) H <sub>2</sub> > S <sup>0</sup> (in absence of O <sub>2</sub> )	1-6	45-96	0.1-4%

1. Gould *et al.* (1994)

3. Leduc and Ferroni (1993)

5. Silver *et al.* (1986)7. Holt *et al.* (1994)

9. Ralph (1979)

2. Blowes *et al.* (1995)

4. Nordstrom (1982)

6. Pronk and Johnson (1992)

8. Ludgren and Dean (1979)

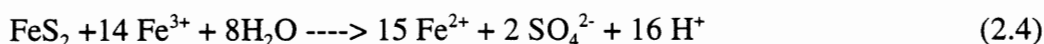
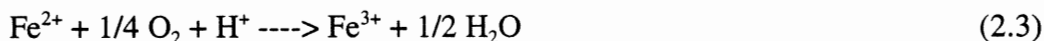
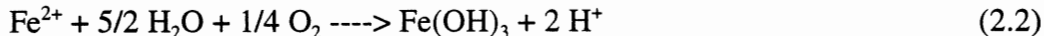
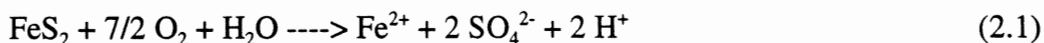
10. Ahonen and Tuovinen (1992)

(Leduc and Ferroni, 1993). This fact has guided the decision to use a natural local sample of ARD microbes in this thesis, as opposed to an artificially prepared mono-species culture. A great deal of detailed work on this subject remains to be done for ARD sites in Nova Scotia.

### 2.3 Reactions of ARD Production: Biological and Chemical

As mentioned in Section 1.2, metal sulphide minerals oxidize in the presence of water and oxygen or ferric iron, forming sulphuric acid and a metal ion. This reaction varies depending on the type of sulphide, Eh, pH, and the presence or absence of bacteria. Following are some examples of specific chemical reactions presented by various authors.

Pyrite oxidation can be described by the following four equations (Paine, 1987):



Equation 2.1 (pyrite oxidation by oxygen) can occur with or without bacteria; Equation 2.2 (oxidation of ferrous iron to a ferric precipitate) occurs with bacteria between pH 2.5 and 4.5, and without bacteria above pH 4.5; Equation 2.3 (ferrous iron oxidation to dissolved ferric iron that is used immediately in Equation 2.4) occurs mainly by bacteria at low pH, and Equation 2.4 (pyrite oxidation by ferric iron) occurs without bacteria at low pH. Elemental sulphur is an intermediate between reduced sulphides and sulphuric acid, and may form during either nonoxidative dissolution, or partial oxidation of a sulphide (Ahonen and Tuovinen, 1992). Figure 2.4 illustrates pyrite oxidation and the relationships between catalysts (bacteria), oxidizing agents and secondary minerals.

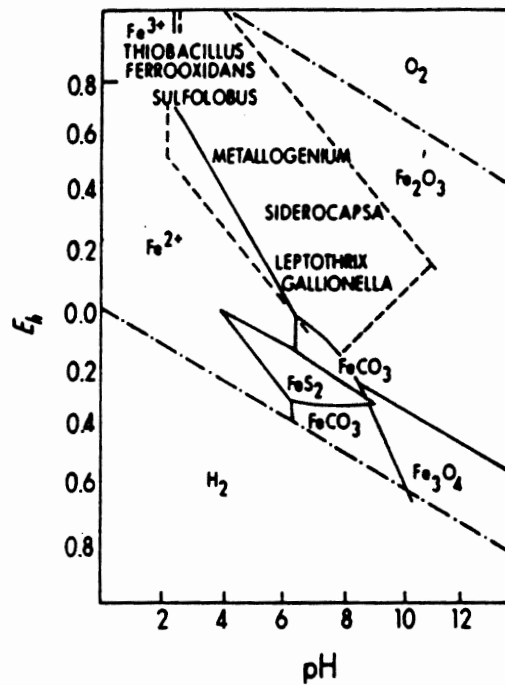


Figure 2.3: Plot of Eh/pH preferred environments of some iron-oxidizing bacteria (from Lundgren and Dean, 1979).

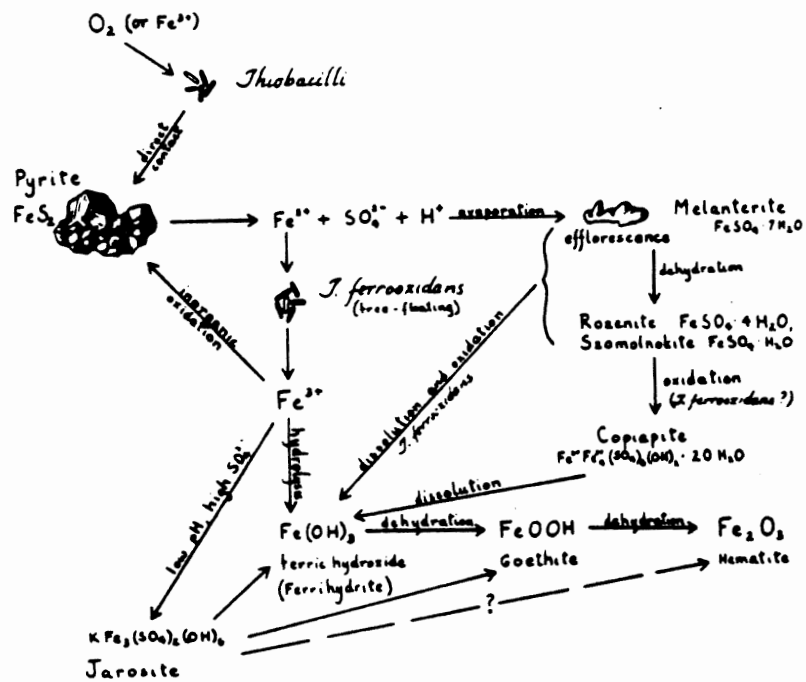
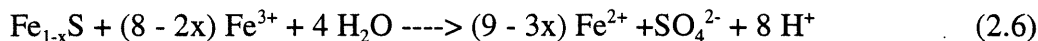
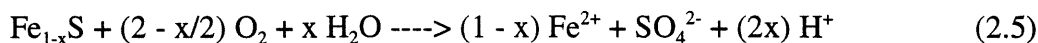


Figure 2.4: Reactions involved in pyrite oxidation, and the relationships between oxidizing agents, secondary minerals and catalysts (from Nordstrom, 1982).

Pyrrhotite oxidation is similar, with different element proportions (Kwong *et al.*, 1995):



Similar oxidation equations have been proposed for many other sulphide minerals including chalcopyrite (Steger and Desjardins, 1978), galena (Silver *et al.*, 1986; Garcia *et al.*, 1995a), and sphalerite (Garcia *et al.*, 1995b).

Oxidation reactions of metal sulphides are exothermic (Gould *et al.*, 1994), meaning that the products are at a lower energy state than the reactants, and the energy is released to make heat. One way to think of the energy transfer is that it can either be used by bacterial metabolism, or released as heat, or both.

## 2.4 Are Bacteria a Major Cause of ARD?

An important question in the study of ARD is how the process of acidification begins. Microbe metabolism is specific to Eh and pH conditions, as explained above, and microbes may also modify these conditions (Ralph, 1979). This leads to the idea proposed by Walsh and Mitchell (1972) of a succession of microorganisms that colonize and alter the environment until conditions are right for the next species. If *Thiobacillus ferrooxidans* is active only below pH 4 to 4.5 (Gould *et al.*, 1994; Holt *et al.*, 1994; Nordstrom, 1982; Walsh and Mitchell, 1972), oxidation may begin at pH 7 with either *Metallogenium spp.* (Walsh and Mitchell, 1972) or purely chemical reactions (Nordstrom, 1982), and as the pH dropped below 4, *Thiobacillus* could take over. If *Thiobacillus ferrooxidans* is metabolically active at pH 7 (Kleinman and Crerar, 1979) (perhaps the microenvironment near the sulphides is more acidic; Nordstrom, 1982) then it can dominate the acidification process from the beginning (Kleinman and Crerar, 1979). In the initial

stages, direct oxidation (see below) is important because ferrous iron would not yet have reached concentrations usable by iron-oxidizing bacteria. Nordstrom (1982) comments that whether bacteria replace each other in succession and which species are responsible requires further study; however, microbes from the soil such as *Thiobacillus spp.* or *Metallogenium spp.* are likely candidates for ARD initiation.

Mechanisms of sulphide oxidation can be divided into two types: direct and indirect. Direct oxidation of a mineral means that the oxidation reaction is triggered or accelerated by a catalyst (bacterium or chemical) acting directly on the mineral, whereas indirect oxidation involves another step between the catalyst and the oxidation. In ARD, sulphur oxidizing bacteria act as direct catalysts to sulphide oxidation, but iron oxidizing bacteria regenerate ferric iron from ferrous iron (Lundgren and Dean, 1979), indirectly oxidizing the sulphides via the  $\text{Fe}^{3+}$  (Ralph, 1979). Sulphides can also be oxidized without bacteria, directly by  $\text{O}_2$  or  $\text{Fe}^{3+}$  from other minerals. In either the biological or chemical case, the rate of regeneration of  $\text{Fe}^{3+}$  is a controlling factor in the rate of the overall  $\text{Fe}^{3+}$  catalysis reaction (Singer and Strumm, 1970). At moderate pH (>4.5) spontaneous  $\text{Fe}^{3+}$  regeneration proceeds fairly quickly, so the energy from this reaction is less useful to iron-oxidizing bacteria. However, at lower pH (2-4.5) spontaneous iron oxidation is slow, and bacteria such as *Thiobacillus ferrooxidans* can catalyze  $\text{Fe}^{3+}$  regeneration  $10^5$ - $10^6$  times faster than abiotic rates (Keenan, 1969, Lacey and Lawson, 1970; cited in Ralph, 1979). Also, this could mean that a few bacteria could have a surprisingly strong effect on the oxidation rate due to the large amounts of  $\text{Fe}^{2+}$  needed by bacteria (as mentioned in Section 2.2.1). Because of the tremendous increase in rate, microbial indirect mechanism of sulphide oxidation by  $\text{Fe}^{3+}$  is certainly important at low pH (i.e. in ARD). Both direct sulphide oxidation by sulphur bacteria



and indirect oxidation occur concurrently (Silverman, 1967, cited in Nordstrom, 1982).

One other mechanism of bacterially increased sulphide oxidation involves re-exposure, and is described by Sanmugasunderam *et al.* (1987) and Ahonen and Tuovinen (1992). Sulphide oxidation produces elemental sulphur that can accumulate on a mineral surface during purely chemical oxidation. If this coating remained in place, it would retard further dissolution or oxidation of the sulphide. However, if sulphur-oxidizing bacteria are present, they will oxidize the elemental sulphur further to sulphuric acid, and re-expose the mineral surface to further attack, indirectly increasing the mineral's oxidation rate.

Other acidophilic organisms may also indirectly increase the rate of sulphide oxidation even though they do not use sulphur or iron for food. Chemolithoautotrophs need other nutrients as well, such as nitrogen. Tsuchiya *et al.* (1974; cited in Ralph, 1979) found a mutualism between *Thiobacillus ferrooxidans* and *Beijerinckia lacticogenes* (a nitrogen-fixing bacterium), meaning that each grew better when the other was present. Other examples of species associations are *Thiobacillus spp.* and *Acidiphilium spp.* (heterotrophic) (Davis and Beveridge, 1995), or *Thiobacillus ferrooxidans* and *T. acidophilus* (Arkesteyn, 1980b, cited in Nordstrom, 1982). As a result, not only do chemolithoautotrophs cause or increase ARD formation, but associated bacteria indirectly encourage the process by helping the sulphur- or iron-oxidizers. Predator interactions also affect the other organisms present (McCready, 1987), and thus the sulphide oxidation rate.

The evidence presented above provides a strong case for the causal effect of sulphur- and iron-oxidizing bacteria and associated organisms in the formation of ARD, either by increasing the rate of a reaction that may also occur spontaneously, or by indirect methods of sulphide

degradation. A great deal more work needs to be done on the species, strains and associations of organisms in ARD sites, especially in the relatively unstudied Meguma slates. Simply stated, bacteria do actively contribute to ARD production.

## CHAPTER 3: DESIGN OF THE OXIDATION EXPERIMENT

### 3.1 Background

A number of studies have been performed that examine bacterially enhanced sulphide oxidation (e.g. Ahonen and Tuovinen, 1992; Kwong and Lawrence, 1994; Sanmugasunderam *et al.*, 1987; MacInnis *et al.*, 1994). This study differs from the others in two significant ways. Firstly, it uses a natural uncultured mixed sample of bacteria without removing the coexisting organisms (including algae and other protists); the sulphide-oxidizing bacteria were not isolated or enriched in an artificial culture medium. Secondly, this is the first comprehensive study that uses rock samples containing a variety of sulphide minerals from the Meguma Supergroup in Nova Scotia. Also, it is now well known that a particular sulphide mineral (e.g. pyrite,  $\text{FeS}_2$ ) can oxidize at substantially different rates depending on such factors as grain size, texture, trace element content, number and type of inclusions, or associated minerals (e.g. Kwong and Lawrence, 1994; Borek, 1994). Simply stated, the oxidation rate and extent is site-specific, and much detailed work remains to be done in this field with the Meguma Supergroup.

### 3.2 Experimental Setup and Procedure

#### 3.2.1 Rock Sample Descriptions

Samples were selected to represent the major sulphide mineral types in the Meguma Supergroup, with a variety of textures (refer to Fig. 1.1 and Table 1.3 for sample locations).

Sample RJ-96-001 (Fig. 3.1) contains mainly large (2mm) euhedral pyrite, uncommonly fractured, with lacy rims of pyrite of the same composition. One bed in the thin section contains anhedral pyrite with abundant lamellar inclusions too fine to probe, associated with chalcopyrite

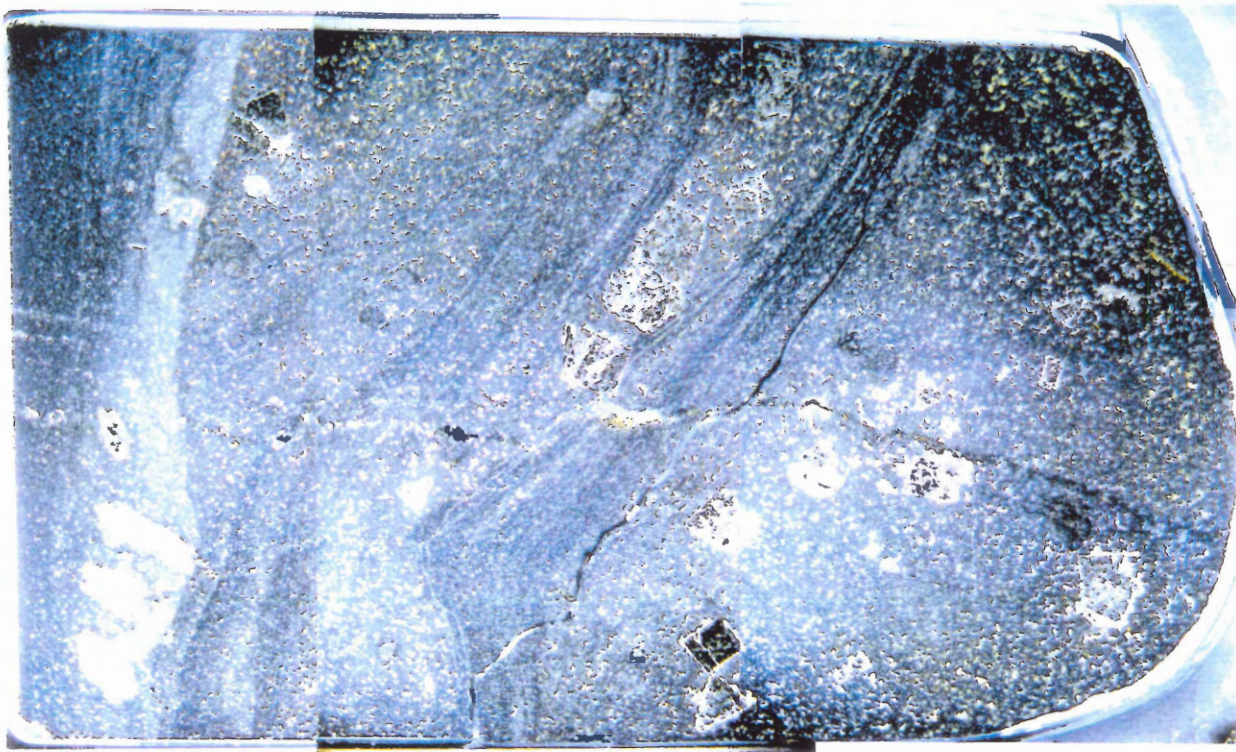


**Figure 3.1:** RJ-96-001. incident light. width=2.6cm. Large euhedral pyrite and one bed with anhedral pyrite. Minor chalcopyrite. Halifax slate.

and fine rims of oxides (Fig. 3.2).

Sample RJ-96-002 (Fig. 3.3) contains large (1-5mm) elongate arsenopyrite, slightly fractured, with pressure shadows of quartz. A minor amount of subhedral pyrite is also present.

Sample RJ-96-003 (Fig. 3.4) is a vein of massive sulphide, mostly hexagonal pyrrhotite (distinguished from monoclinic pyrrhotite by XRD analysis, Appendix C), with chalcopyrite rims (Fig. 3.5), and inclusions of galena, chalcopyrite, arsenopyrite and oxides. Subgrains of hexagonal pyrrhotite are visible under crossed polars and vary from large and equant to small and elongate (Fig. 3.6). Rare fractures cut across subgrains.

Sample BH-20-I (Fig. 3.7) contains large, elongate (approximately 1x5 mm), monoclinic pyrrhotite oriented parallel to cleavage and cross-cutting bedding. Short sides of grains are irregular and commonly rimmed with rutile. Long sides are smoother. Minor sulphide inclusions in pyrrhotite include chalcopyrite, sphalerite, and trace galena. Small (0.1-0.3 mm) euhedral pyrite grains are scattered throughout the matrix. Elongate, irregular subgrains of monoclinic pyrrhotite are visible under crossed polars (Fig. 3.8).

Sample CR-95-002 (Fig. 3.9) is a hornfels containing small (0.1-0.4 mm) monoclinic pyrrhotite associated with ilmenite and rutile (Fig. 3.10), and rare inclusions of (Co,Ni)AsS (solid solution between gersdorffite and cobaltite). Oxidation revealed lamellae in the pyrrhotite (Fig. 4.24) within equant subgrains. Large andalusites are present, indicating contact metamorphism from the nearby granite pluton (Fig. 1.1). Contact metamorphism may also have been a factor in the formation of the sulphide texture.

Sample CR-95-016 (Fig. 3.11) contains pyrite, monoclinic pyrrhotite, and minor chalcopyrite. The rock is thinly bedded with various sulphide textures. Pyrrhotite occurs in

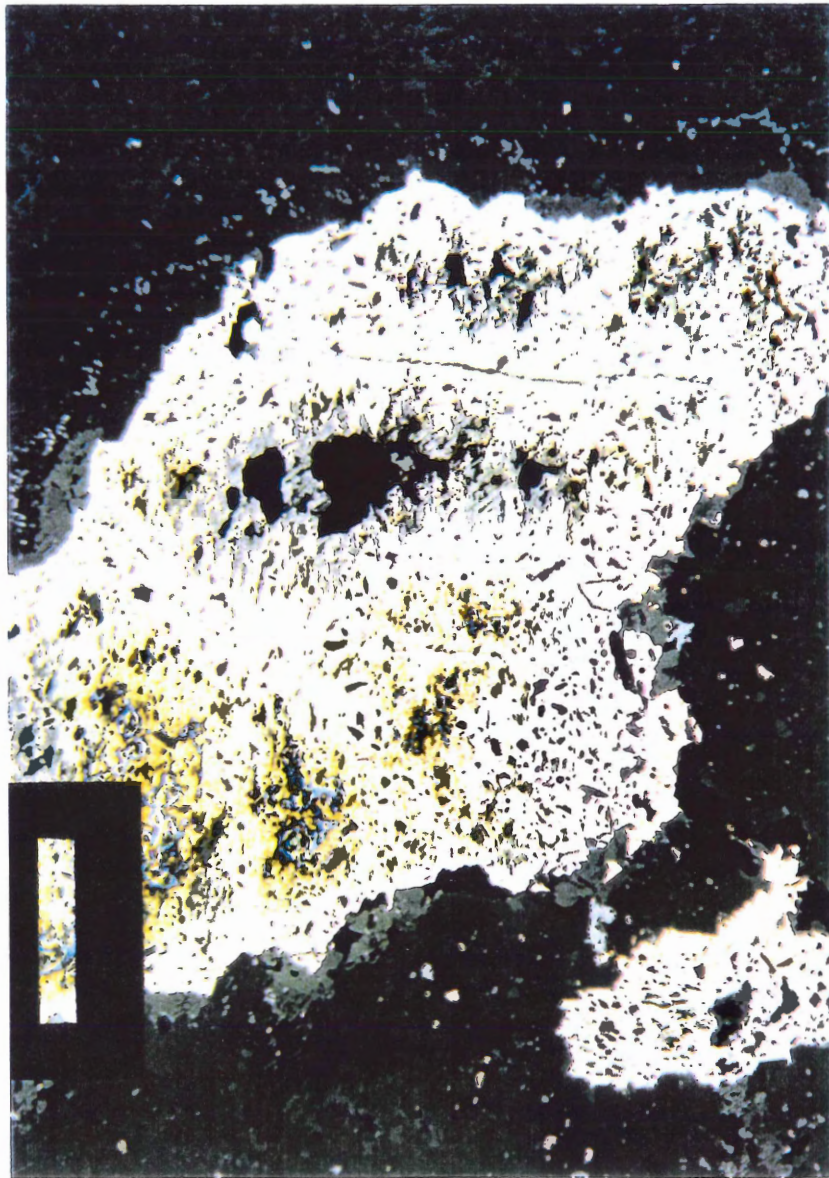


**Figure 3.2:** RJ-96-001, anhedral pyrite with grey lamellae, an oxide rim, and minor chalcopyrite. Scale bar = 0.62mm.

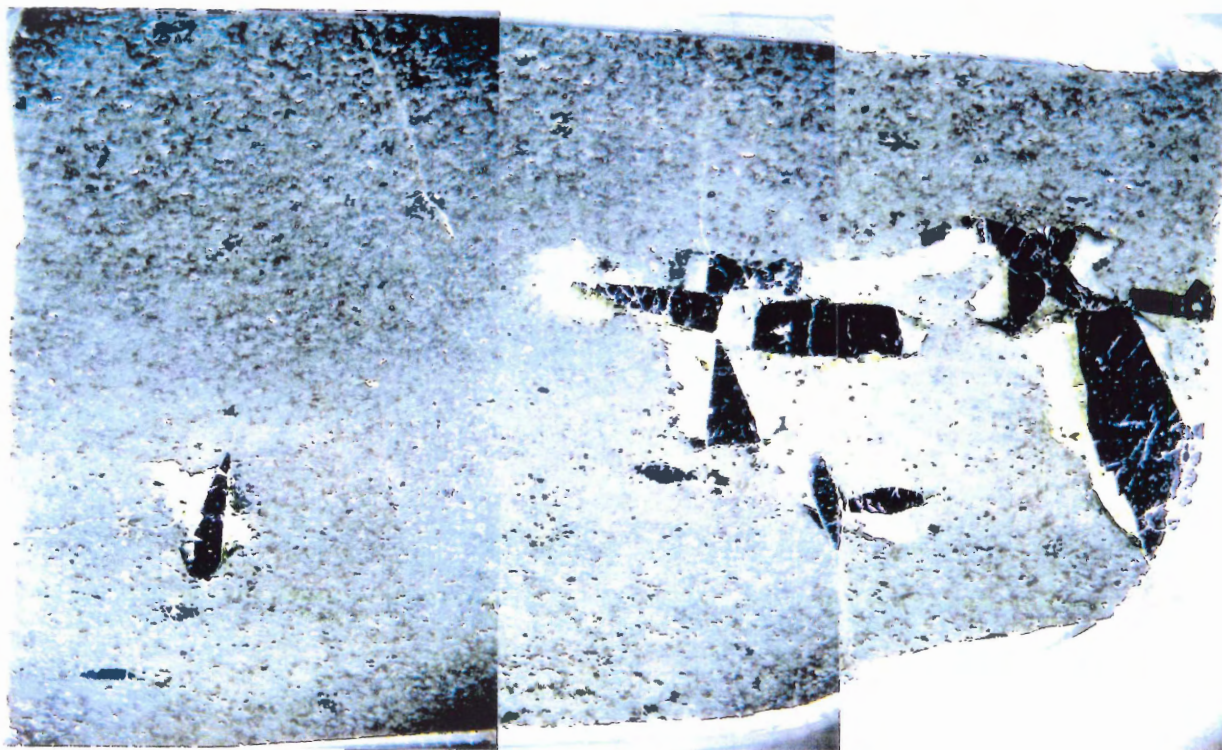


**Figure 3.3:** RJ-96-002, incident light, width= 2.6cm. Large arsenopyrite with pressure shadows of quartz. Goldenville quartzite.

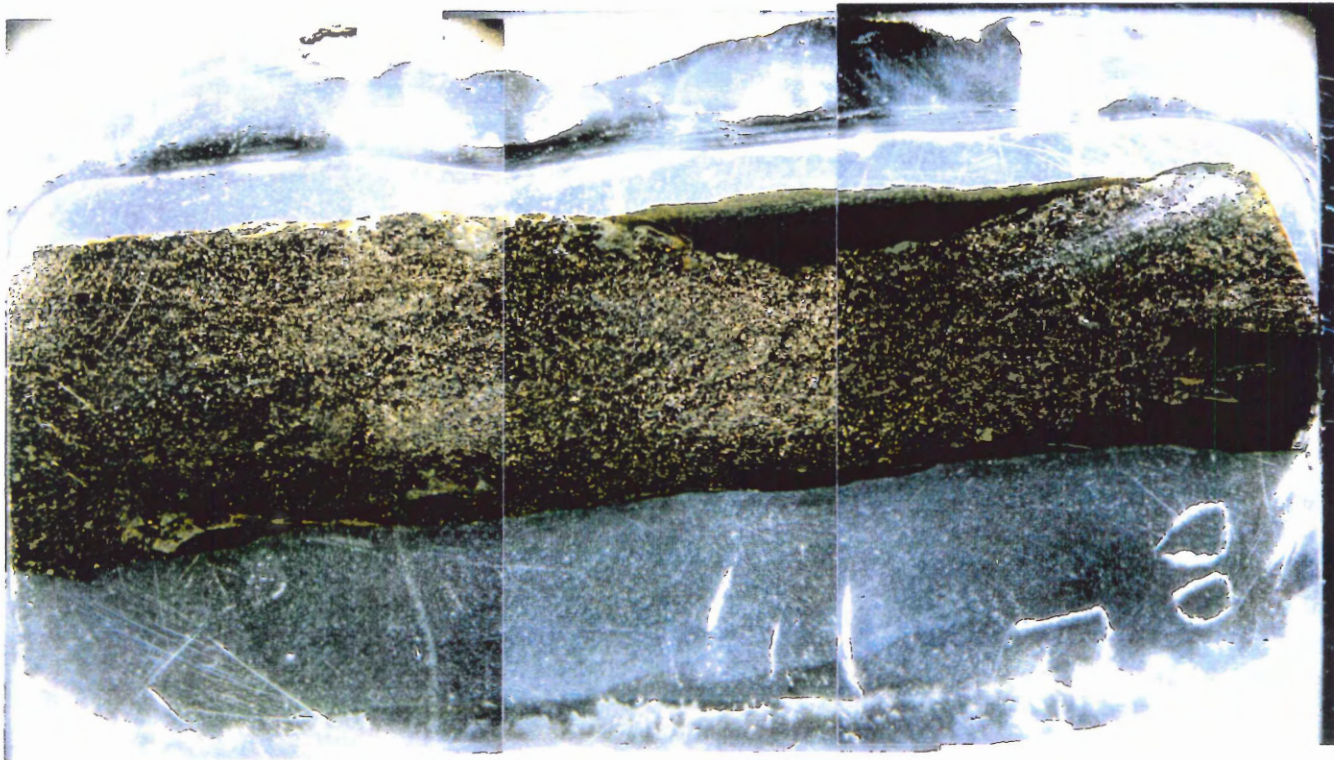


**Figure 3.4:** RJ-96-003, incident light, width~2.6cm. Vein of massive sulphide dominated by hexagonal pyrrhotite, minor chalcopyrite, galena, arsenopyrite.



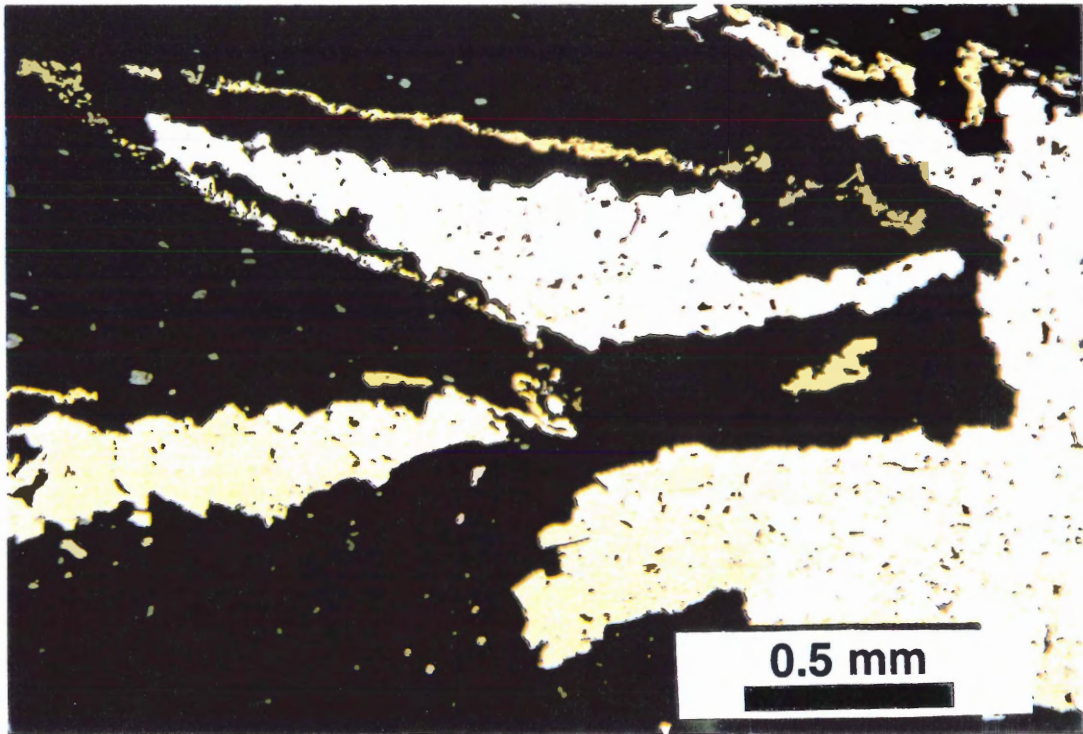


Figure 3.5: RJ-96-003, hexagonal pyrrhotite rimmed with chalcopyrite.

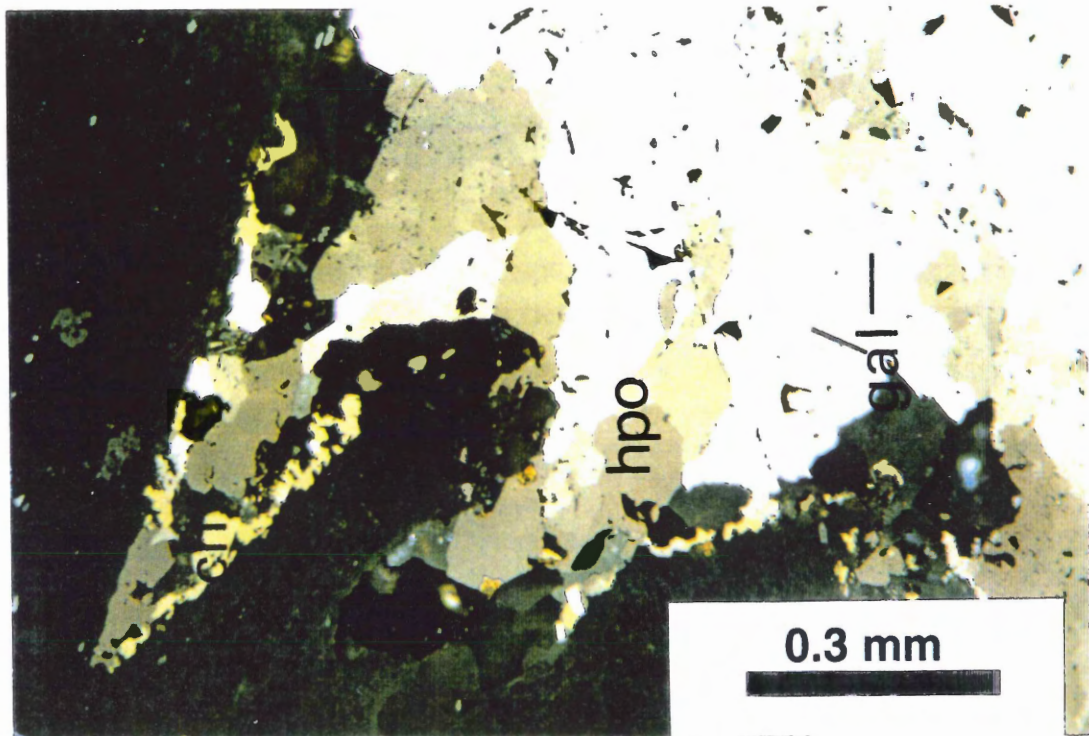
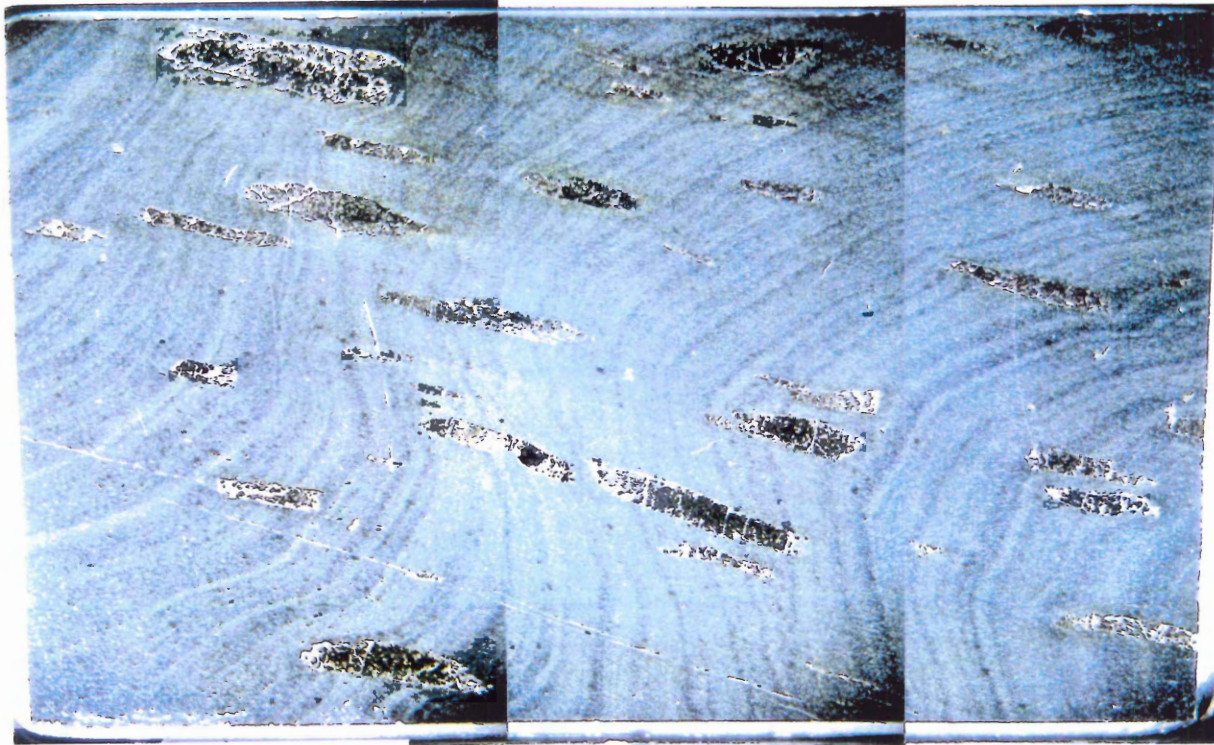


Figure 3.6: RJ-96-003, subgrains of hexagonal pyrrhotite



**Figure 3.7:** BH-20-1. incident light, width=2.6cm. Monoclinic pyrrhotite aligned with cleavage, cross-cutting bedding. Halifax slate.

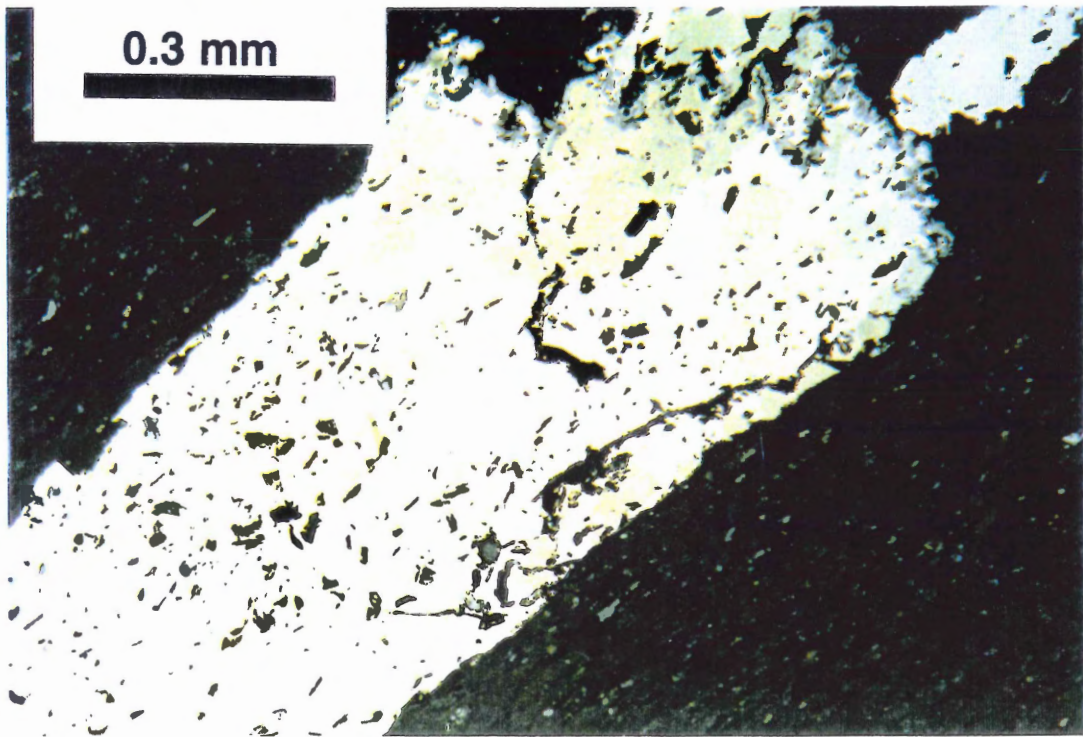
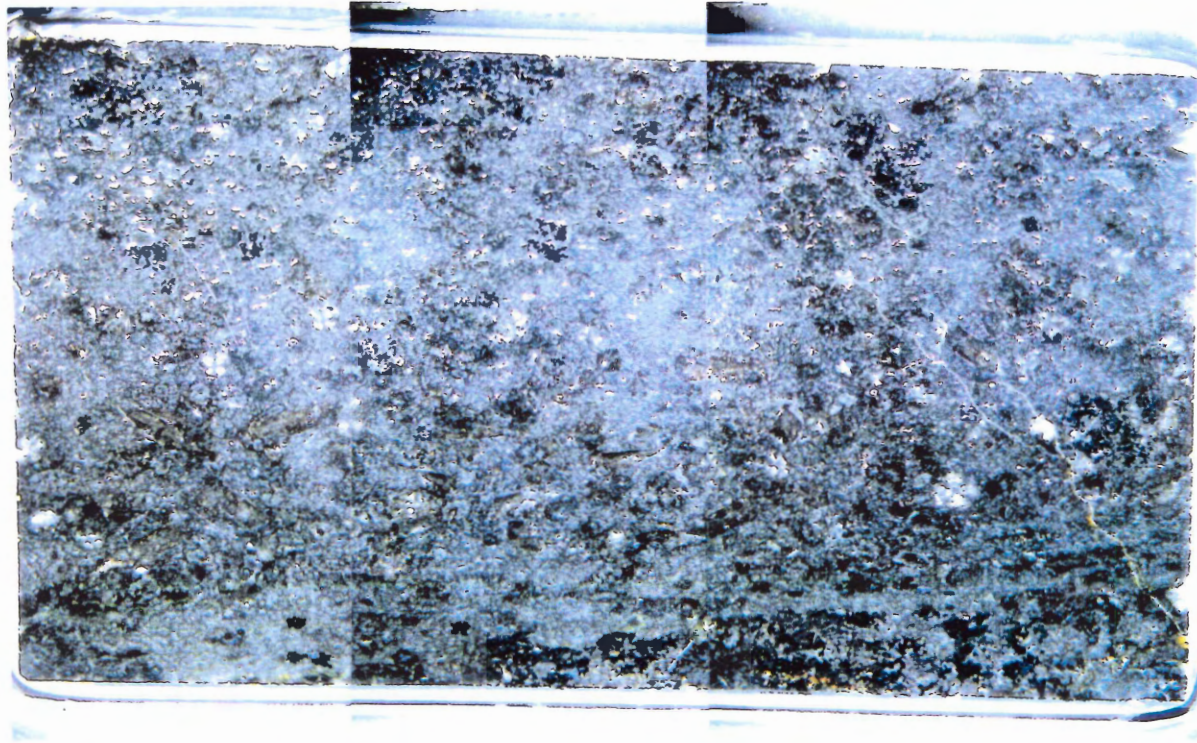
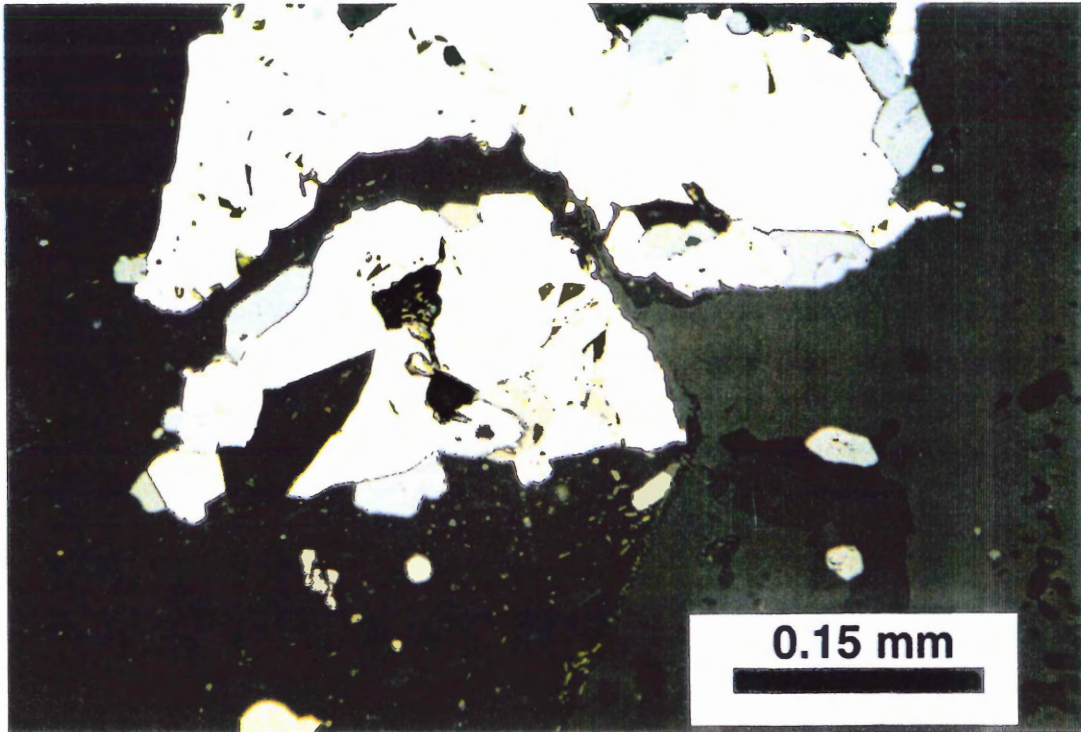


Figure 3.8: BH-20-I. subgrains of monoclinic pyrrhotite.



**Figure 3.9:** CR-95-002, incident light, width=2.6cm. Contact metamorphism formed a hornfels texture. Very fine sulphide grains, large andalusites, uniform rock texture. Halifax slate/hornfels.



**Figure 3.10:** CR-95-002, fine grains of monoclinic pyrrhotite (white) associated with oxides (brownish grey is ilmenite, steel grey is rutile).

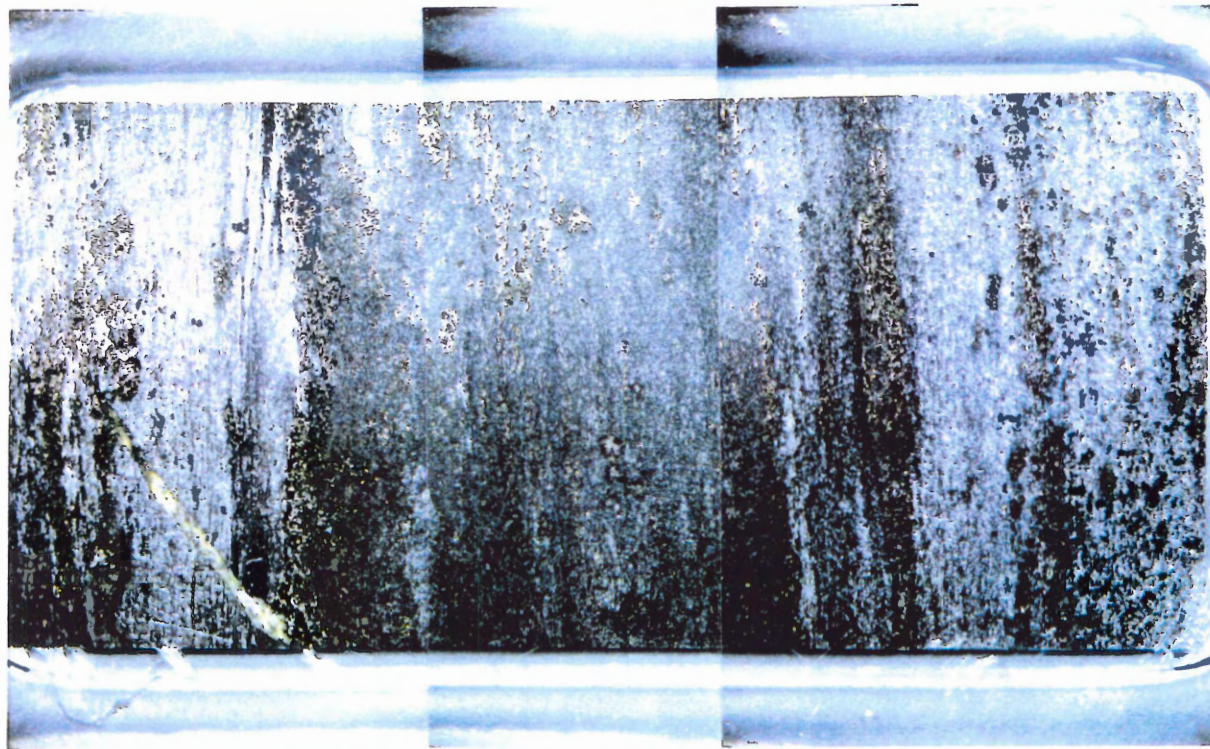


**Figure 3.11:** CR-95-016. incident light, width=2.6cm. Fine sulphide grains aligned with bedding. Goldenville-Halifax Transition Zone.

three textures. Pyrite and pyrrhotite form fine beds of large elongate grains (up to 0.4 x 1.0 mm). These minerals interfinger in a few places. Pyrrhotite also forms globular grains rimmed by garnet (0.1 to 0.4mm in diameter), which are scattered among small elongate grains parallel to bedding. Figure 3.12 shows both of these textures.

### *3.2.2 Preparation of Rock Samples*

Two polished thin sections from each of the six samples were made from adjacent slices of rock so that the pair would be as similar as possible. The slices were cut extra thickly (approx. 1mm instead of the standard 30 $\mu$ m) to allow for volume loss during oxidation and repolishing. While not in use, the thin sections were stored in a desiccator to slow oxidation in air.

Before carbon coating for microprobe work, the thin sections were photographed to document the initial surface appearance. The photomicrographs were taken in reflected light with a blue filter. The JEOL 733 electron microprobe (at the Department of Earth Sciences, Dalhousie University, under the direction of B. MacKay) aided in sulphide mineral identification and documentation of mineral chemistry. Results are given in Appendix A. The probe is equipped with four wavelength dispersive spectrometers and an Oxford Link eXL energy dispersive system, the latter of which was used for all elements. Resolution of the energy dispersive detector was 137 eV at 5.9 KeV. Each spectrum was acquired for 40 seconds with an accelerating voltage of 15 Kv and a beam current of 15 nA. The size of the probe spot was approximately 1 micron. Link's ZAF matrix correction program corrected the raw data. Calibration used cobalt metal. Precision on cobalt metal ( $x=10$ ) was  $\pm 0.5\%$  at one standard deviation. Accuracy for major elements was  $\pm 1.5$  to 2.0% relative. The natural geological

sulphide standards used as controls were chalcopyrite, pyrrhotite, sphalerite (Dr. L.J. Cabri, CANMET), galena (ASTIMEX Scientific, Mount Minm 25-53), and arsenopyrite (CANMIN Vol.14, pp.364-386, 1976, arsenopyrite 200).

Before beginning the experiment, the thin sections were repolished to remove the carbon coating so the surfaces had no protective barrier that might inhibit oxidation. Some carbon likely stayed in cracks or pits in the surface, but as all thin sections were treated the same, they are comparable to each other.

Sterilization was necessary to minimize the chance of bacterial contamination of the filtered treatment. All the thin sections were sterilized, even the ones to be placed in the bacterial treatment, so the sterilization procedure could not create a second variable between the treatments. Soaking in methanol leaches water out of cells and denatures proteins, effectively killing bacteria (Dr. M. Silver, pers. comm., 1996). Therefore the twelve thin sections were soaked in laboratory grade methanol for 86 hours, rinsed in filtered ARD to remove methanol residue that may harm growth in the bacterial treatment, and placed in the experimental jars (Section 3.2.3) using sterile tongs. A test of the effect of methanol on surface appearance of sulphides revealed slight colour changes, but as all samples were exposed to methanol for the same amount of time and only the differences in oxidation rate between the treatments and among different minerals and textures were of interest, this small change would not affect the final results. Only quantitative analyses require that any and all oxidation be due to the experimental treatments.

One extra thin section from sample BH-20-I was used as a control for overall sterilization success; it was not soaked in methanol, its jar was not autoclaved, and the ARD was clear, but



not filtered. After only two days, the control exhibited growth of rust-coloured material, whereas the sterilized treatment did not, indicating that sterilization was important and effective in the experiment.

### *3.2.3 Preparation of ARD Samples*

A quarry near the Halifax International Airport (HIA) contains a small pond of ARD with a pH of approximately 3.0 to 3.5. The water contains stringy gelatinous rust-coloured clouds of biogenic material with patches of yellow, green, or brown (Fig. 3.13), as well as some cattails, waterboatman beetles, bloodworms, rotifers, and other varieties of pond life. It is surprising that these organisms can survive in such acidic conditions.

Water from this pond was collected for use in the oxidation experiment. Considering the low pH, the presence of sulphide minerals in the quarry rock, and the colonies of material with the colour of oxidized iron, it is very likely that sulphur- and iron-oxidizing bacteria are present in a natural mixture of species. Seven litres of rust-coloured sludge and five litres of clear water surrounding the sludge were collected in 1-litre mason jars. These were stored in a refrigerator so that the organisms remained inactive, requiring little oxygen, with the lids tight so they would not spill or be contaminated.

ARD for the sterile treatment (clear water) was double filtered with a pre-sterilized membrane vacuum filter with a 0.2 micron pore size to physically remove bacteria. The filtrate was temporarily stored in autoclaved mason jars (for autoclave specifications, see Section 3.2.5). Filtration was used instead of the autoclave because heat causes a precipitate to form from the ARD, changing the chemistry of the water. As the bacterial treatment would not be sterilized,

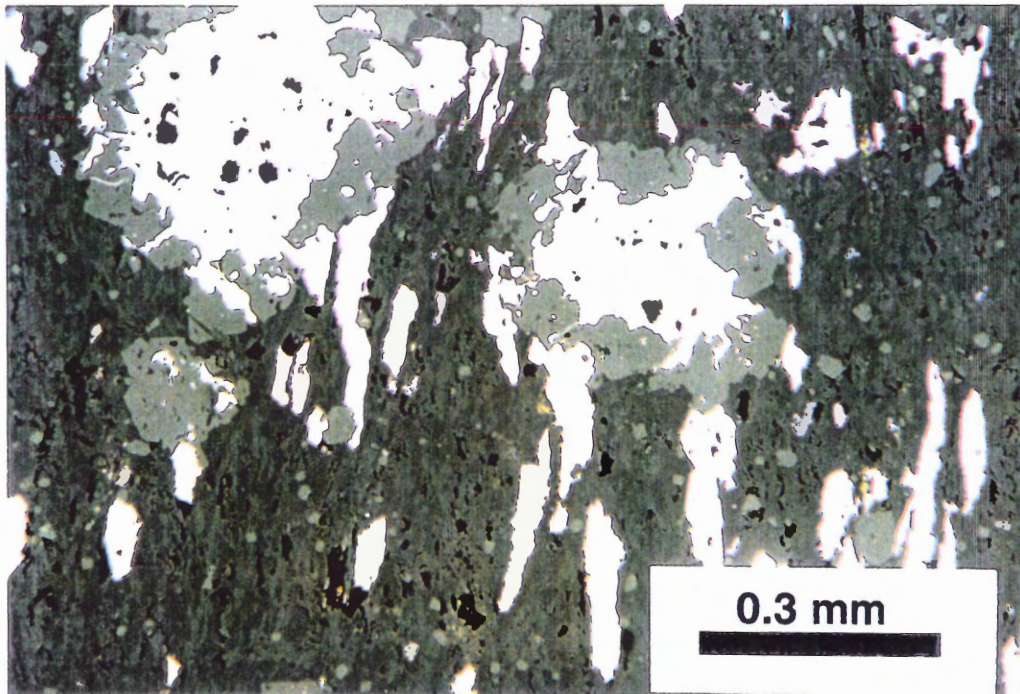


**Figure 3.12:** CR-95-016, two pyrrhotite textures: globular and rimmed by garnet, and elongate grains.



**Figure 3.13:** Quarry near the Halifax International Airport, showing rust-coloured gelatinous growth in the water.

this would create an unwanted chemical difference between the treatments. The ARD was filtered twice because the membrane pore size was 0.2 microns *on average*, so there was a very small chance that a bacterium could fit lengthwise through one of the larger pores. The probability of making a sterile filtrate was squared by filtering twice. After two days in the refrigerator, two jars of filtered water remained clear, but the others turned slightly cloudy. There are a number of possible explanations. Iron may have been oxidized by extra exposure to oxygen, creating a rusty cloudy colour, but all jars were treated the same, so it is unlikely that some were exposed to more oxygen than others. Some jars may have been contaminated by bacteria, but the refrigerator is not at the optimum growth temperature of sulphur- and iron-oxidizing bacteria, and so it is unlikely that they could grow fast enough to show cloudiness in two days. Comparability among thin sections was of primary interest, so the clear and cloudy water were combined to make a homogeneous treatment.

ARD for the bacterial treatment (sludge water) was shaken to dislodge bacteria from the colony. The free-floating organisms were decanted from the collection jar by pouring through a narrowly opened lid. The massive colonies were not added to the experiment because the treatment requires only inoculation, and some degree of visibility through the water was desirable to observe changes in the sulphide surfaces.

#### 3.2.4 Apparatus

The apparatus was designed to sterilely contain 13 thin sections (6 in the bacterial treatment, 6 in the sterile treatment, and 1 control of the overall sterilization procedure) covered with ARD, with plenty of oxygen available. The temperature was held constant at 25°C to encourage microbial growth. Thirteen 500mL mason jars individually held each thin section,

and a sterile air supply continuously aerated the 300mL of ARD in each jar. The air was sterilized with an in-line PTFE 50mm membrane filter with an average pore size of 0.2 microns. The bubbles entering the water caused gentle turbulence, so all the water was uniformly oxygenated. An alternate design could use closed air-tight containers with only a shallow ARD cover over the thin section to allow oxygen diffusion. Because the amount of air needed for growth of organisms and rapid oxidation of sulphides was unknown, this alternate method was rejected in favour of continuous air supply and a larger volume of water. More water was necessary so that evaporation would have less effect, allowing the experiment to run a longer time. Figure 3.14 shows the completed design.

A major limitation in designing such an apparatus is using only autoclavable materials. Many plastics melt or warp in the autoclave, so air tubing, tube splitters, containers and stoppers all need to meet this requirement.

The following apparatus was used: 13 glass 500 mL mason jars, 13 rubber stoppers with input and output holes, 26 glass tubes, Nalgene non-toxic autoclavable premium tubing (Lab/FDA/USP VI Grade) 1/4"ID, plenum (13-way air divider), in-line 0.2 micron PTFE 50mm membrane filter, pre-filter with aquarium wool, a room maintained at 25°C and a pressurized air nozzle connected to an air pump for the whole building.

### *3.2.5 Procedure*

Each piece of apparatus down flow from the air filter was autoclaved at 16 lbs steam pressure for 15 minutes, on the unwrapped cycle. The Nalgene hose expanded when hot, and tended to slip off connections, so the jars and plenum were autoclaved separately with the hose plugged with wool to maintain sterility after autoclaving.

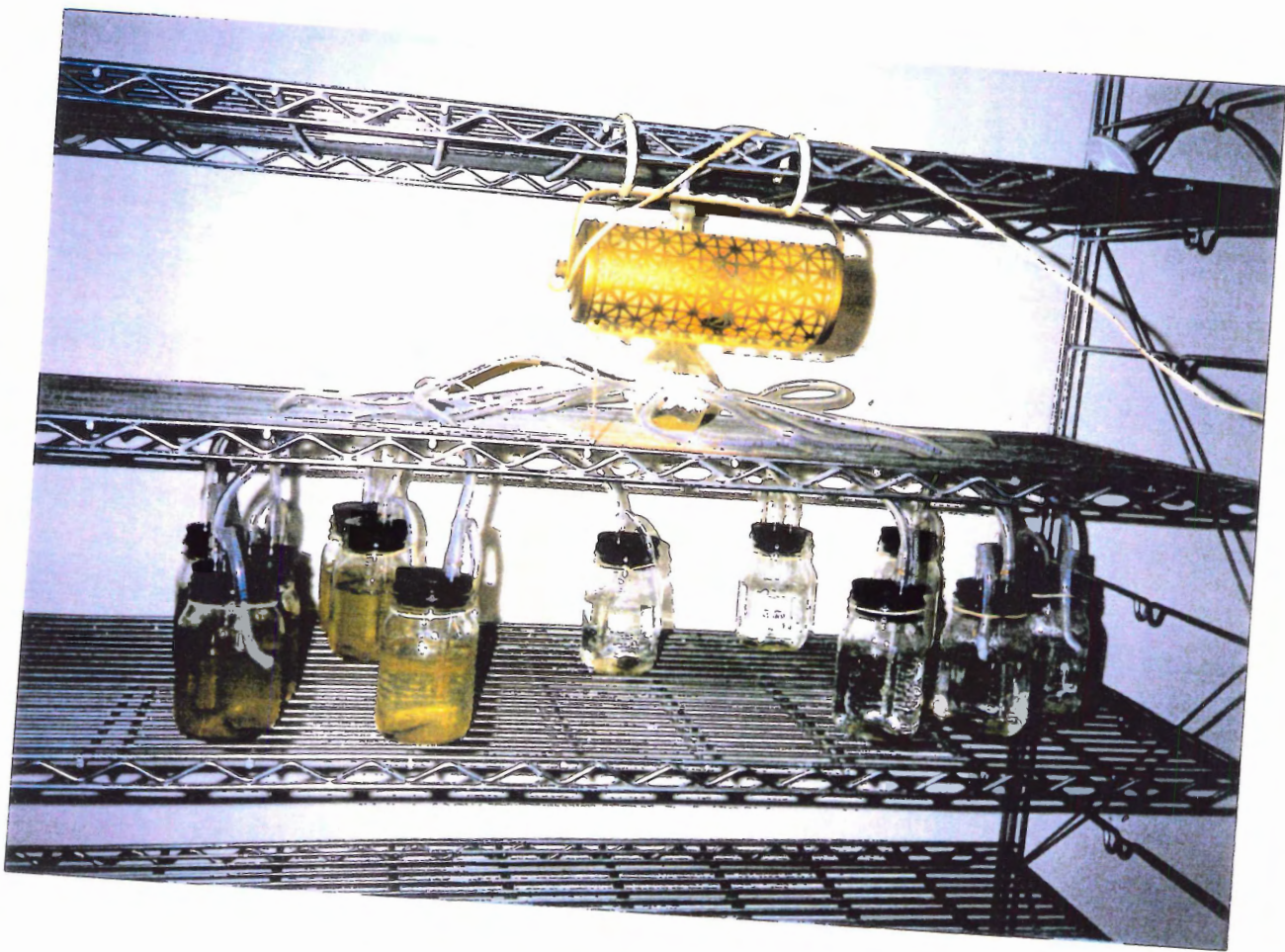


Figure 3.14: Experimental setup design.

After soaking in methanol, thin sections were rinsed in sterile ARD to remove the residue, and transferred to the sterile jars using autoclaved tongs, minimizing the time exposed to air in the room. ARD was carefully poured into the jars up to a mark placed at 300 mL. Again, time exposed to air was minimized.

Hose connection was done sequentially with the air already flowing through the first tubes so that positive pressure would maintain sterility. Wool was removed and the hose connected immediately.

Air flow rate was adjusted with compression of the output hose. Air can flow into a jar only at the rate it can flow out. Adjustment produced gentle bubbling in each jar.

To observe the thin sections under a microscope, they were transferred to petri dishes with 25 mL filtered ARD (just enough to cover the thin section surface) using sterile tongs. The sterile treatment was transferred first before the tongs were contaminated. Between each transfer, the tongs were passed through a flame as a further guard against contamination. While observing, the tongs were re-autoclaved in preparation for the return procedure. Observations and photographs were taken through the cover of the dish. To photograph the sulphide surfaces in the bacterial treatment, the organisms had to be removed with a fine brush (autoclaved). Figure 3.15 shows an example of sulphides before and after brushing. The return transfer used the same procedure as before.

The experiment was allowed to run for 42 days (six weeks). Photomicrographs were taken before oxidation began, 2 days into the experiment, and at 42 days. Final surficial appearance was also documented with the SEM.

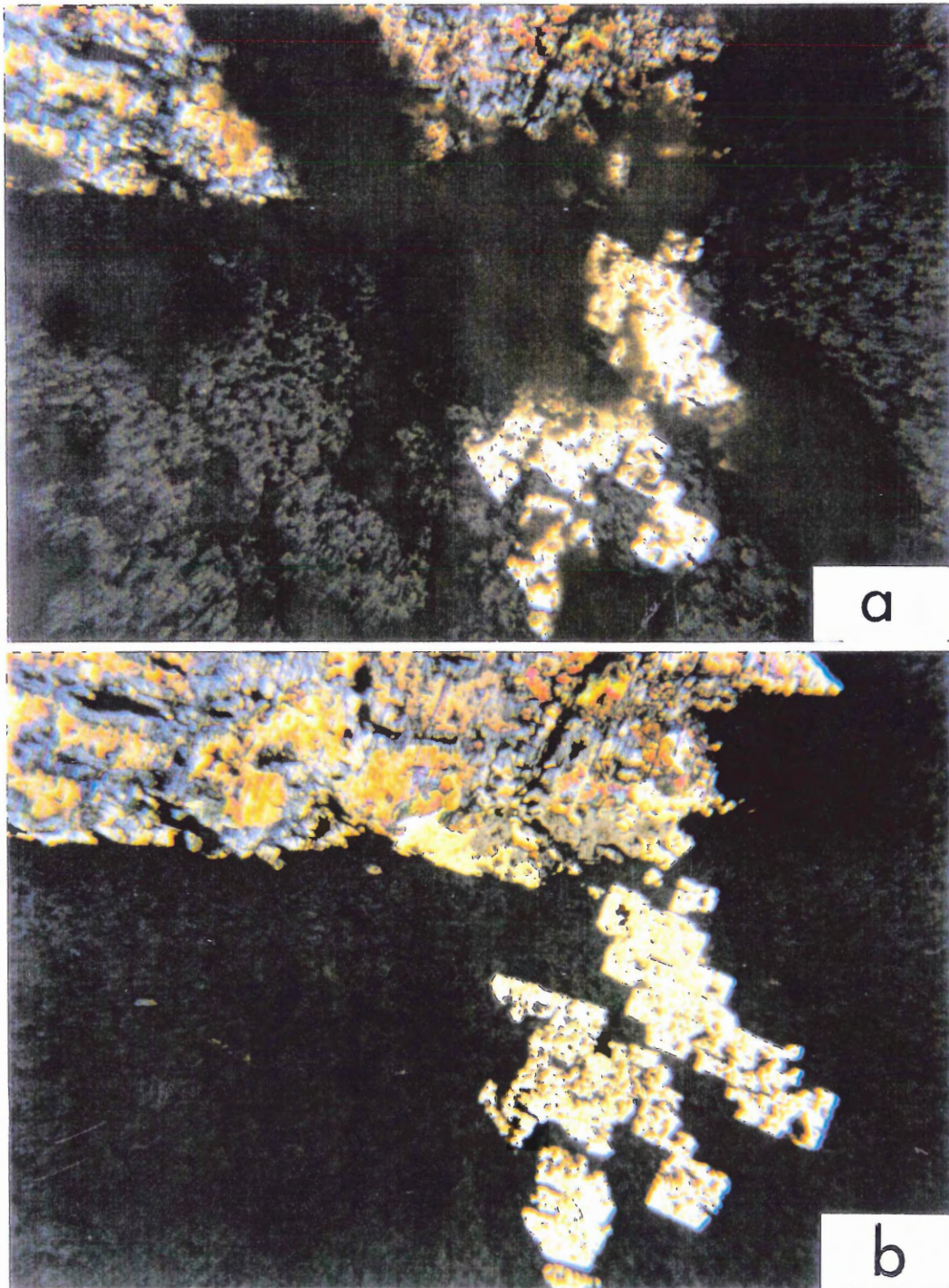


**Figure 3.15:** Sulphide minerals (BH-20-I microbial treatment) (a) before and (b) after brushing. See Figure 4.2 for mineral descriptions.

## CHAPTER 4: RESULTS AND DISCUSSION

### 4.1 Results

#### *4.1.1 Electron Microprobe Results*

Microprobe analyses were used to confirm sulphide mineral identification. BH-20-I contains monoclinic pyrrhotite, pyrite, chalcopyrite, sphalerite and galena. RJ-96-001 contains pyrite and chalcopyrite. RJ-96-002 contains arsenopyrite and very minor pyrite. RJ-96-003 contains hexagonal pyrrhotite (also see Appendix C), galena, chalcopyrite and arsenopyrite. CR-95-002 contains monoclinic pyrrhotite, minor chalcopyrite and cobaltite. CR-95-016 contains monoclinic pyrrhotite, chalcopyrite, and pyrite. Figure 4.1 gives the scatter of pyrrhotite compositions across samples CR-95-016, CR-95-002, RJ-96-003, and BH-20-I. This is a broader spread than found by Robinson (1996), partly because it includes hexagonal pyrrhotite. Also, some of the points from CR-95-016 were measured after oxidation. These plot much farther away from the main group of points, and they have lower totals. They were clearly affected by oxidation, perhaps by element loss or interference by the tarnish. Analyses from orange-tarnished grains contained less sulphur and more iron than blue-tarnished grains, and a spot without tarnish had intermediate sulphur content (Appendix A). Repolishing would be necessary to study the composition of the starting material. Also in this sample, pyrrhotite subgrains that oxidized at different rates were probed, revealing a difference in trace Cu amount. The probe point sample size was small, however, so more study would be needed to be certain. If it is real, the Cu difference could be due to tarnish, original mineralogical composition, or a precipitate.

Preferentially oxidized lamellae within pyrrhotites of sample CR-95-002 are



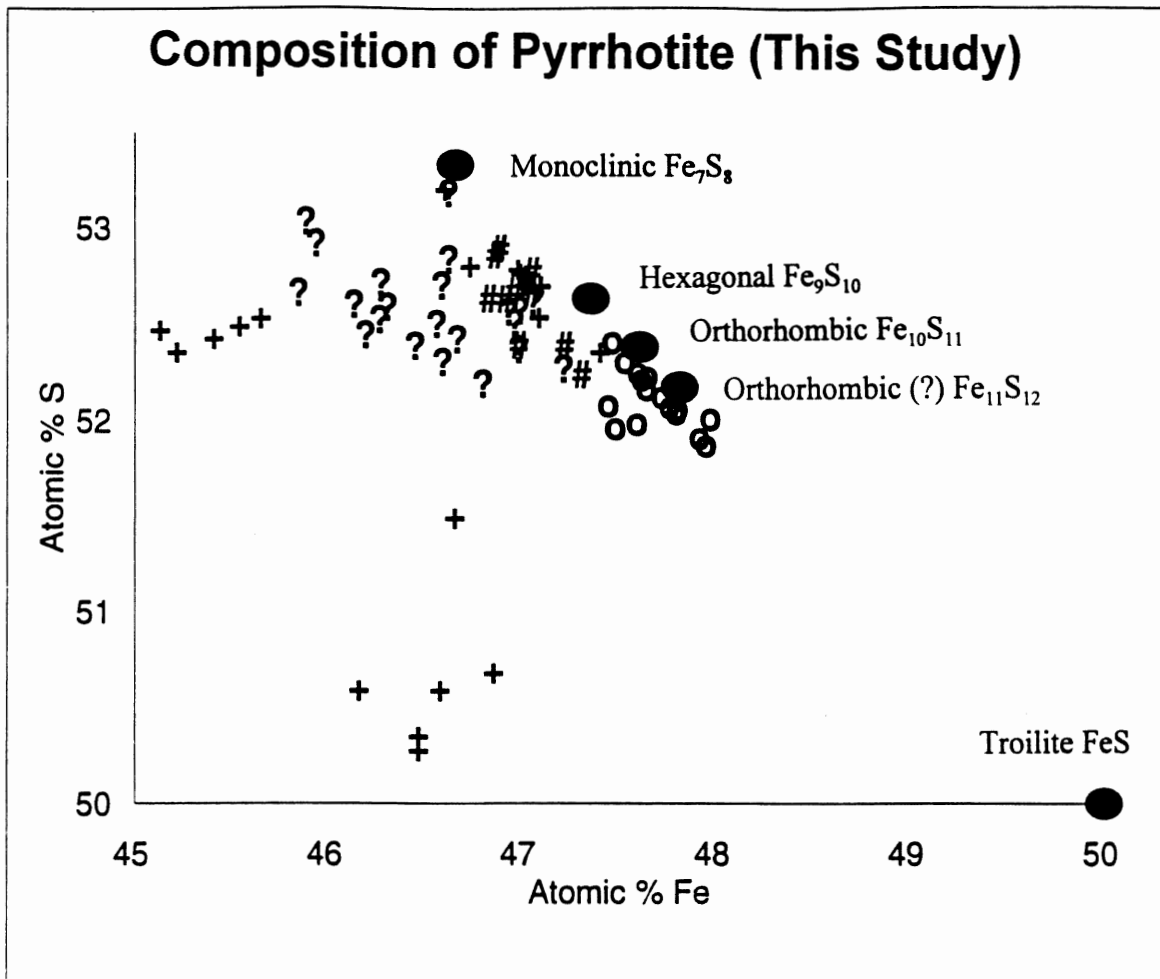


**Figure 4.1:** Plot of atomic % S versus Fe for pyrrhotite compositions used in this study, in comparison to five ideal forms of pyrrhotite (large black circles). Symbols: + (CR-95-016), ? (CR-95-002), o (RJ-96-003), and # (BH-20-I). The broad distribution indicates the presence of both monoclinic and hexagonal pyrrhotite. Points plotted far from the ideal types were measured after oxidation, so the results may have been affected by element loss or interference by the tarnish. Ideal forms of pyrrhotite from Craig and Scott (1974).

compositionally indistinguishable from their host (see Appendix A), eliminating the possibility that compositional variations were the reason for stronger corrosion, unless trace elements below detection limit are involved.

#### 4.1.2 Relative Rates of Oxidation by Image Analysis

In each of the following samples, the relative amount of oxidative dissolution or corrosion was judged by surface appearance. In reflected light, colour changes and etched scratches, cracks or pits were interpreted as oxidation or corrosion. In general, stronger or darker colours and darker polishing scratches indicated a greater degree of corrosion. The use of colour to observe oxidation is supported by the work of Steger (1982), who found that pyrrhotite followed a sequence of colour changes with increasing oxidation: steel-grey to orange-brown to blue-purple to blue-green to orange-brown. Steger further suggests that the blue-purple is due to an insoluble secondary product of  $\text{Fe}^{2+}$  oxidation, such as  $\text{Fe}(\text{OH})(\text{SO}_4) \cdot x\text{H}_2\text{O}$ , the orange-brown is due to ferric oxide, and the other colours are mixtures of the two precipitates. Blue, purple, orange, yellow or brown tarnish have also been noted on chalcopyrite (Chen *et al.*, 1980; Kwong and Lawrence, 1994), pyrite, and sphalerite (Kwong and Lawrence, 1994). Scanning electron microscope (SEM) pictures in this study confirmed that tarnish is associated with corrosion, because more strongly coloured and etched sulphide grains had lower and more irregular topography, consistent with loss of material by oxidative dissolution.

#### Sample BH-20-I

Figure 4.2 shows monoclinic pyrrhotite (cream), pyrite (white), chalcopyrite (yellow) and sphalerite (grey) at 0, 2, and 42 days of oxidation. This sample was in the microbial treatment. It

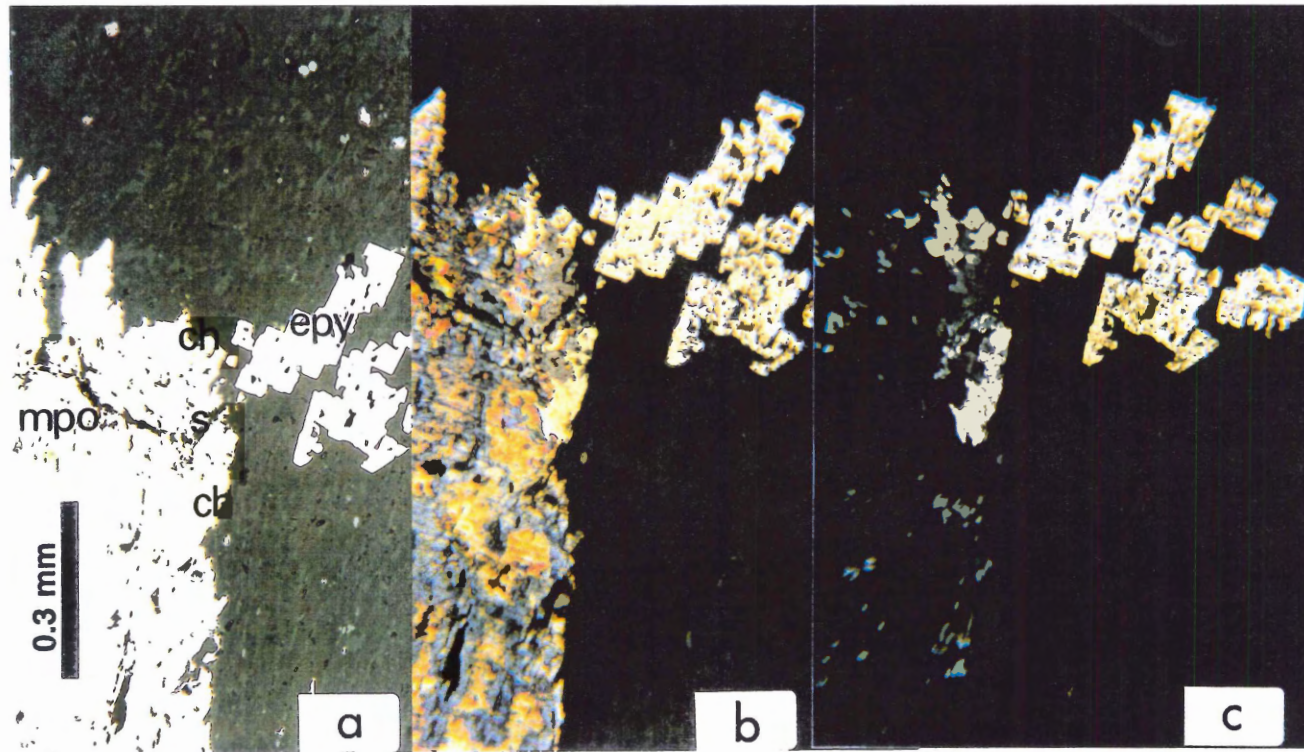


**Figure 4.2:** Photomicrographs of sample BH-20-I from the microbial treatment, taken in reflected, plane polarized light with a blue filter, showing surface characteristics at (a) 0 days (b) 2 days and (c) 42 days of oxidation. Monoclinic pyrrhotite (mpo), which developed etched polishing scratches and colour changes, clearly oxidized much more than euhedral pyrite (epy), sphalerite (s), or chalcopyrite (ch). Sphalerite and pyrite developed slight signs of oxidation (discolouration and scratches), but chalcopyrite remained unchanged. Also see Figure 4.3 and 4.4.

is clear by the colour changes (from cream to multicolours to black) and appearance of etched polishing scratches that monoclinic pyrrhotite has changed much more than pyrite, chalcopyrite or sphalerite. Sphalerite has a little discolouration, pyrite polishing scratches became visible after 42 days, but is otherwise unchanged and chalcopyrite is still perfectly clean. SEM images of this area (Figs. 4.3 and 4.4) clearly illustrate the topographical differences among monoclinic pyrrhotite, chalcopyrite and sphalerite, and the polishing scratches on pyrite.

In the sterile treatment, again monoclinic pyrrhotite is the most darkly coloured in comparison to chalcopyrite, sphalerite and pyrite, but it is not as strongly oxidized as the monoclinic pyrrhotite in the microbial treatment. Compare Figure 4.5, the sterile treatment, to 4.2, the microbial treatment. Pyrite and sphalerite also have less visible effects of oxidation in the sterile treatment. Chalcopyrite looks very similar in the two treatments, however, in the sterile treatment it appears to have a very small amount of tarnish. This chalcopyrite is unique, all other samples of chalcopyrite have not changed detectably. Figure 4.6 shows chalcopyrite and monoclinic pyrrhotite from the sterile treatment in the SEM. Pyrrhotite has only a slightly rougher surface, as opposed to the obvious difference in Figure 4.3. Also, sterile pyrite (Fig. 4.7) is smooth compared to the etched scratches in the microbial treatment (Fig. 4.4).

#### Sample RJ-96-003

Figure 4.8 shows hexagonal pyrrhotite (cream), chalcopyrite (yellow), and galena (light grey) in crossed polars (to show subgrains), plain polarized light (to show initial colours), at two days of oxidation in the microbial treatment, and at six weeks. The hexagonal pyrrhotite turned dark brown, and then almost black indicating very strong oxidation. The chalcopyrite remained

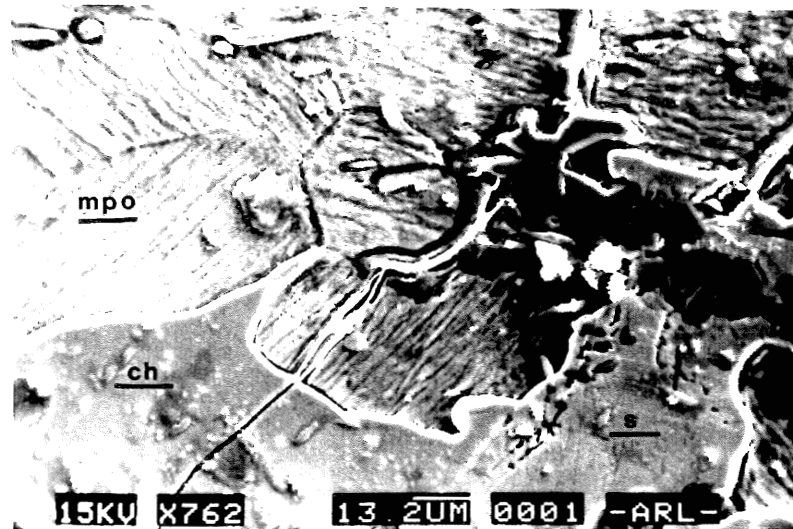


**Figure 4.3:** SEM image of sample BH-20-I from the microbial treatment showing surface features after 42 days of oxidation. Monoclinic pyrrhotite (mpo) has a much lower topography than that of chalcopyrite (ch) or sphalerite (s), indicating greater loss of material by oxidative dissolution. Subgrains of mpo are also visible.

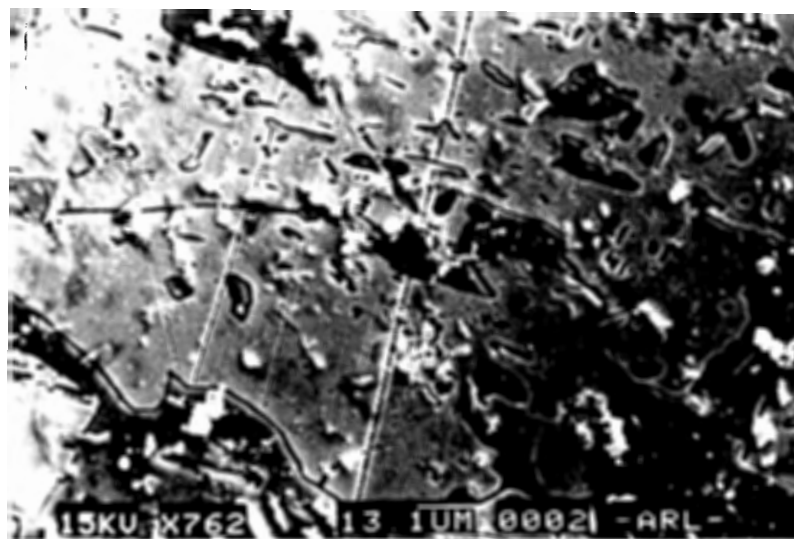


**Figure 4.4:** SEM image of sample BH-20-I from the microbial treatment showing polishing scratches on euhedral pyrite after 42 days of oxidation.

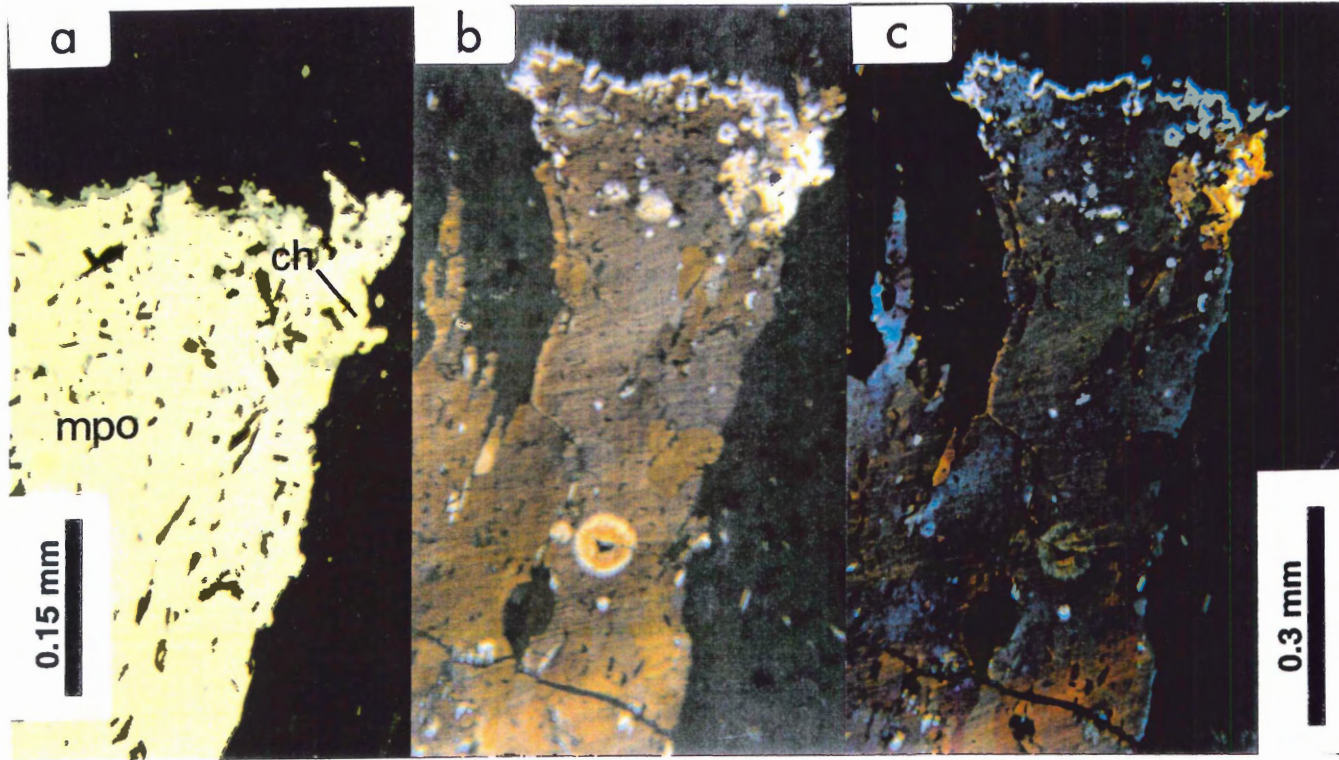


**Figure 4.5:** Photomicrographs of sample BH-20-I from the sterile treatment, taken in reflected, plane polarized light with a blue filter, showing surface characteristics at (a) 0 days (b) 2 days and (c) 42 days of oxidation. Monoclinic pyrrhotite (mpo) developed colour changes and etched polishing scratches, clearly oxidizing more than the chalcopyrite (ch), which shows only slight tarnish. Mpo oxidized less than in Figure 4.2. Also see Figures 4.6 and 4.7.

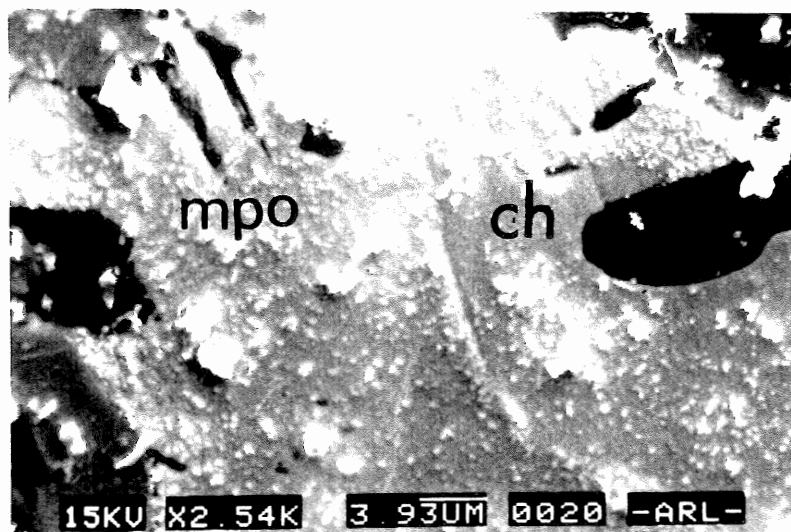


**Figure 4.6:** SEM image of sample BH-20-I from the sterile treatment showing only a slight difference in topography between monoclinic pyrrhotite (mpo) and chalcopyrite (ch). This indicates that mpo oxidized much less than in the microbial treatment (Fig. 4.3).

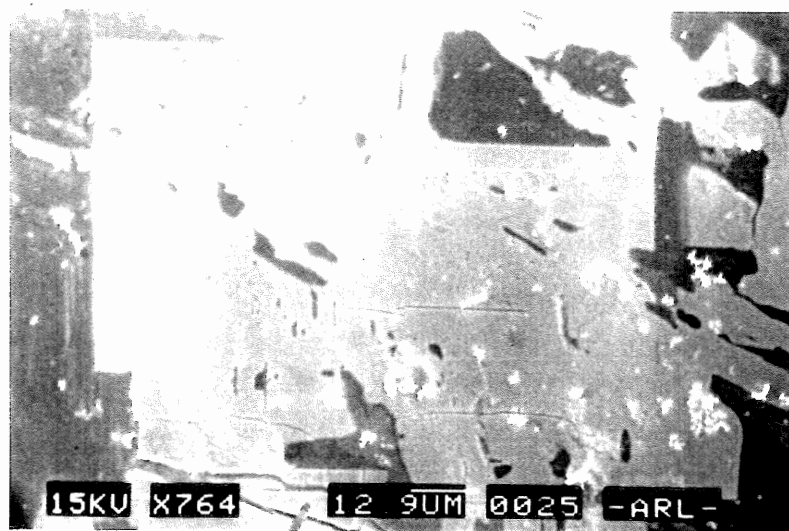


**Figure 4.7:** SEM image of sample BH-20-I from the sterile treatment showing no polishing scratches on euheedral pyrite after 42 days of oxidation.

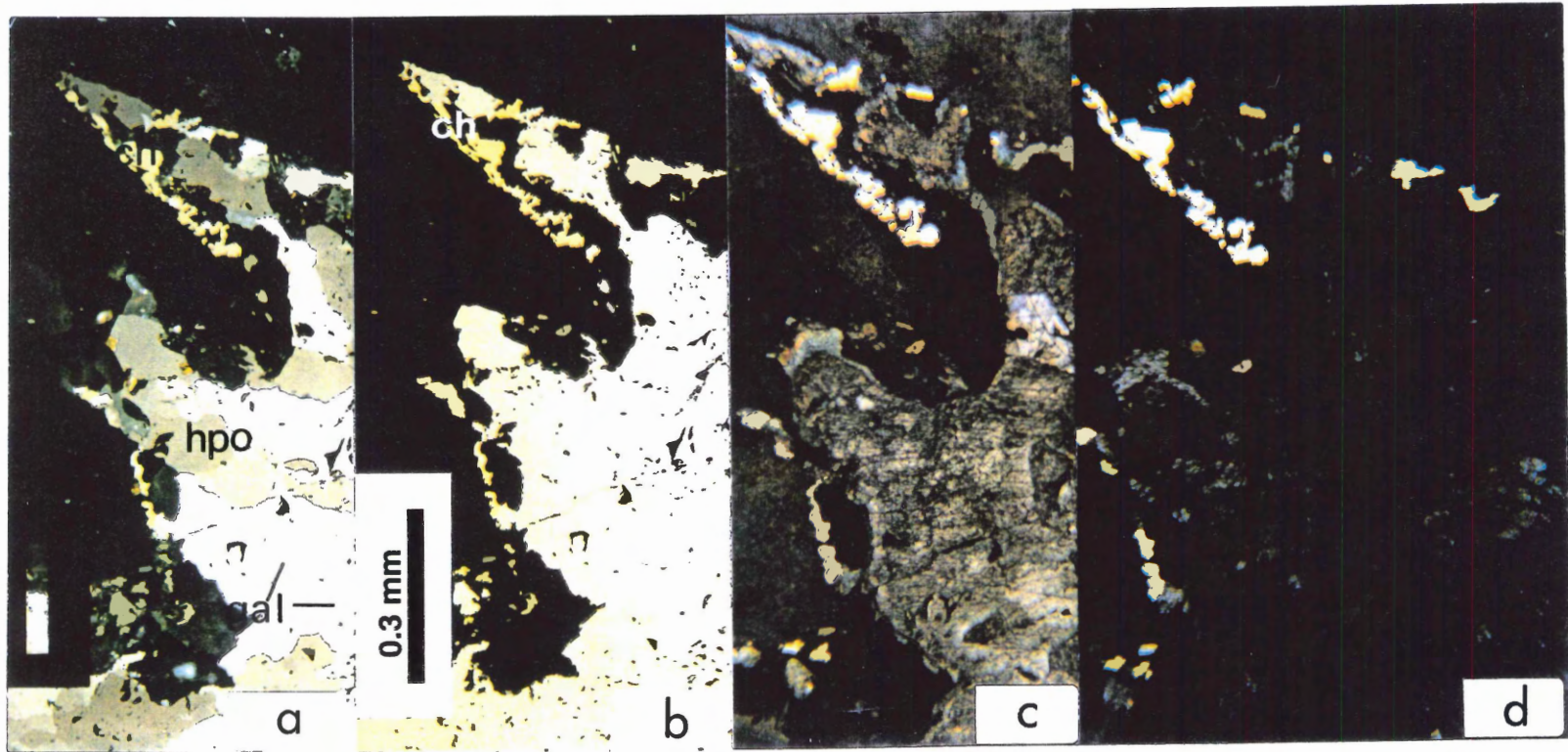


**Figure 4.8:** Photomicrographs of sample RJ-96-003 from the microbial treatment, taken in reflected light with a blue filter, showing surface characteristics at (a) 0 days (under crossed polars) (b) 0 days (under ppl) (c) 2 days (under ppl) and (d) 42 days (under ppl) of oxidation. Chalcopyrite (ch) remained unaltered, hexagonal pyrrhotite (hpo) corroded strongly (dark, with scratches), and galena (gal) corroded the most. Also see Figures 4.9 and 4.10.



clean bright yellow. Galena oxidized even faster than the hexagonal pyrrhotite. At only two days, it is recognizable only by its dark outline within the hexagonal pyrrhotite. SEM images shown in Figures 4.9 and 4.10 show the differences in surface texture among chalcopyrite, hexagonal pyrrhotite and galena. Chalcopyrite is as smooth as the matrix, and the other two are covered with tiny crystals of possible secondary minerals. Galena has a lower topography than pyrrhotite. This sample also contains a small amount of arsenopyrite that did not alter at all, even after six weeks (see Section 4.2 for a possible explanation).

In the sterile treatment, the relative order of oxidation among the minerals is the same, but hexagonal pyrrhotite has oxidized much less than in the microbial treatment. Figure 4.11 shows hexagonal pyrrhotite and galena before, during and after oxidation. At two days, the galena has turned black, but the hexagonal pyrrhotite is only slightly discoloured in patches. At six weeks, a secondary mineral coating covered the hexagonal pyrrhotite, but not the galena, and clean unoxidized hexagonal pyrrhotite can be seen surrounding the galena where the coating was thin. The SEM (Fig. 4.12) shows that the coating is confined to the surface, and the hexagonal pyrrhotite has not been corroded beneath it. It is also very clear in Figure 4.13 that galena has been substantially more corroded than pyrrhotite, and both have different surface textures than in the microbial treatment (Fig. 4.10).

#### Sample RJ-96-001

This sample contains two different textures of pyrite. The euhedral pyrite changed very little over six weeks. In the microbial treatment some polishing scratches became visible (Fig. 4.14), but not in the sterile treatment (Fig. 4.15). Figure 4.16 illustrates a close SEM view of the

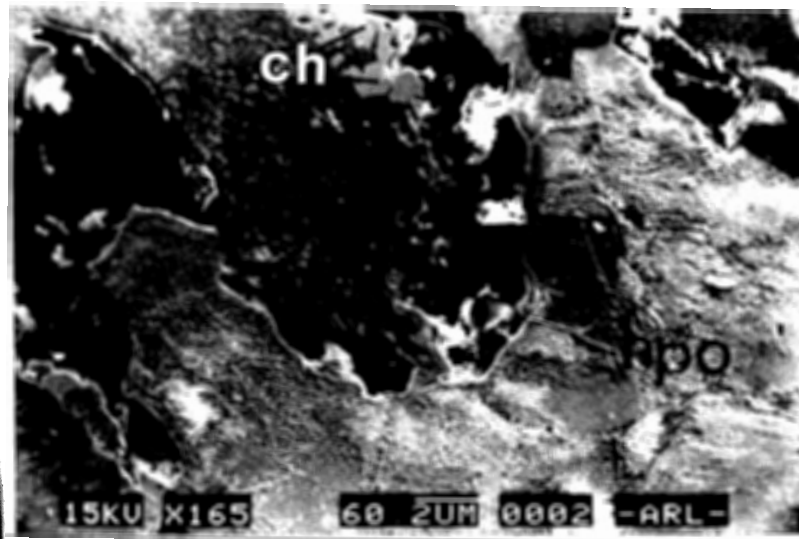


**Figure 4.9:** SEM image of sample RJ-96-003 from the microbial treatment showing surface features after 42 days of oxidation. Hexagonal pyrrhotite (hpo) is much rougher and appears more corroded than chalcopyrite (ch).

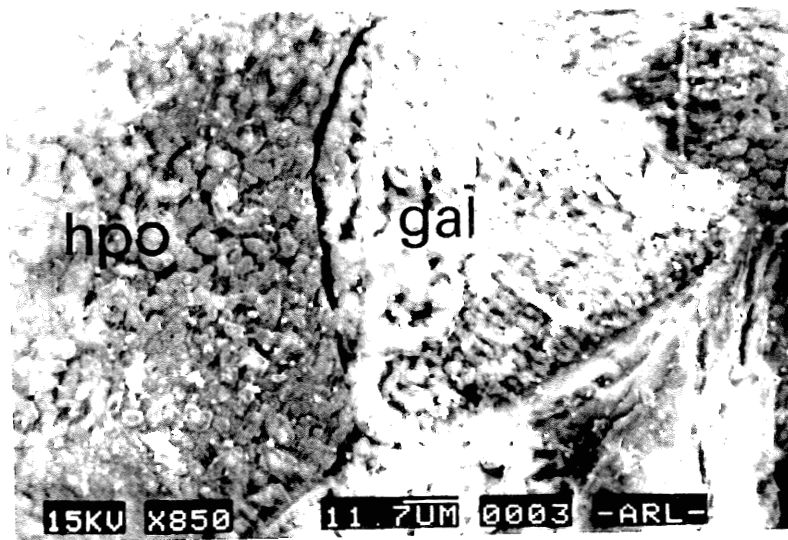


**Figure 4.10:** SEM image of sample RJ-96-003 from the microbial treatment showing surface features after 42 days of oxidation. Galena (gal) has a lower topography than that of hexagonal pyrrhotite (hpo), indicating greater loss of material by oxidative dissolution.

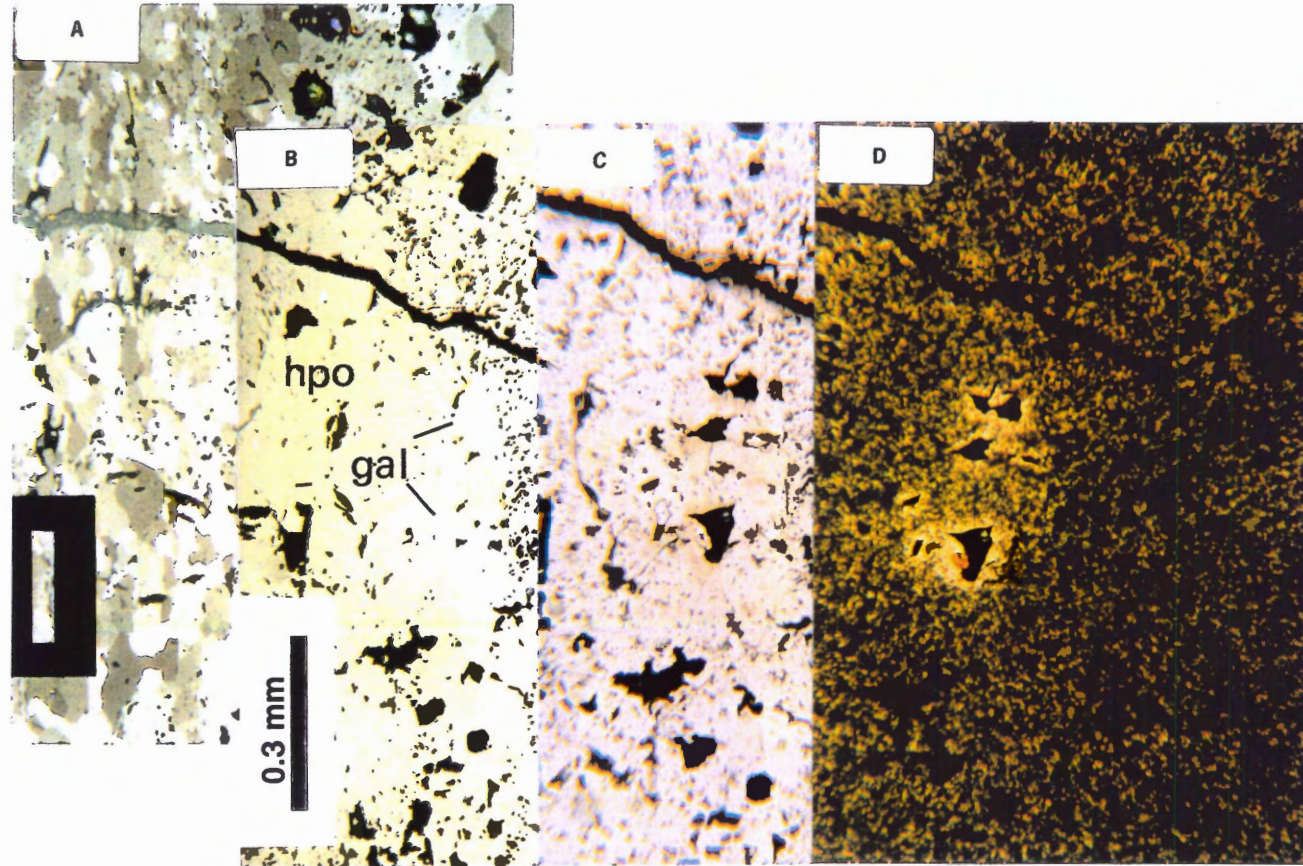


**Figure 4.11:** Photomicrographs of sample RJ-96-003 from the sterile treatment, taken in reflected light with a blue filter, showing surface characteristics at (a) 0 days (under crossed polars) (b) 0 days (under ppl) (c) 2 days (under ppl) and (d) 42 days (under ppl) of oxidation. Galena (gal) turned black indicating strong corrosion, and hexagonal pyrrhotite (hpo) remained cream coloured, although a coating had developed by 42 days, obscuring the smooth surface of hpo except near the galena (Fig. 4.12).

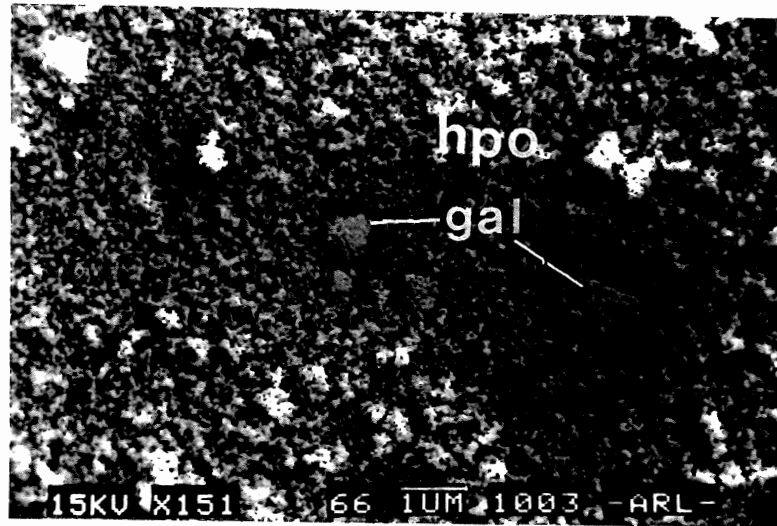


**Figure 4.12:** SEM image of sample RJ-96-003 from the sterile treatment showing surface features after 42 days of oxidation. Galena (gal) appears rougher than the hexagonal pyrrhotite (hpo) visible through the thinner areas of the coating.

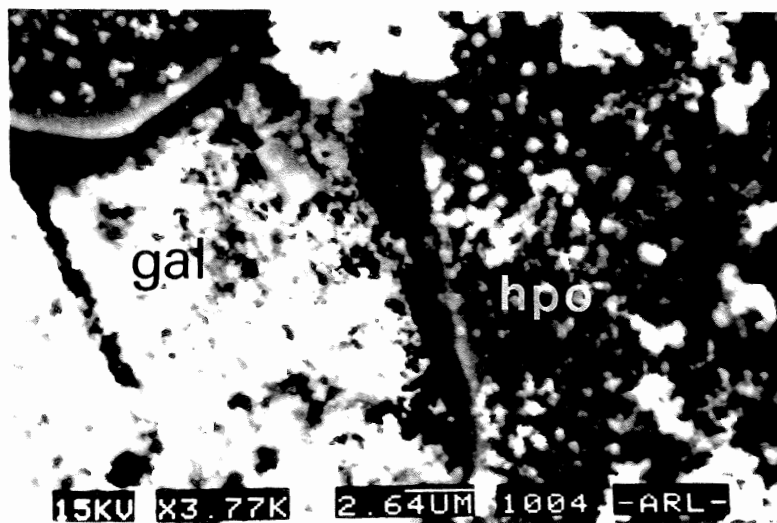


**Figure 4.13:** SEM image of sample RJ-96-003 from the sterile treatment showing surface features after 42 days of oxidation. Galena (gal) has a lower topography than that of hexagonal pyrrhotite (hpo), indicating greater loss of material by oxidative dissolution. The surface textures of both minerals are very different from the microbial treatment (Fig. 4.10).

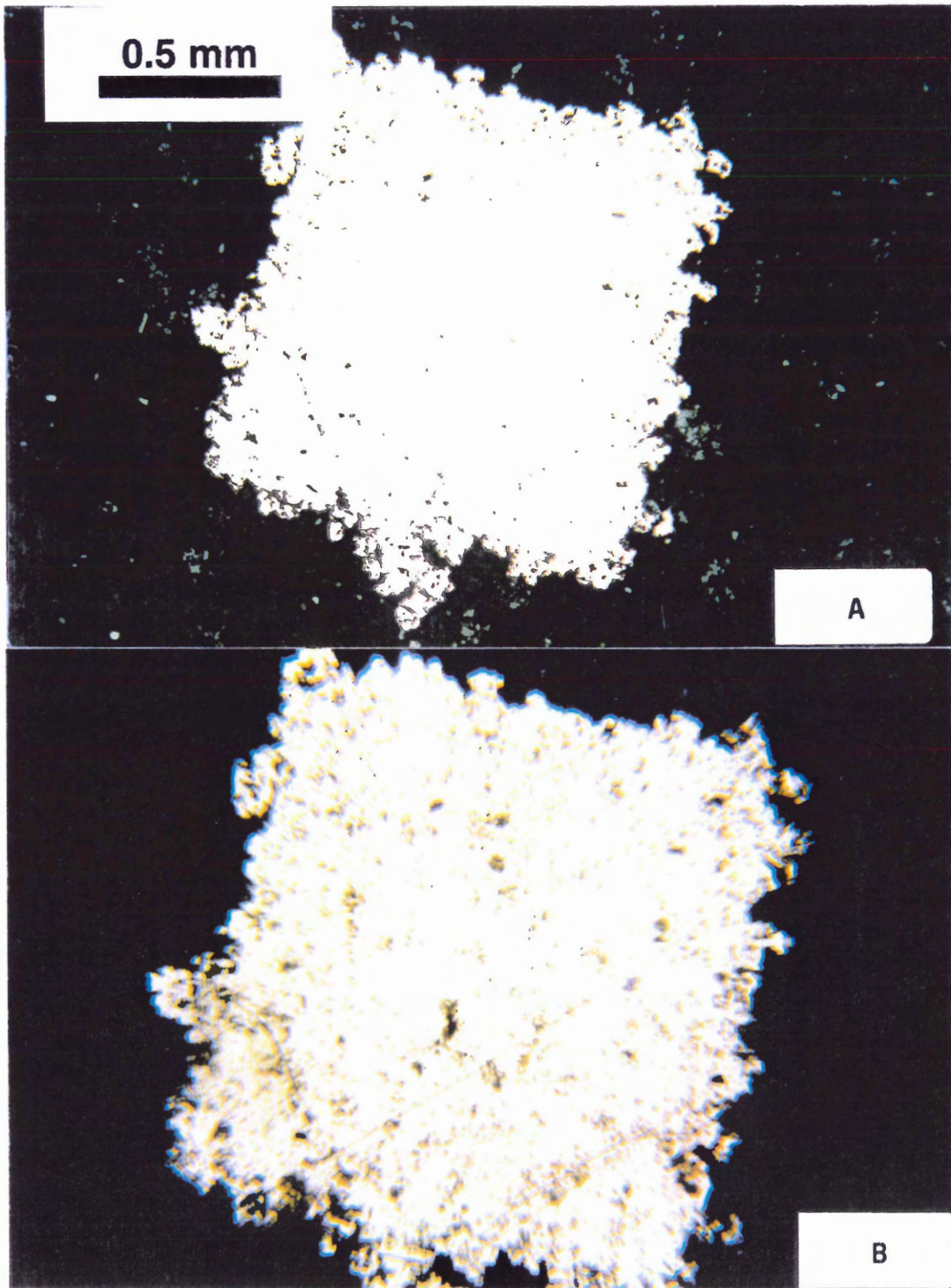


**Figure 4.14:** Photomicrographs of euhedral pyrite in sample RJ-96-001 from the microbial treatment, taken in reflected, plane polarized light with a blue filter, showing surface characteristics at (a) 0 days and (b) 42 days of oxidation. Note the appearance of polishing scratches in contrast to the sterile treatment (Fig. 4.15).

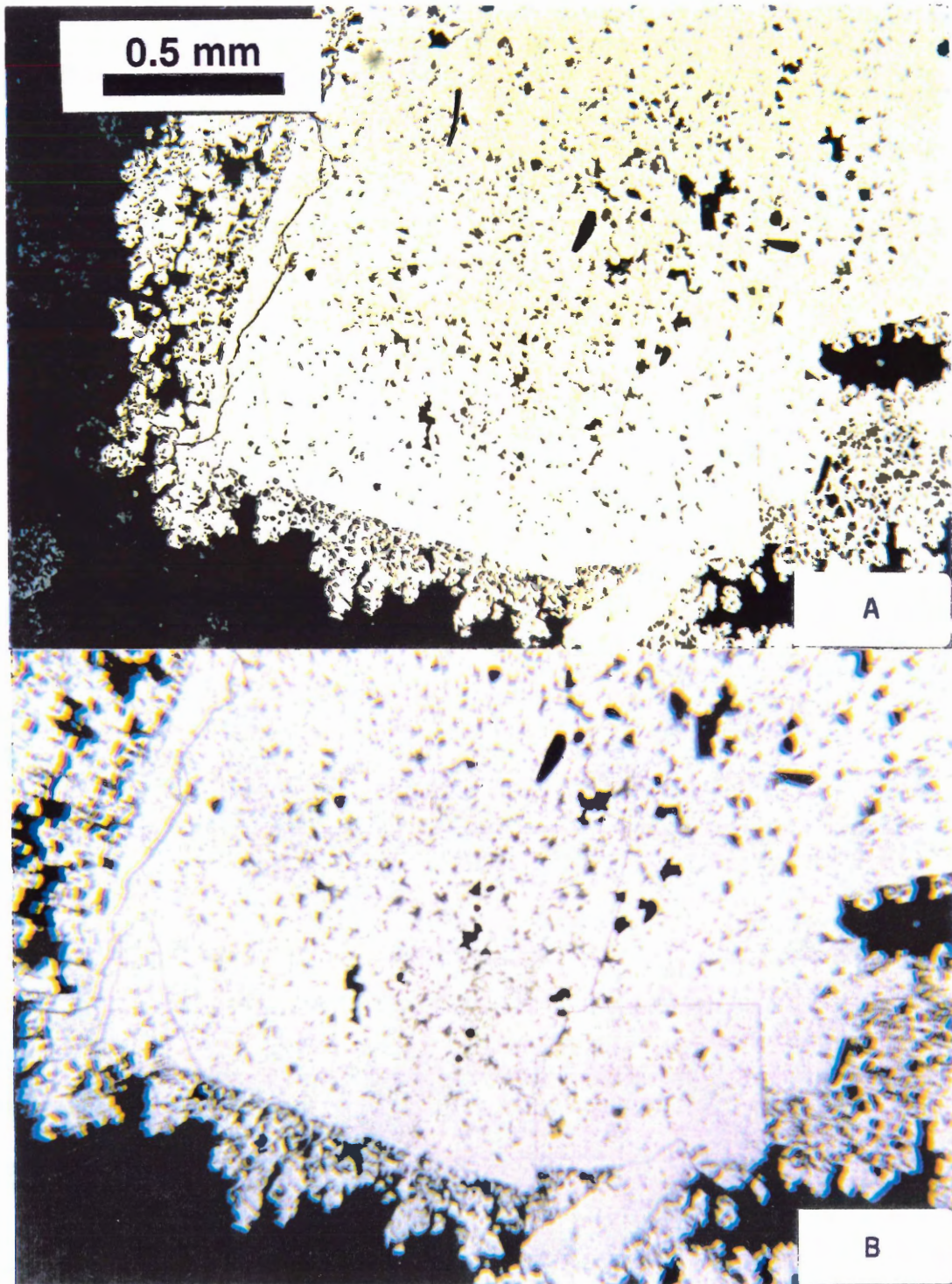


**Figure 4.15:** Photomicrographs of euhedral pyrite in sample RJ-96-001 from the sterile treatment, taken in reflected, plane polarized light with a blue filter, showing surface characteristics at (a) 0 days and (b) 42 days of oxidation. Note the lack of polishing scratches in contrast to the microbial treatment (Fig. 4.14).



**Figure 4.16:** SEM image of sample RJ-96-001 from the microbial treatment showing etched polishing scratches in euhedral pyrite after 42 days of oxidation.

polishing scratches in the microbial treatment. The other form of pyrite, anhedral with fine grey lamellae that were too fine to be analysed with the microprobe, produced extremely different results. At two days there was little change, but by six weeks the pyrite had turned black (Fig. 4.17), and its location was visible only by contrast with the adjacent unchanged chalcopyrite. This texture looked indistinguishable between the treatments in reflected light, both were black, but SEM images suggest that the microbial treatment sample has been corroded a little more than the sterile treatment. The surfaces are both very irregular. Figures 4.18 and 4.19 show the highly ridged surfaces of the anhedral pyrites in each treatment. The pyrite topography is lower than that of the matrix or inclusions. In the microbial treatment, secondary minerals have developed on the centre of the grain (Fig. 4.20). The radial or "spiny ball" texture is typical of the secondary mineral schwertmannite [ $\text{Fe}_8\text{O}_8(\text{OH})_6\text{SO}_4$ ] (Bigham, 1994). This mineral has also been noted to result from microbial pyrrhotite oxidation (Bigham, 1994).

#### Sample RJ-96-002

Arsenopyrite (Fig. 4.21) was oxidized visibly, but not as much as the pyrrhotites in samples BH-20-I or RJ-96-003. Brown discolouration and corrosion occurred to a greater degree in the microbial treatment than in the sterile treatment. In the microbial treatment, there seemed to be differential corrosion across a boundary within the grain. This indicates that subgrains of different orientation may oxidize at different rates, or that the visibility of the oxidation may be related to crystallographic orientation within the plane of the thin section (see Section 4.2).



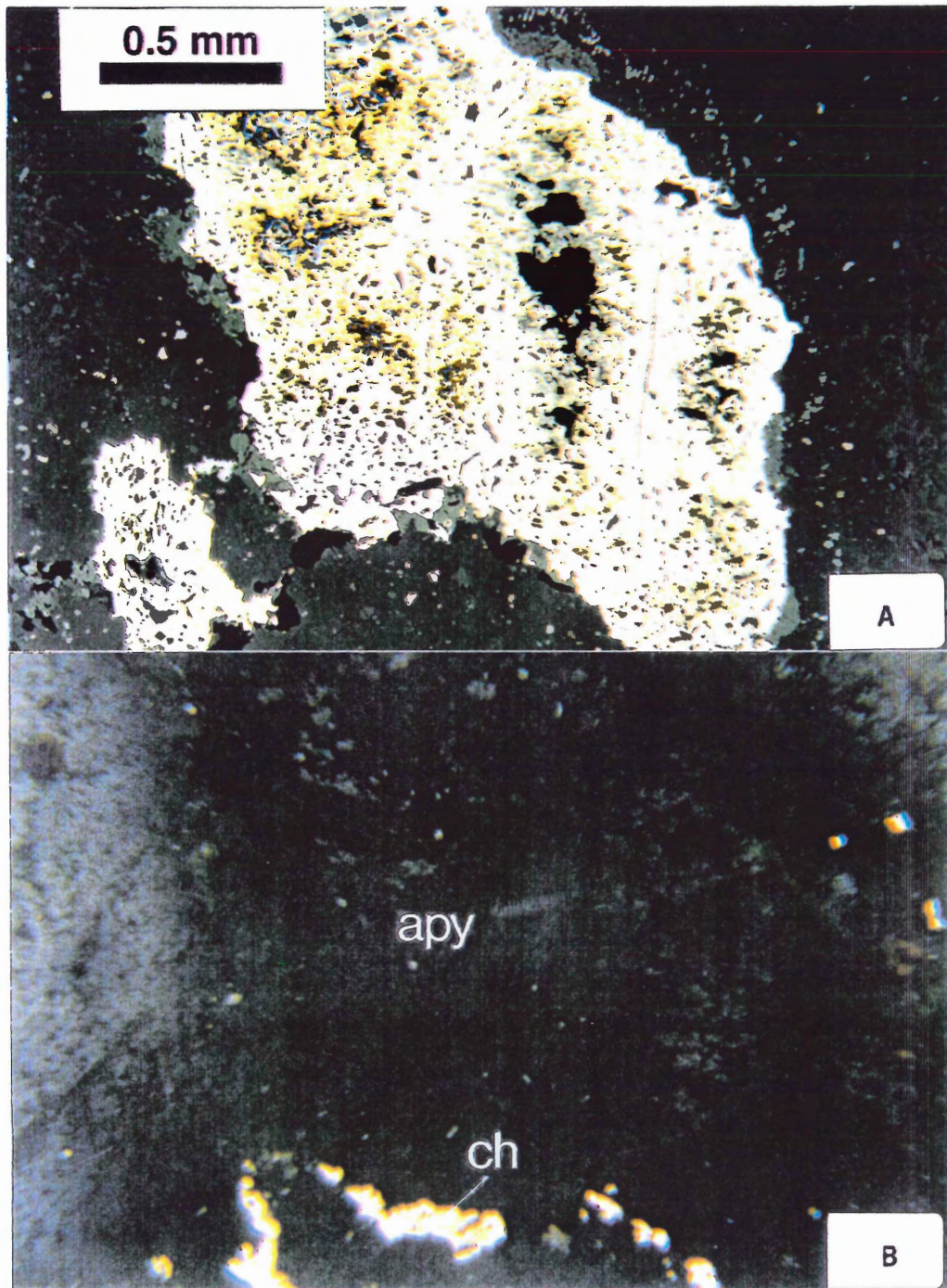


**Figure 4.17:** Photomicrographs of anhedral pyrite (apy) and chalcopyrite (ch) in sample RJ-96-001 from the sterile treatment, taken in reflected, plane polarized light with a blue filter, showing surface characteristics at (a) 0 days and (b) 42 days of oxidation. The anhedral pyrite turned black, indicating very strong corrosion, in sharp contrast to chalcopyrite which remained unchanged. See also Figures 4.18 and 4.19.



**Figure 4.18:** SEM images of anhedral pyrite in sample RJ-96-001 from the microbial treatment showing the surface after 42 days of oxidation. (a) An overview of the ridged anhedral pyrite grain surrounded by dark smooth matrix and with possible secondary minerals in the center (Fig. 4.20). (b) Deepest pit in the grain indicating very strong corrosion. Rounded oxide inclusions (ox) provide a baseline for topographic comparison, assuming the oxides have not changed and represent the level of the original polished surface. Ridges may be fine grey lamellae of the type seen in Figure 4.17.

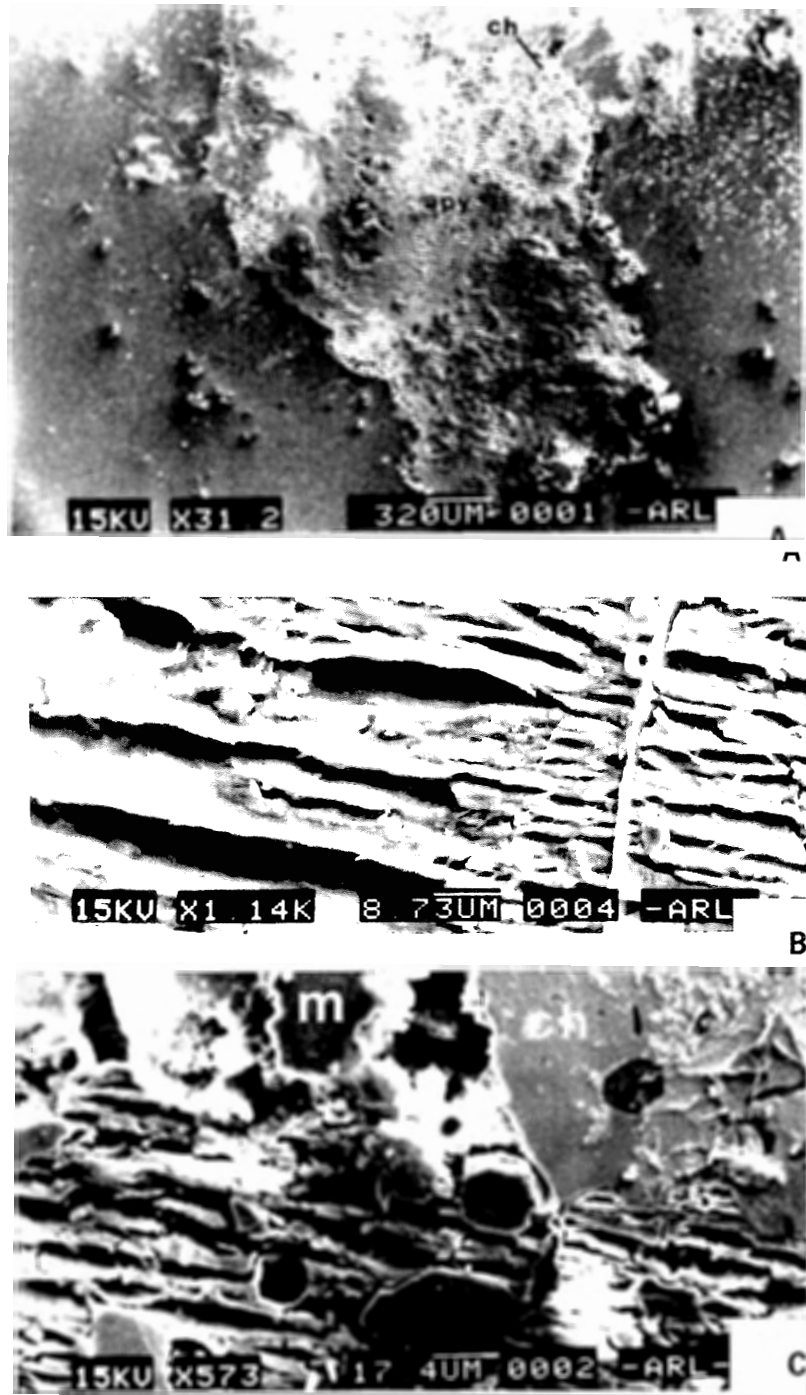


**Figure 4.19:** SEM images of anhedral pyrite (apy) in sample RJ-96-001 from the sterile treatment showing the surface after 42 days of oxidation. (a) An overview of the ridged anhedral pyrite grain surrounded by dark smooth matrix, with smooth chalcopyrite (ch) at the top. (b) Ridge size changes close to a crack. (c) Anhedral pyrite has a lower, much rougher topography than the matrix (m) and chalcopyrite (ch), indicating loss of material by oxidative dissolution.

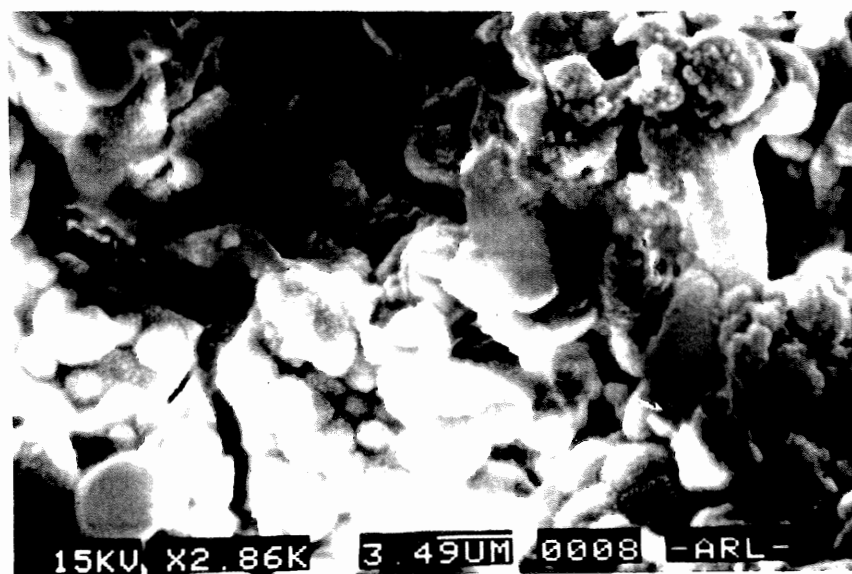


**Figure 4.20:** SEM image of a globular, slightly spiny secondary precipitate on anhedral pyrite in sample RJ-96-001 from the microbial treatment showing the surface after 42 days of oxidation. The texture suggests that it is schwertmannite (Bigham, 1994).

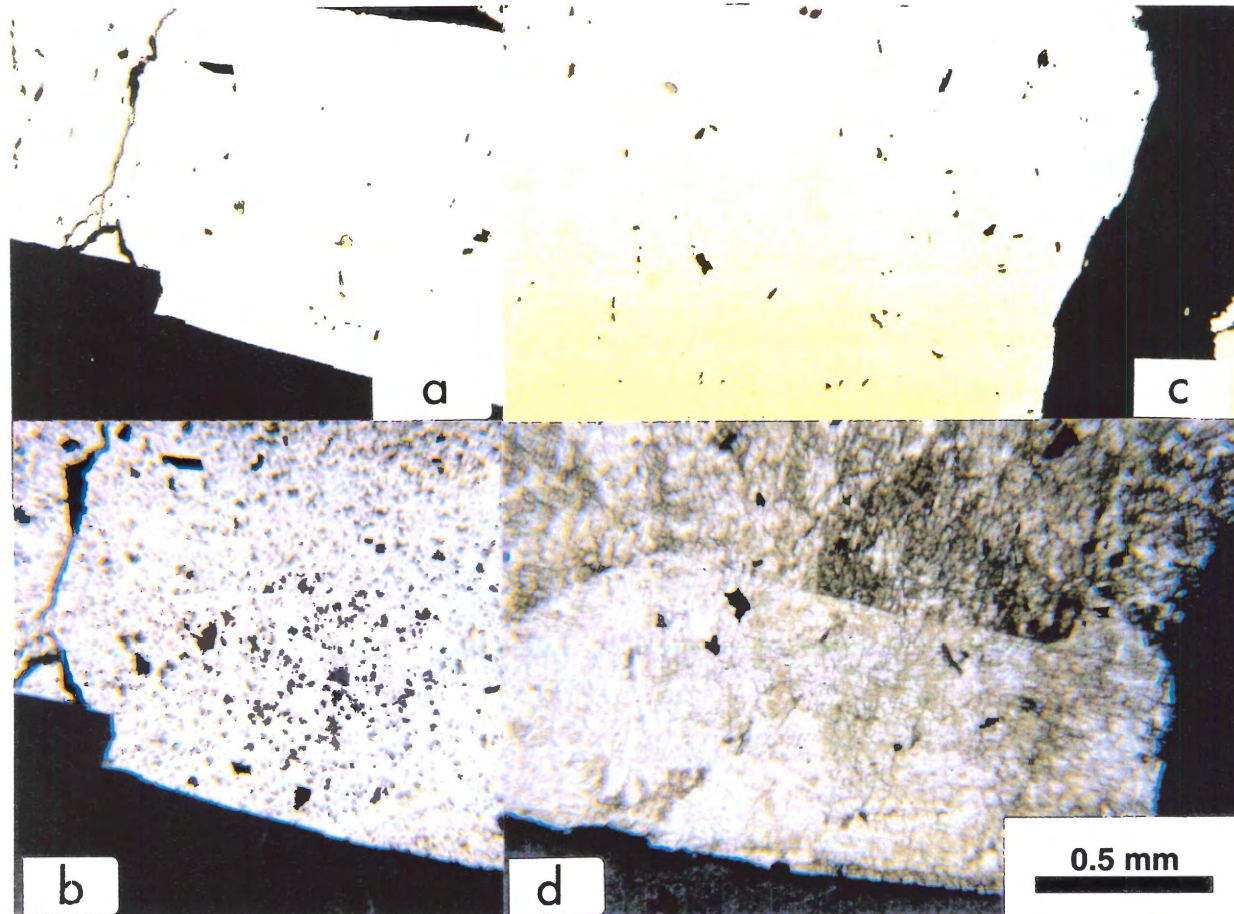


**Figure 4.21:** Photomicrographs of arsenopyrite in sample RJ-96-002 taken in reflected, plane polarized light with a blue filter, showing surface characteristics at (a) 0 days oxidation, sterile treatment (b) 42 days, sterile treatment, (c) 0 days, microbial treatment, and (d) 42 days of oxidation, microbial treatment. It is clear by the discolouration that arsenopyrite in the microbial treatment oxidized faster than in the sterile treatment. Speckles on the sterile treatment may be precipitates from the water. The discolouration is certainly visible, but not nearly as severe as on the pyrrhotites, galena, or anhedral pyrite in the other samples.

### Sample CR-95-016

Sulphides in this sample were pyrite, monoclinic pyrrhotite, and chalcopyrite.

Chalcopyrite did not oxidize in either treatment, as in the other samples. Pyrite remained fairly white at two days, although some grains developed a secondary mineral coating after six weeks. Monoclinic pyrrhotite turned a uniform light brown in many areas, but when it occurred in a cotecule texture it was far from uniform. Here, subgrains within a pyrrhotite grain from the microbial treatment turned very different colours, ranging from cream to dark purple or blue (Fig 4.22). One explanation is that crystal lattice orientation is important in determining the rate of oxidation (see Section 4.2). Another possible explanation is that trace elements affect the oxidation rate. Microprobe data (Appendix A) suggest that a higher concentration of Cu in the pyrrhotite (2.4% instead of 1.3%) increases the oxidation rate, however, the probe point sample size was small.

Separate pyrrhotite grains also oxidized at very different rates, again with a range of colour from deep blue-purple to light orange (Fig. 4.23). Polishing scratches were more visible on the deep blue grains indicating stronger oxidation. Subsequent microprobe analysis (Appendix A) suggests that grains relatively depleted in Fe oxidized faster, but this may also be partly due to differing tarnish compositions.

### Sample CR-95-002

The sulphides in this sample were pyrrhotite with rare tiny inclusions of a sulphide compositionally intermediate between cobaltite and gersdorffite. Both treatments of this sample behaved similarly, with slightly stronger oxidation in the microbial treatment. The tiny inclusions

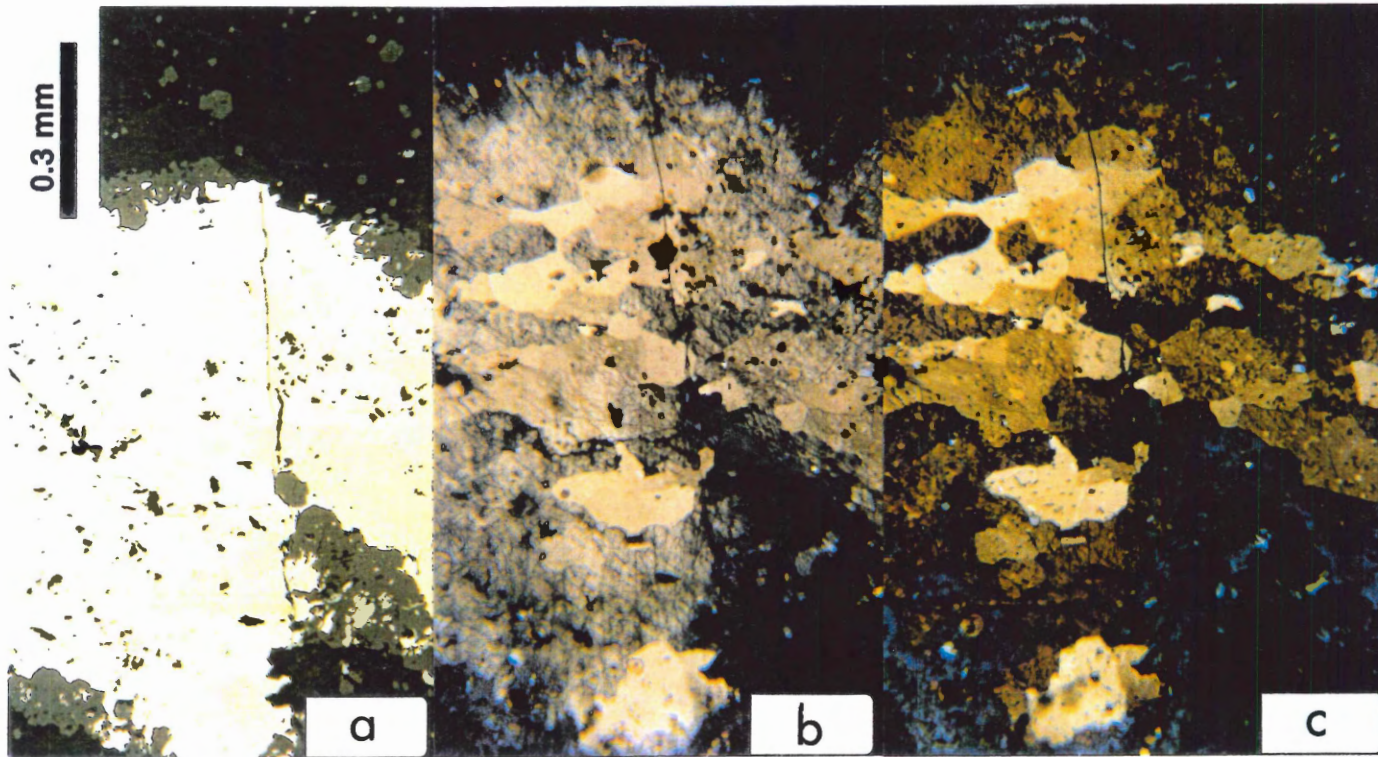


**Figure 4.22:** Photomicrographs of a pyrrhotite grain in sample CR-95-016 taken in reflected, plane polarized light with a blue filter, showing surface characteristics at (a) 0 days (b) 2 days and (c) 42 days of oxidation. Subgrains have oxidized at very different rates. Some subgrains are still cream coloured (unaltered), and some are deep blue-purple (oxidized). Preliminary microprobe analysis (Appendix A) indicates a possible Cu variation that may have caused the differential oxidation rates.

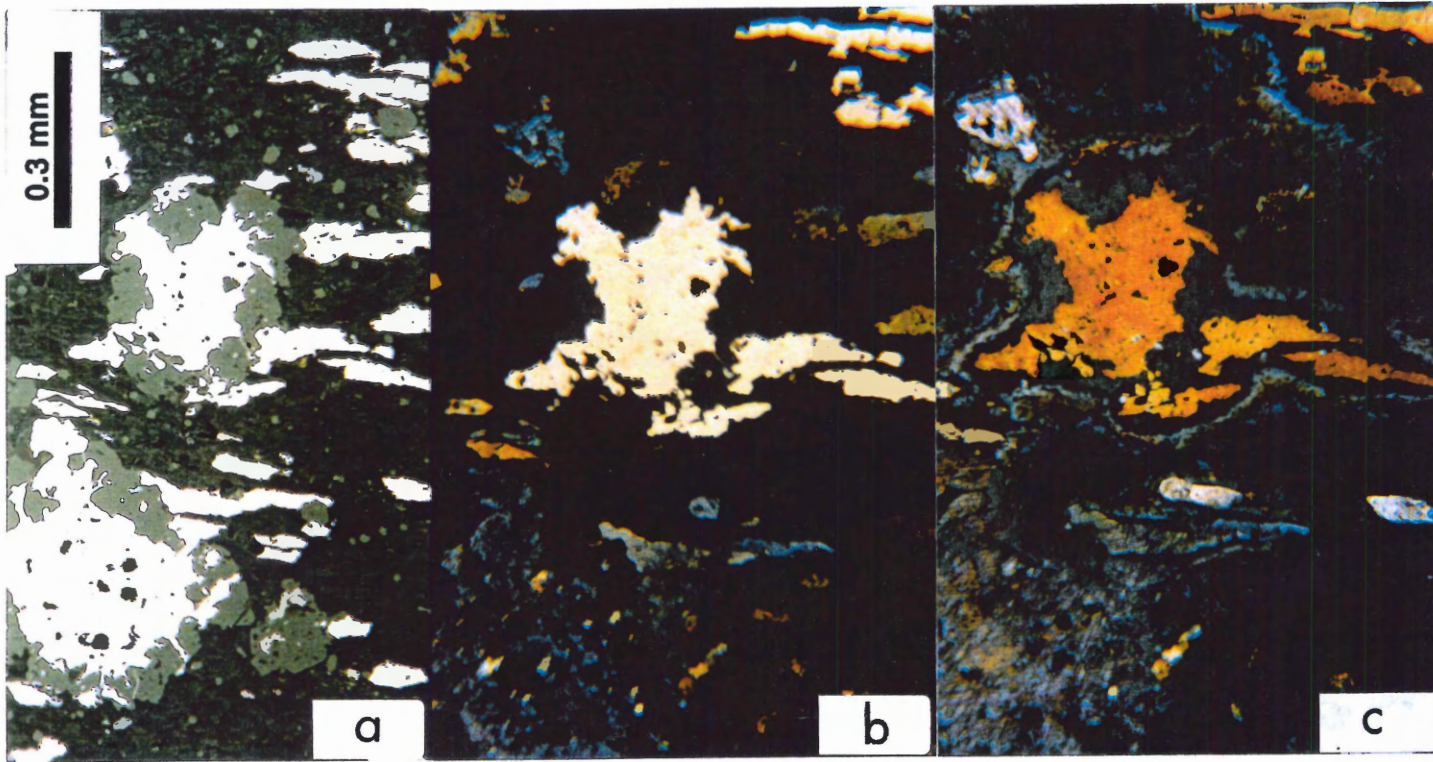


**Figure 4.23:** Photomicrographs of two pyrrhotite grains in sample CR-95-016 taken in reflected, plane polarized light with a blue filter, showing surface characteristics at (a) 0 days (b) 2 days and (c) 42 days of oxidation. These two grains and their smaller neighbours have oxidized at very different rates (cream or light orange versus dark blue-purple). Preliminary microprobe analysis indicates a possible difference in the proportion of iron to sulphur between the two grains that may explain the different oxidation rates.



remained white and unoxidized; however, the pyrrhotite did oxidize, and at two days fine parallel lamellae within the pyrrhotite became visible by their different colour (Fig. 4.24). It is interesting that the lamellae had been undetectable to begin with, and only oxidation revealed their presence. At six weeks, these lamellae had turned black, while the surrounding material was still brown. SEM pictures of this area (Fig. 4.25) give further evidence that this colour difference was due to differential oxidation rates, because the lamellae surfaces are significantly lower than their host. The darker subgrains of the host have lower topography as well. Microprobe analysis after oxidation indicates no significant difference between the host and lamellae (Appendix A). Perhaps the lamellae have a different crystal structure (i.e. polymorph) that corroded preferentially. "Anomalous" pyrrhotite has the same chemical formula as monoclinic pyrrhotite ( $\text{Fe}_7\text{S}_8$ ), is anti-ferrimagnetic like hexagonal pyrrhotite, and has an unknown stability field (Craig and Scott, 1974). This form of pyrrhotite is a good candidate for the lamellae if a different structure is the cause of differential oxidation, because it has the same composition as the surrounding monoclinic pyrrhotite, and it could be stable at different conditions. XRD analysis may provide an identification, although the lamellae are a small percentage of the pyrrhotite present, so the peaks would require interpretation. Trace element concentration may also be the reason for differential lamellar oxidation.

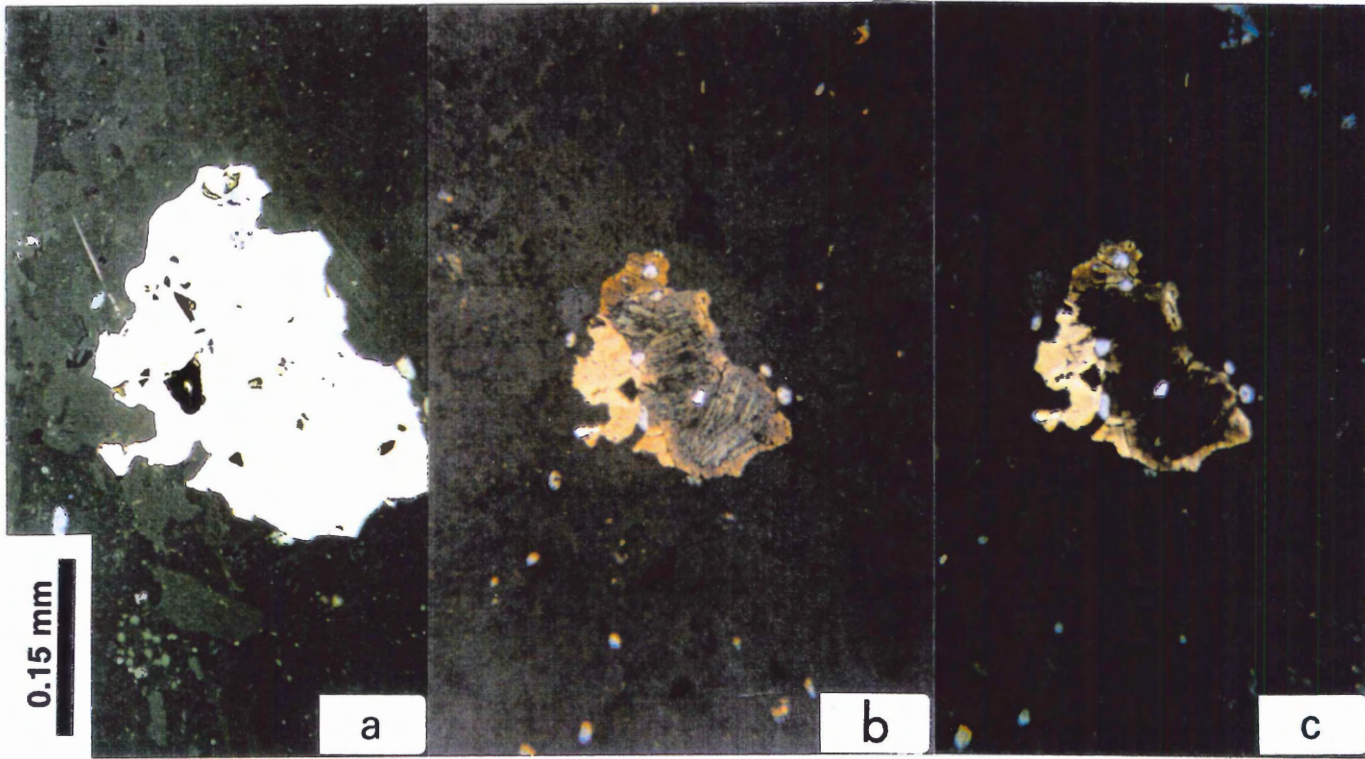


**Figure 4.24:** Photomicrographs of pyrrhotite in sample CR-95-002 taken in reflected, plane polarized light with a blue filter, showing surface characteristics at (a) 0 days (b) 2 days and (c) 42 days of oxidation. This grain contains lamellae that oxidized at different rates (black at 42 days). See also Figure 4.25.

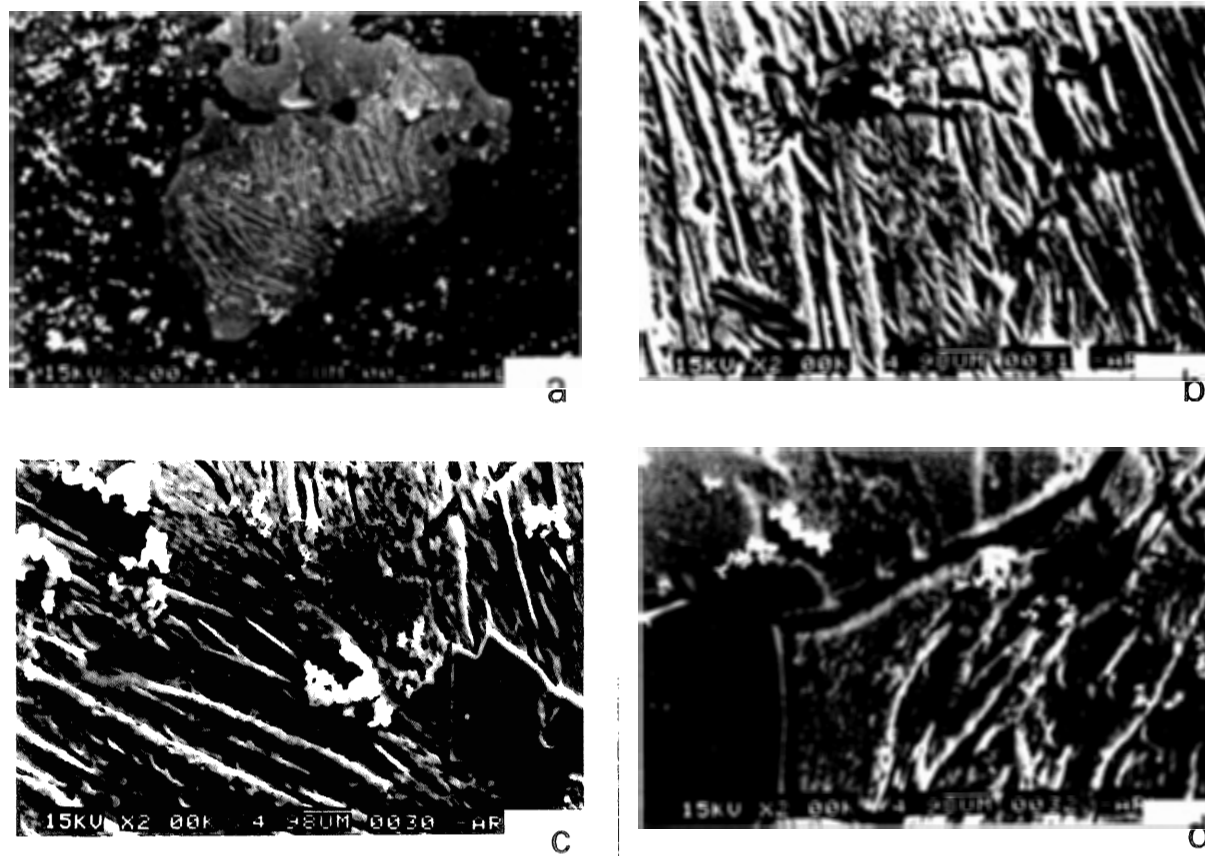


**Figure 4.25:** SEM images of pyrrhotite lamellae in sample CR-95-002 from the sterile treatment showing the surface after 42 days of oxidation. (a) Overview of the lamellar grain. (b) Lamellae appear to follow cleavage planes. (c) Lamellae end before subgrain boundary. (d) Subgrains of different colours have different depths of etching.

### Summary of Observations

Table 4.1 describes the relative order of oxidation among sulphide minerals in each sample. Overall, the relative order of oxidation of sulphide minerals in the microbial treatment was galena > hexagonal pyrrhotite > monoclinic pyrrhotite > anhedral pyrite >> arsenopyrite, sphalerite > euhedral pyrite > chalcopyrite. In the sterile treatment, the relative order was galena > anhedral pyrite > monoclinic pyrrhotite >> hexagonal pyrrhotite, sphalerite, arsenopyrite > euhedral pyrite > chalcopyrite. The pyrrhotites had a greater difference in oxidation rates between the treatments than the other sulphide minerals, causing the order of oxidation among minerals to change.

Most sulphides (monoclinic pyrrhotite, galena, sphalerite, arsenopyrite, and euhedral pyrite) oxidized significantly more in the microbial than in the sterile treatment. Exceptions were hexagonal pyrrhotite, which displayed an extreme difference, anhedral pyrite, which was very strongly oxidized in both treatments, and chalcopyrite, which was unoxidized throughout.

#### *4.1.3 Preliminary Analyses of Secondary Precipitates: XRD and SEM*

X-ray diffraction analysis (Fig. 4.26) of the rust-coloured precipitate in the microbial treatment (Fig. 4.27) gives strong evidence against any crystalline structure. Absolutely no reasonable peaks are present. Judging by the colour, this is an amorphous substance with  $\text{Fe}^{3+}$  comprising a major part of its constituents.

Fine crystals are visible in SEM images displayed in Figures 4.10 (RJ-96-003, microbial treatment) and 4.20 (RJ-96-001, microbial treatment). These could be secondary minerals that formed on the sulphide surfaces during oxidation. As described in Section 4.1.2, the texture of

**Table 4.1:** Order of Oxidation among Sulphide Minerals for Each Sample  
(when multiple sulphides per sample occur)

Sample	Treatment	Order of oxidation
BH-20-I	microbial	galena > monoclinic pyrrhotite >> sphalerite > euhedral pyrite > chalcopyrite
	sterile	monoclinic pyrrhotite >> euhedral pyrite, chalcopyrite
RJ-96-001	microbial	anhedral pyrite >> euhedral pyrite
	sterile	anhedral pyrite >> euhedral pyrite
RJ-96-002	microbial	arsenopyrite
	sterile	arsenopyrite
RJ-96-003	microbial	galena > hexagonal pyrrhotite >> arsenopyrite, chalcopyrite
	sterile	galena >> hexagonal pyrrhotite > arsenopyrite, chalcopyrite
CR-95-002	microbial	monoclinic pyrrhotite (lamellae > host)
	sterile	monoclinic pyrrhotite (lamellae > host)
CR-95-016	microbial	monoclinic pyrrhotite > pyrite > chalcopyrite
	sterile	monoclinic pyrrhotite > pyrite > chalcopyrite

Sample ident.: rachel02

7-Mar-1997 15:43

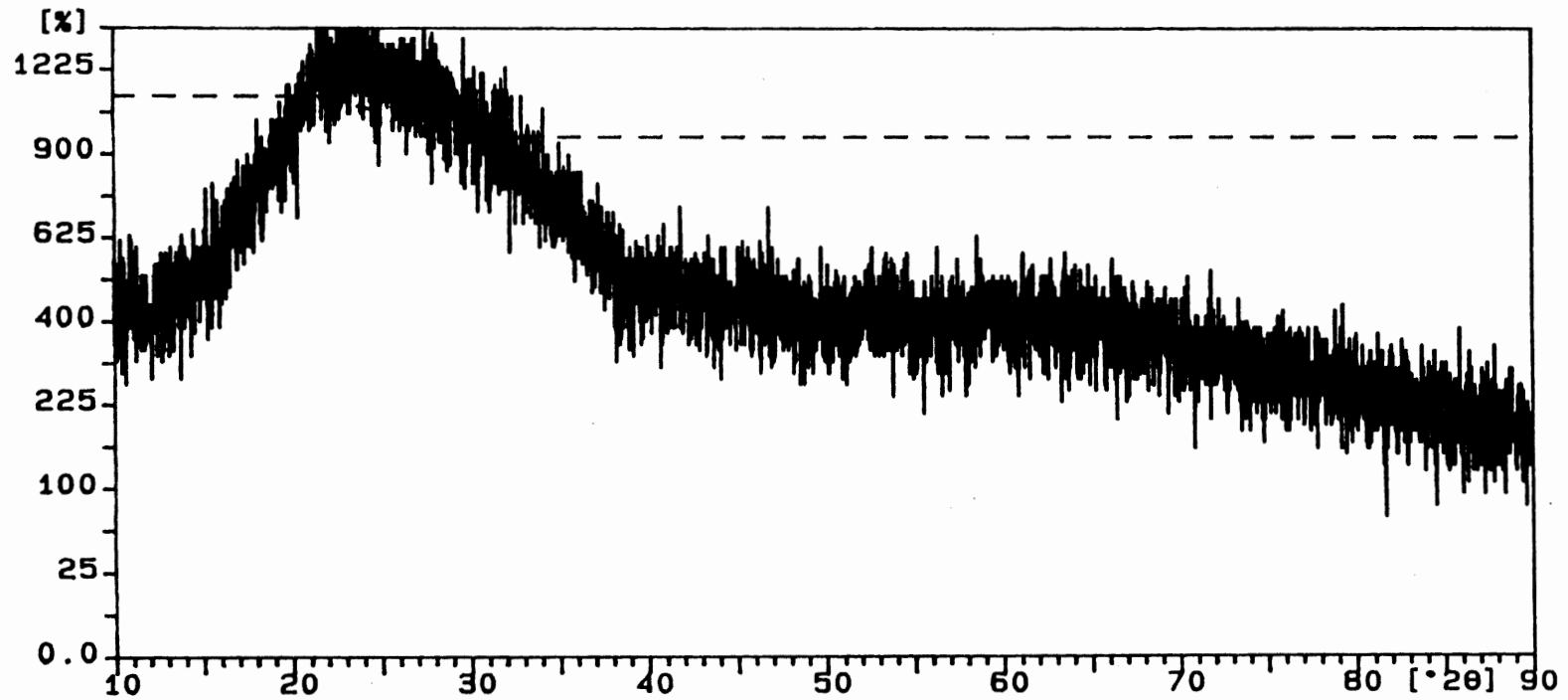


**Figure 4.26:** XRD analysis with no peaks at all, indicating the amorphous nature of the rust-coloured precipitate that formed in all samples of the microbial treatment.

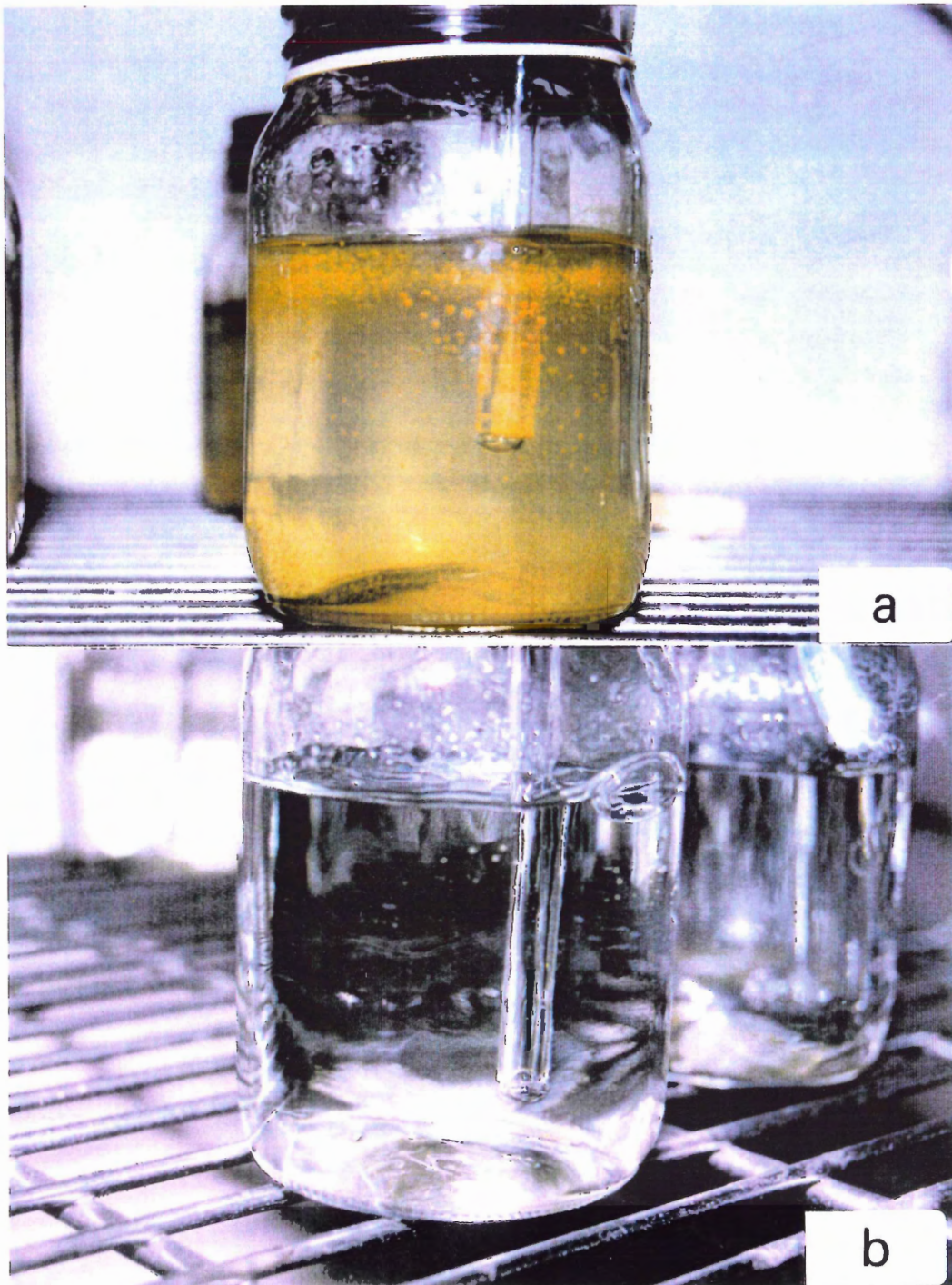


**Figure 4.27:** (a) Rust-coloured precipitate in the microbial treatment. (b) No precipitate in the sterile treatment.

material in Figure 4.20 suggests the mineral schwertmannite (Bigham, 1994).

#### 4.1.4 Evidence for Microbial Activity

As seen in Figure 4.27, a prolific amount of rust-coloured precipitate formed in the microbial treatment, contrasting strongly with the sterile treatment, which remained clear. If this precipitate contains  $\text{Fe}^{3+}$  as suggested in Section 4.1.3, then precipitation of  $\text{Fe}^{3+}$  by oxidation of  $\text{Fe}^{2+}$  may have occurred. This is supported by water chemistry data (Appendix B) which indicate a drop in the dissolved iron concentration in the microbial treatment in comparison to the initial concentration and that in the sterile treatment. As discussed in Section 2.2.1 and 2.4, at pH between 2 and 4.5 (experimental pH: 3.16 to 3.76) spontaneous iron oxidation is slow, but iron-oxidizing bacteria can catalyze  $\text{Fe}^{3+}$  production  $10^5$  to  $10^6$  times faster than abiotic rates (Keenan, 1969, Lacey and Lawson, 1970; cited in Ralph, 1979). Also, since large amounts of  $\text{Fe}^{2+}$  are necessary to fuel metabolism,  $\text{Fe}^{3+}$  precipitates far in excess of cell substance (Lundgren and Dean, 1979). These microbial characteristics explain perfectly the contrast of  $\text{Fe}^{3+}$  precipitate volume between the treatments. It is safe to conclude that iron-oxidizing bacteria were present and active in the microbial treatment, and not the sterile treatment.

Images from environmental scanning electron microscope (ESEM) and scanning electron microscope (SEM) reveal a variety of microstructures, some clearly bacteria, and some that may be caused by bacteria (Fig. 4.28). Due to time constraints, individual species of bacteria were not identified, but some images are consistent with the presence of a rod-shaped bacterium such as *Thiobacillus spp.*



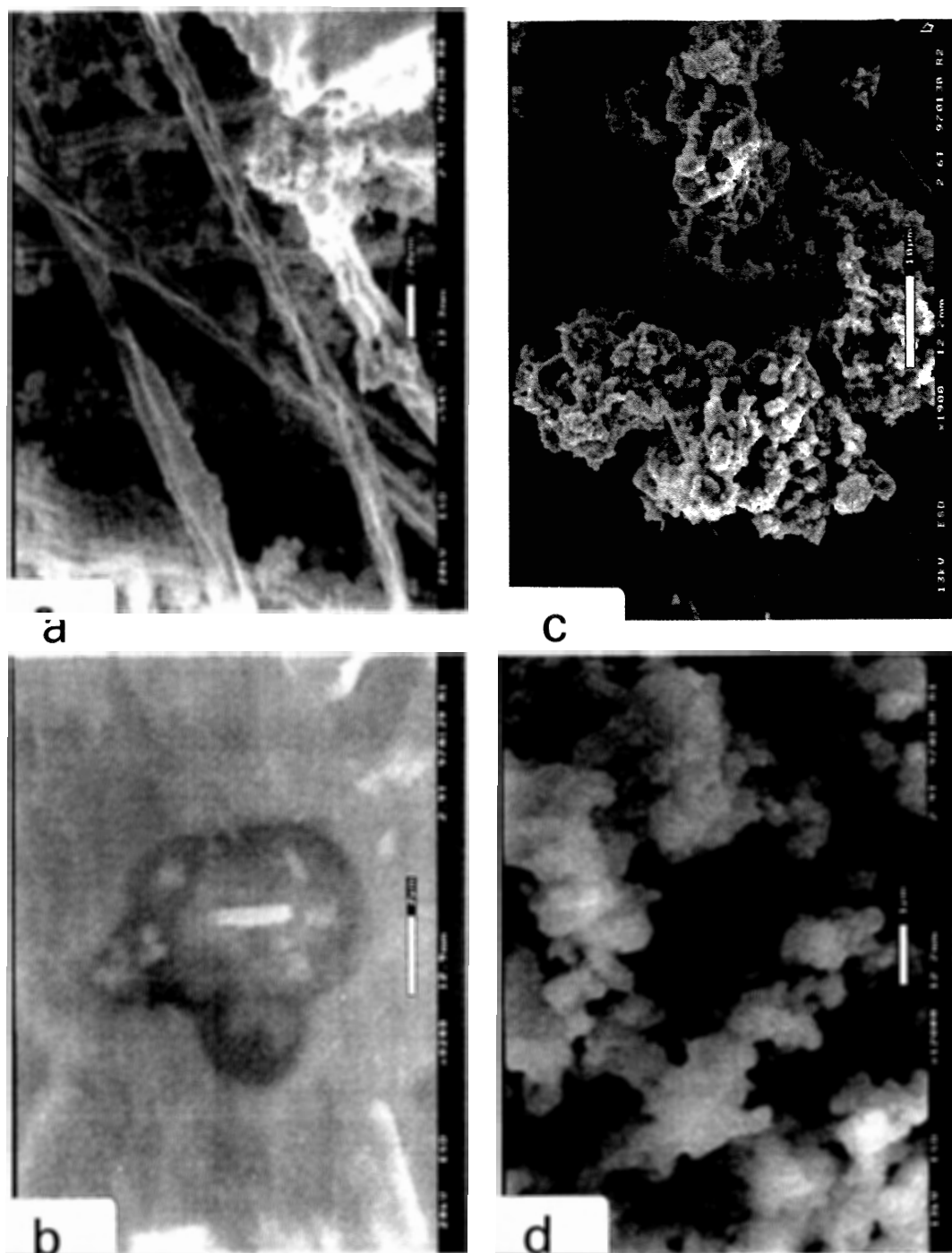


**Figure 4.28:** Images taken with the ESEM as evidence for microbial activity. (a) Relatively thick strands that are probably algae, (b) a rod-shaped structure in a pit that is consistent with a sulphide-oxidizing bacterium surrounded by corroded rock, (c) rust-coloured precipitate from the microbial treatment that may be biogenic, and (d) a close-up of the same type of material as in (c).

## 4.2 Discussion

### 4.2.1 Factors Affecting Oxidation Sensitivity among Sulphides

Controls on oxidation rate of sulphide minerals are varied and can be difficult to measure because many controls can be acting on a single sample. Following is a discussion of some of the possible reasons why the sulphides in this study oxidized in the order they did.

#### Electrochemistry

Mineral stability in its environment is a major factor. Each mineral has a different stability zone that can be calculated from its Gibbs free energy of formation, given specific parameters such as Eh, pH, temperature, pressure, or mineral composition. This stability zone can be plotted on a phase diagram with Eh on the y-axis and pH on the x-axis, holding P and T constant (Garrels, 1960). If the Eh and pH of a mineral's environment are within this stability zone, the mineral will remain intact. If not, the mineral will change by chemical reaction to form another, more stable mineral under the new conditions. Figure 4.29 illustrates an example of an Eh-pH stability diagram for pyrrhotite and pyrite. Figure 4.30 shows the locations of various natural environments in Eh-pH space. ARD would plot at low pH (acid) and high Eh (oxidizing) conditions. Since pyrrhotite has a very small stability field (at high pH and low Eh) under the conditions shown in the figure, it is clear that the mineral is thermodynamically unstable in ARD. Pyrite, on the other hand, is stable over a much wider range of pH and Eh conditions, so it tends to oxidize less easily than pyrrhotite.

In relation to the stability fields, galvanic reactions can affect the amount of sulphide

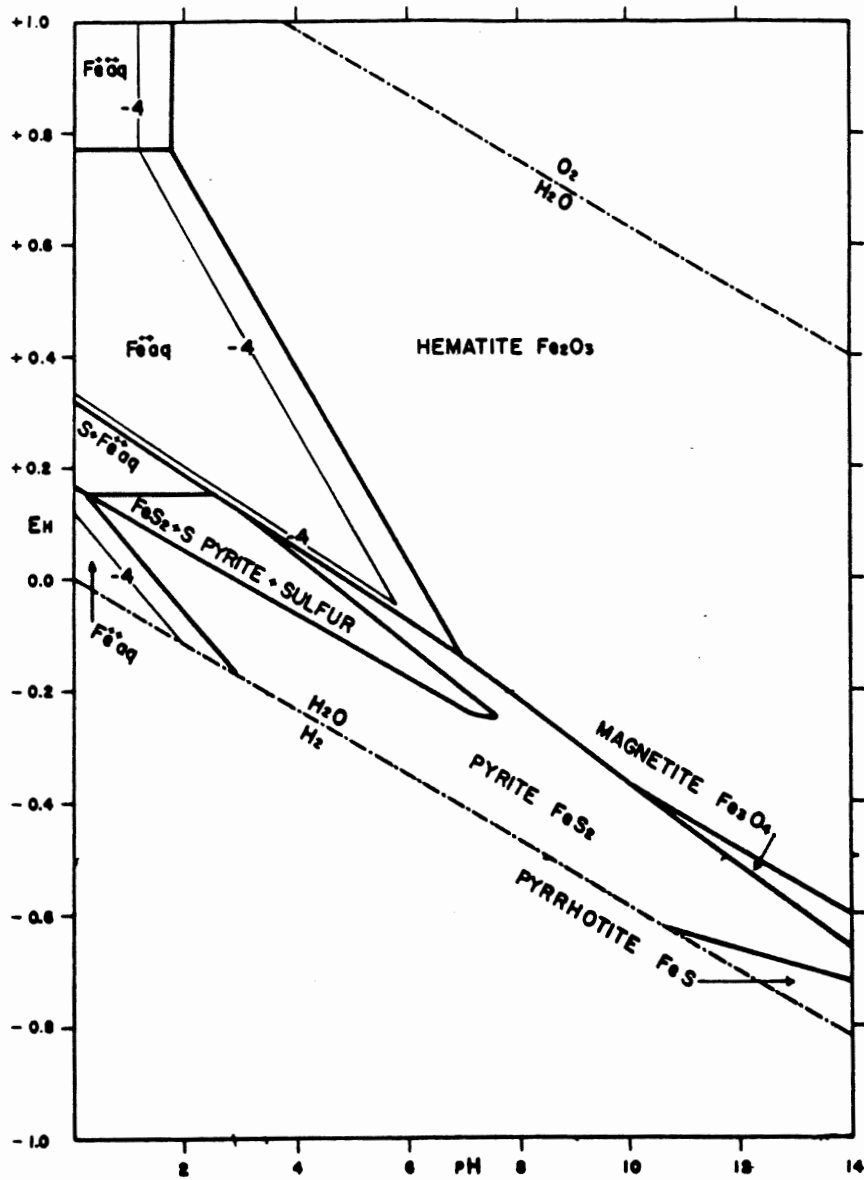


**Figure 4.29:** An example of an Eh/pH plot that shows the stability fields of iron oxides and iron sulphides in water at 25°C, 1 atm. total pressure, with an activity of dissolved sulphur of  $10^{-1}$  (Garrels, 1960). Note that pyrrhotite has a very small stability field (at high pH and low Eh), whereas pyrite has a much wider stability field. It is clear that pyrrhotite is more unstable than pyrite in ARD conditions (see Figure 4.30).

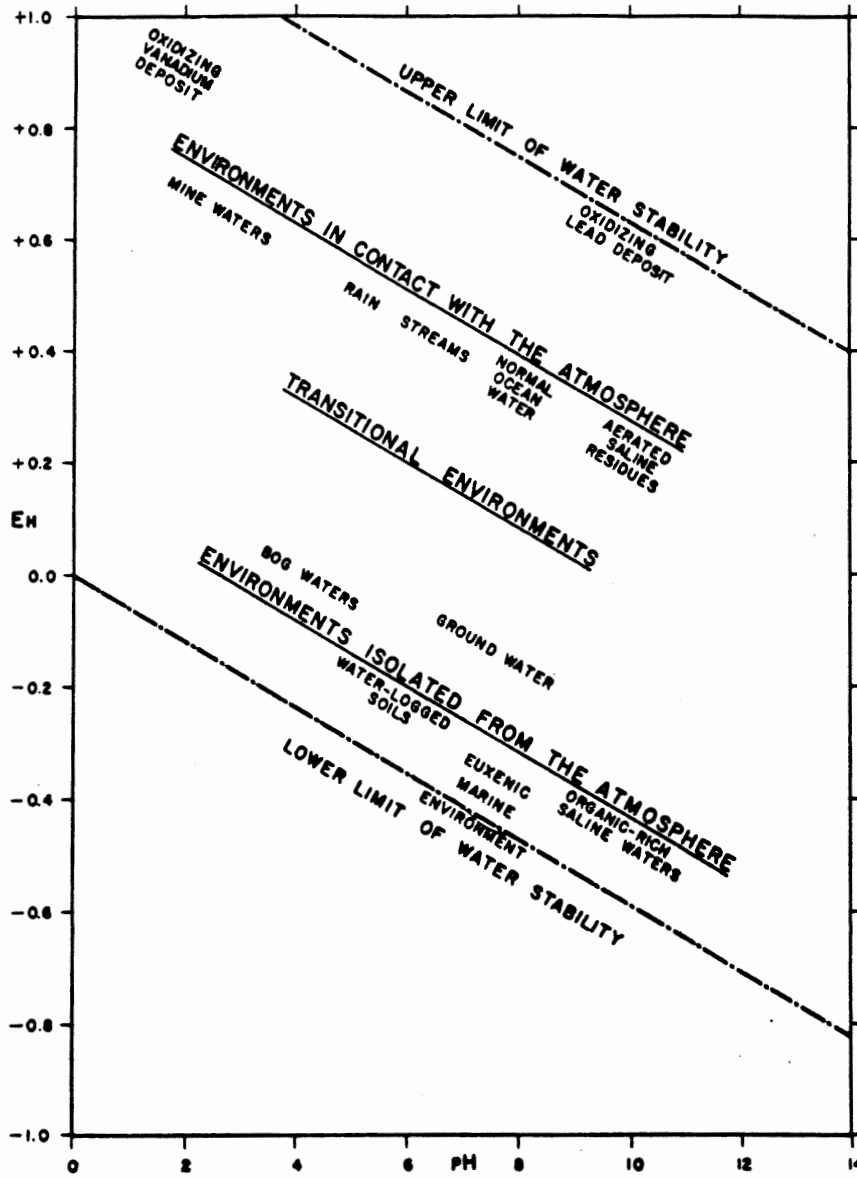


**Figure 4.30:** An Eh vs pH plot showing stability fields for various types of water environments (Garrels, 1960). Note that ARD waters ("mine waters") plot at high Eh and low pH (i.e. oxidizing, acid conditions).

oxidation. As explained by Natarajan (1990) and Kwong (1995), different types of sulphide in close proximity in an oxygenated aqueous medium can act like a battery, with one sulphide behaving like the cathode and the other like the anode. Preferential oxidative dissolution will occur at the anode (the sulphide with lower rest potential), protecting the cathode from oxidation. Table 4.2 lists the rest potentials of pyrite, chalcopyrite, galena, sphalerite and pyrrhotite (FeS). It seems reasonable to use this list to predict which sulphides will oxidize first (i.e. those with lower rest potential). Rest potential is the equilibrium electrode potential when the net anodic or cathodic current is zero (Kwong, 1995).

Two possible examples of galvanic interactions in this study are illustrated in Figures 4.31 and 4.32. In the first example (Fig. 4.31), monoclinic pyrrhotite is clearly the most strongly oxidized, and the white pyrite closest to the pyrrhotite appears less oxidized than the pyrite farther away (cream coloured). It is possible that the closer pyrite was galvanically protected. In the second example (Fig. 4.32), unaltered arsenopyrite is surrounded by hexagonal pyrrhotite, which is strongly altered. The arsenopyrite in RJ-96-002 (Fig. 4.21) oxidized more, indicating that the small inclusion may have been galvanically protected.

However, the list of rest potentials is not completely reliable in the prediction of relative oxidation. Galena is listed after sphalerite and before chalcopyrite, but it oxidized faster than pyrrhotite. Perhaps the iron impurity in the galena (see Appendix A) changed its rest potential, or perhaps other factors came into play, such as crystal lattice effects (discussed below). Also, these rest potentials were determined for pure sulphide compounds in pure acid solutions of  $H_2SO_4$  or  $HClO_4$ , rather than for natural rock samples immersed in ARD "chemical soup."

**Table 4.2:** List of rest potentials of some common sulphide minerals. In a galvanic cell, the mineral with lower rest potential would oxidize first (modified from Kwong, 1995).

Mineral	Formula	Rest Potential (V vs. SHE)	Conditions solution	temperature
pyrite	FeS <sub>2</sub>	0.63	1.0M H <sub>2</sub> SO <sub>4</sub>	25 °C
chalcopyrite	CuFeS <sub>2</sub>	0.52	1.0M H <sub>2</sub> SO <sub>4</sub>	20 °C
galena	PbS	0.28	1.0M H <sub>2</sub> SO <sub>4</sub>	20 °C
sphalerite	ZnS	-0.24	1.0M H <sub>2</sub> SO <sub>4</sub>	20 °C
pyrrhotite	FeS	-0.28	1.0M H <sub>2</sub> SO <sub>4</sub>	20 °C

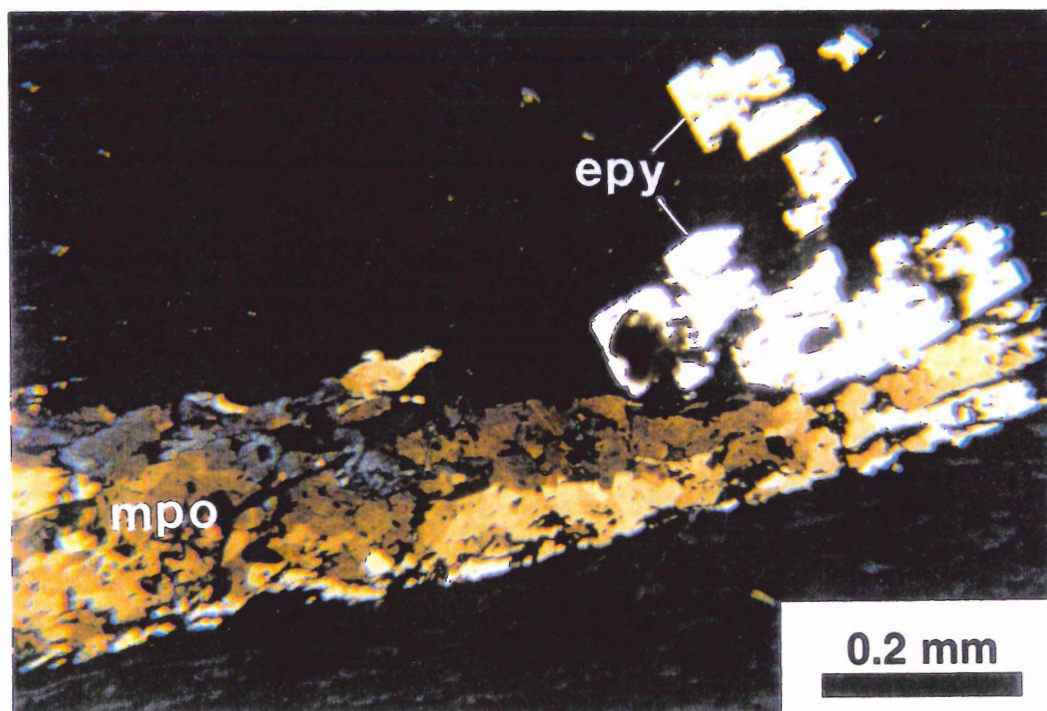


**Figure 4.31:** A possible example of galvanic interactions (sample BH-20-I, 2 days oxidation, reflected plane polarized light with a blue filter). The two grains of euhedral pyrite (epy) have slightly different colours: the one farthest from monoclinic pyrrhotite (mpo) has turned yellowish, whereas the pyrite in contact with the pyrrhotite is still pure white. A galvanic cell may have protected the latter pyrite from oxidation.

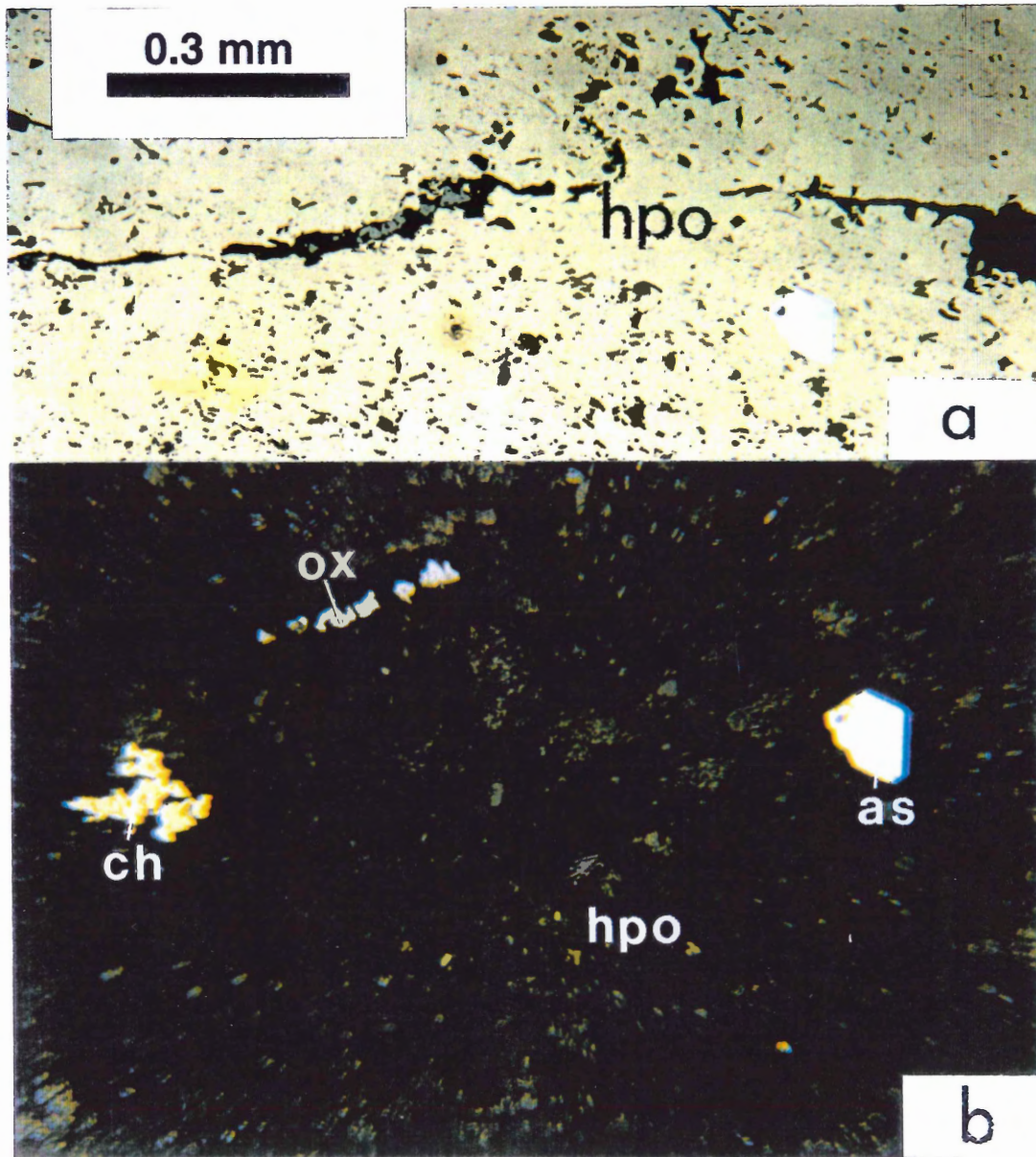


**Figure 4.32:** Another possible example of galvanic interactions. (a) 0 days (b) 42 days oxidation (sample RJ-96-003, reflected plane polarized light with a blue filter). Even after 42 days of oxidation time, arsenopyrite (as), chalcopyrite (ch), and an oxide (ox) remained the same colour as they began, whereas hexagonal pyrrhotite (hpo) was etched and altered to a very dark brown. To compare, the arsenopyrite in Figure 4.21 did change colour. Perhaps this small inclusion was galvanically protected.



### Crystal Lattice Effects

Because oxidative dissolution occurs on the atom level, one must consider the arrangement of these atoms. Weak bonds are more likely to break than strong bonds, and although an ideal crystal consists of an identically repeated group of bonds, this is not always true in natural samples. Lattice structure can be interrupted by impurities, vacancies, dislocations, cracks, or simply the edge of the grain, all of which affect the stability of the mineral (Callister, 1993). Grain surfaces are less stable than the interior because the surface atoms cannot bond outside the mineral, so bond locations are not satisfied. Subgrain boundaries have the same problem (Fig. 4.33). Figure 4.34 shows an SEM picture of monoclinic pyrrhotite subgrain boundaries that appear as grooves where the lattice has been preferentially oxidized. This reasoning also applies to polishing scratches, which begin as small grooves in the surface, so that the surface area is locally increased. Because more atoms along the scratch are unstable in comparison to the surrounding surface, the scratches are preferentially etched during oxidation. This justifies the use of etched polishing scratches as indicators of oxidative dissolution.

Experimental evidence from this study also indicates differential oxidation of various crystal lattice orientations. In Figure 4.35, one can see that different subgrains turned different colours. Therefore, the orientation of the intersection plane between the crystal and the thin section surface is important in determining the stability of that surface. This is related, more immediately, to cleavage planes that reflect lattice orientations with respect to the polished surface (Fig. 4.36).

One further point concerns the texture of the mineral. Anhedral pyrite oxidized much faster than euhedral pyrite. The anhedral grains had irregular edges and were full of fine lamellar

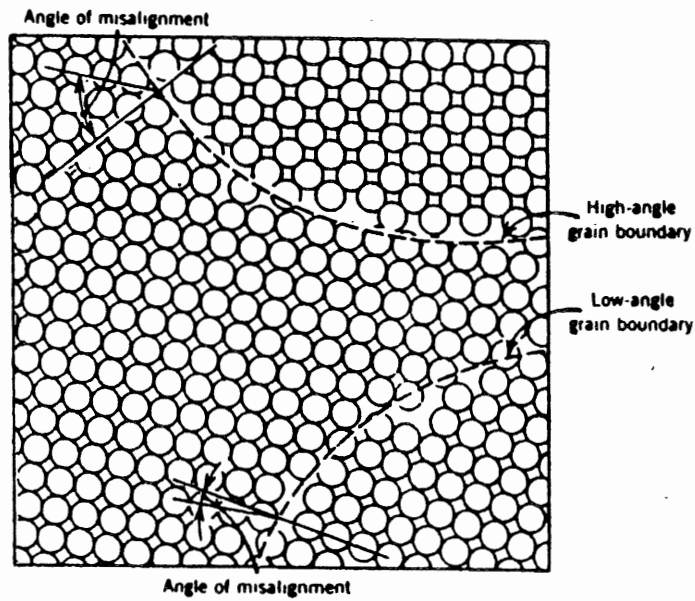


**Figure 4.33:** Structure of sub-grain boundaries, showing interrupted lattice structure causing unsatisfied bond locations (from Callister, 1993).

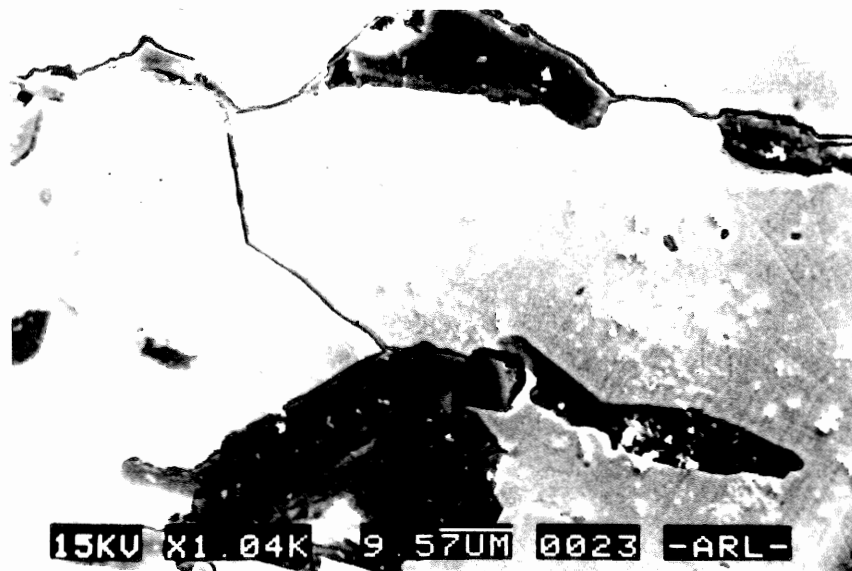


**Figure 4.34:** SEM image of monoclinic pyrrhotite (BH-20-I, sterile treatment) showing subgrain boundaries that have been etched preferentially into grooves.

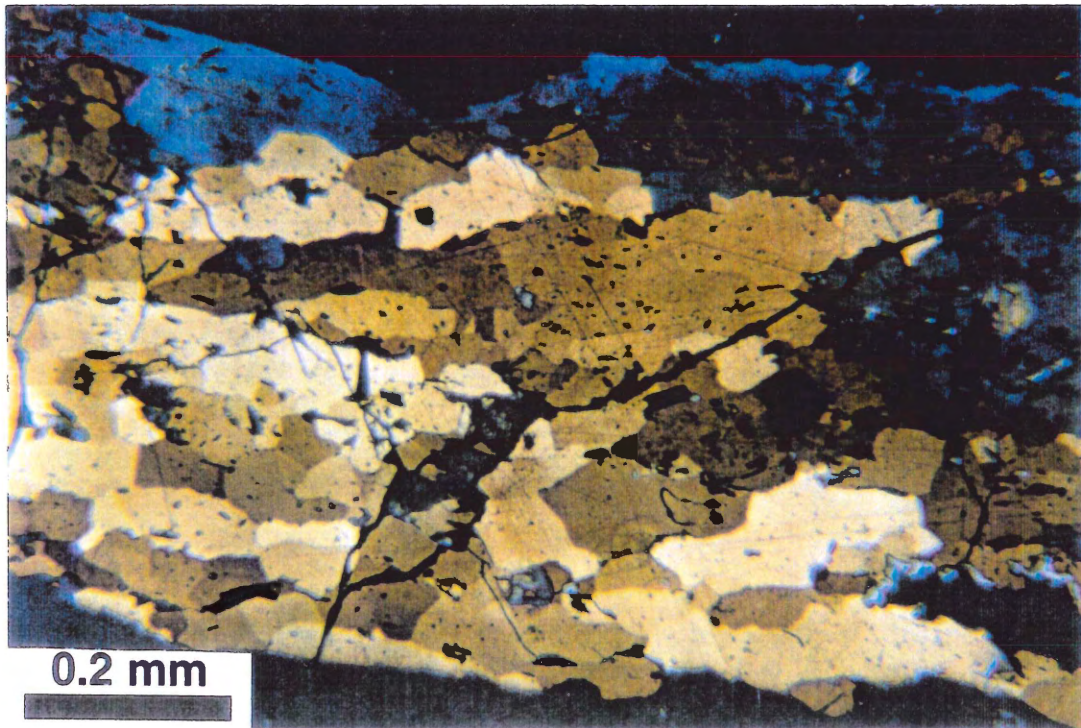


**Figure 4.35:** Monoclinic pyrrhotite subgrains from BH-20-I (sterile treatment) appear as different colours after 42 days of exposure. Grain orientation is likely the cause, either by differential oxidation, or reflectance of cleavage planes (see Fig. 4.36).

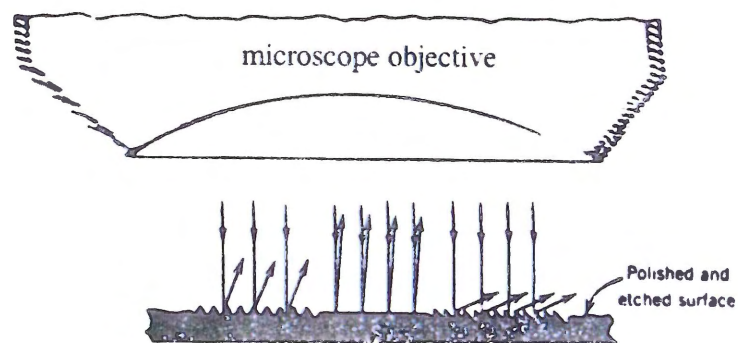


**Figure 4.36:** An illustration of how different crystallographic orientations are etched to create different surface patterns that reflect light in various directions. If light is not reflected vertically into the microscope objective, the subgrain will appear dark (from Callister, 1993).

inclusions that interrupted the pyrite lattice, whereas the euhedral grains had smooth edges and fewer inclusions. This texture could be a result of pyrrhotite replacement by  $\text{FeS}_2$ , either pyrite or marcasite (fig. 3.6 in Robinson, 1996, displays pyrrhotite rimmed with anhedral  $\text{FeS}_2$ ). It is reasonable to assume there would be internal lattice imperfections, causing the anhedral grains to be less stable and oxidize more easily.

#### *4.2.2 Why were the Oxidation Rates Different Between Treatments?*

The most obvious explanation for the significant difference in oxidation rates between the treatments is the metabolism of sulphide-oxidizing bacteria, through direct or indirect means. As discussed in section 2.4, direct oxidation by bacteria would involve active metabolism of sulphide atoms from the mineral surface, while an indirect effect could be created by oxidation of ions in solution (e.g.  $\text{Fe}^{2+}$ ), where the products (e.g.  $\text{Fe}^{3+}$ ) then oxidize the sulphide mineral. In other words, it is not a requirement that bacteria attach themselves to sulphide grains to have a significant effect on their oxidation rate.

There are two other factors that could be involved in the difference between treatments, but their effects are thought to be minimal. There was a small initial pH difference between the two treatments, possibly due to bacterial metabolism during storage in the refrigerator. Also, the metabolism or decay of the other microorganisms may have some effect on the chemistry or oxidation potential of the water. Initially, the sterile treatment was pH = 3.16 (4.5 after oxidation with CR-95-016), and the microbial treatment pH was between 3.62 and 3.76 (4.7 after oxidation with CR-95-016).

It is interesting that bacteria caused such a large difference between the treatments for the

monoclinic and hexagonal pyrrhotites. The pyrrhotites had a greater difference in oxidation rates between the treatments than the other sulphide minerals, causing the order of oxidation among minerals to change (see section 4.1.2). One possible reason for this discrepancy could be that catalysis by microorganisms was facilitated by a higher concentration of iron, favouring the oxidation of hexagonal pyrrhotite over monoclinic, and both pyrrhotites over euhedral pyrite, sphalerite, arsenopyrite and chalcopyrite. Another possibility could be preferential microbial oxidation of crystallographic regimes with differing iron valence states within the pyrrhotites. The commonly used formula  $\text{Fe}_{1-x}\text{S}$  for pyrrhotite is simplified. The more complex formula involves varying proportions of  $\text{Fe}^{2+}$  and  $\text{Fe}^{3+}$  and vacancies within the crystal lattice:  $(\text{Fe}^{2+}, \text{Fe}^{3+}, \text{V})\text{S}$  (Schwarz, 1974; also discussed in MEND, 1991; Pratt *et al.*, 1994). This might explain the preferential microbial oxidation of hexagonal pyrrhotite over monoclinic, if the two minerals had different proportions of ferric and ferrous iron, and if microbes catalyzed oxidation of one proportion better than the other.

#### 4.2.3 Experimentation with Mixed Microbial Species

The main reason to use mixed species is to approximate nature more closely. If one uses a pure culture of bacteria, for example *Thiobacillus ferrooxidans*, it is possible to see its role in sulphide oxidation, but this is not the only species involved in ARD formation. Other species of bacteria can metabolize secondary minerals formed by primary mineral oxidation, re-exposing the sulphide surface and allowing further oxidation. Otherwise the secondary mineral coating may inhibit continuing oxidation (Sanmugasunderam *et al.*, 1987; Ahonen and Tuovinen, 1992). Also, oxidation of different minerals is species-specific (Leduc and Ferroni, 1993). Species vary in their

ability to oxidize different sulphide minerals, so in an experiment involving many sulphides, one should include more than one bacteria species, or the results will be biased.

Predators of sulphide-oxidizers (Protists such as rotifers, zooflagellates and ciliates) are part of the natural system as well (McCready, 1987). When disturbance of sulphide-bearing rock exposes a large volume of minerals for bacterial consumption, there may be a bloom of bacteria, followed by a bloom of their predators. These interactions must influence the rate of sulphide oxidation.

It is clear that the proliferation of bacteria in a particular medium in nature depends on the check and balance provided by predators (Bergeron, 1997). Therefore, a multi-species experiment may better represent nature than a mono-species one.

## **CHAPTER 5: CONCLUSIONS, RECOMMENDATIONS AND FUTURE WORK**

### **5.1 Conclusions**

Two conclusions can be drawn from the evidence collected:

1. Sulphide-oxidizing bacteria are very important in the formation of acid rock drainage because they significantly increase the rate of oxidation. This thesis confirms the findings of previous studies on the role of sulphide-oxidizing bacteria, and also demonstrates the importance of this role for the first time in Nova Scotian rocks with a natural mixed sample of bacteria and other microorganisms.
2. In confirmation of previous work (e.g. Kwong and Lawrence, 1994; Borek, 1994), sulphide mineralogy and texture both strongly affect the oxidation rate. Accurate prediction of potential locations of acid drainage formation must involve an examination of these two factors, because the oxidation rates are site-specific.

### **5.2 Recommendations**

If this experiment were to be repeated, some improvements could be as follows.

This study used reflected light micrographs for comparison before and after oxidation, and scanning electron microscope (SEM) pictures for description and documentation of the results. Time constraints prevented the use of initial SEM pictures for comparison as well, but this would have been a useful addition. One problem with this is the carbon coating necessary for use of the SEM. The carbon coating needs to be polished away before oxidation, and this would change any fine polishing scratches already photographed. However, the average size of scratches could still be compared. The SEM provides clearer pictures with better resolution than the ESEM or

confocal microscope, making it very useful for examination of fine surface detail.

A possible improvement of the experimental design would be to allow observation of the thin sections with a microscope without removal from the experiment. This would require shallow containers, like petri dishes, with a continuous supply of oxygenated water, and the proximity of a temperature-controlled room to a microscope. This would reduce the risk of contamination, and allow observation of secondary minerals and microorganisms undisturbed by transfer. This was not done for this study because of apparatus limitations and the length of time the experiment was allowed to run. The longer the time, the more evaporation could take place, so starting with a large volume of water was best.

### **5.3 Future Work**

This thesis qualitatively examined the relative rates of sulphide mineral oxidation using photomicrographs. The obvious next step would be to quantify the oxidation using a very different experimental design. In order to measure significant changes in water chemistry, a larger volume of sulphides would need to be oxidized. The sulphides could be crushed to maximize the surface area. Visual comparison would not be tremendously useful in this instance, but chemical analyses of the water, and XRD analyses of the sulphides and secondary minerals before and after oxidation, as well as monitoring of pH and Eh throughout the experiment would provide useful quantitative data on oxidation rates. A new method of rock sample sterilization would need to be found in a quantitative experiment, because methanol has a slight tendency to oxidize sulphides. For the study completed in this thesis, slight oxidation by methanol did not compromise the results because it was qualitative differences between the treatments and among sulphide minerals



that was of interest, and all samples were in the methanol for the same length of time, so they were comparable to each other. In a quantitative study, however, the only oxidation occurring should be due to experimental conditions.

It would be beneficial to know what species of sulphide-oxidizing bacteria are active in Nova Scotian ARD sites, as well as local predator-prey interactions. An understanding of these relationships may help in the design of remediation techniques.

The experiment in this thesis could be expanded to include more sulphide textures and sample locations, allowing a broader perspective. Applicability and certainty of experimental results increase in proportion to sample size.

Preliminary evidence in this study (Appendix A), and previous work (e.g. Chen *et al.*, 1980; Kwong and Lawrence, 1994) indicate that trace metal type and concentration may have an effect on the oxidation rate of sulphide minerals. An experiment that compares the oxidation rates of sulphides with various trace element compositions in the Meguma Supergroup would shed some light on this complex issue for this area.

The effects of matrix composition or aqueous environment chemistry were not examined in this thesis. An experiment keeping sulphide mineralogy, texture and composition constant, but varying matrix samples or water chemistry would clarify the role of these variables in the rate of sulphide oxidation. One other variable that could be tested is the difference between the saturated and unsaturated zones, with respect to sulphide oxidation rate.

## REFERENCES

- Ahonen, L., and Tuovinen, O.H. 1992. Alterations in surfaces and textures of minerals during the bacterial leaching of a complex sulfide ore. *Geomicrobiology Journal*, **10**: 207-217.
- Alpers, C.N. and Blowes, D.W. (eds.). 1994. *Environmental Geochemistry and Sulfide Oxidation*. American Chemical Society, Washington, D.C. 681p.
- Bergeron, L. 1997. Slimmed down diet is best for soil-cleaning bacteria. *New Scientist*, **2064**: 16.
- Bigham, J.M. 1994. Mineralogy of ochre deposits formed by sulfide oxidation. *In* The environmental geochemistry of sulfide mine-wastes: short course handbook, Vol. 22, pp. 103-132.
- Binney, W.R., Jenner, K.A., Sangster, A.L., and Zentilli, M. 1986. A stratabound zinc-lead deposit in Meguma Group metasediments at Eastville, Nova Scotia. *Maritime Sediments and Atlantic Geology*, **22**: pp. 65-88.
- Blowes, D.W., Lortie, L., Gould, W.D., and Jambor, J.L. 1995. Microbiological, chemical, and mineralogical characterization of the Kidd Creek Mine Tailings Impoundment, Timmins Area, Ontario. *Geomicrobiology Journal*, **13**: 13-31.
- Borek, S.L. 1994. Effect of humidity on pyrite oxidation. *In* *Environmental Geochemistry and Sulfide Oxidation*. Edited by C.N. Alpers and D.W. Blowes. American Chemical Society, Washington, D.C., pp. 31-44.
- Callister, W.D. Jr. 1993. *Materials science and engineering: an introduction*, 3rd ed. John Wiley & Sons, Inc. New York, NY. pp. 68-87.
- Cameron, G.W. and Hood, P.J. 1975. Residual aeromagnetic anomalies associated with the Meguma Group of Nova Scotia and their relationship to gold mineralization. Geological Survey of Canada, Paper 75-1C, pp. 197-211.
- Canadian Council of Resource and Environmental Ministers. 1987. *Canadian Water Quality Branch, Inland Waters Directorate*, Environment Canada, Ottawa, p.3-2.
- Chen, T.T., Dutrizac, J.E., Owens, D.R., and LaFlamme, J.H.G. 1980. Accelerated tarnishing of some chalcopyrite and tennantite specimens. *Canadian Mineralogist*, **18**: 173-180.
- Craig, J.R. and Scott, S.D. 1974. Sulfide phase equilibria (Chapter 5). *In* *Reviews in mineralogy*, Volume 1, *Sulfide Mineralogy*. Edited by P.H. Ribbe. Mineralogical Society of America, pp. CS-1 - CS-110.

Davis, B.S., and Beveridge, T.J. 1995. The geomicrobiology of the oxic zone at Kidd Creek mine tailings: An ecological study of Acidophilic bacteria, their role in the formation of acid mine drainage (A.M.D.) and removal of toxic heavy metals from the environment through biomineralization. *In* Biotechnology and the Mining Environment: Proceedings of the eleventh annual general meeting of Biominet, SP95-1, Ottawa, Ontario, January 16, 1995. Natural Resources Canada, pp. 69-85.

Department of Energy, Mines, and Resources. 1954, 1980, 1982. 1:50 000 scale NTS sheets.

Evangelou, V.P. and Zhang, Y.L. 1995. A review: pyrite oxidation mechanisms and acid mine drainage prevention. *Critical Reviews in Environmental Science and Technology*, **25**(2): 141-199.

Garcia, O. Jr., Bigham, J.M., and Tuovinen, O.H. 1995a. Oxidation of galena by *Thiobacillus ferrooxidans* and *Thiobacillus thiooxidans*. *Canadian Journal of Microbiology*, **41**: 508-514.

Garcia, O. Jr., Bigham, J.M., and Tuovinen, O.H. 1995b. Sphalerite oxidation by *Thiobacillus ferrooxidans* and *Thiobacillus thiooxidans*. *Canadian Journal of Microbiology*, **41**: 578-584.

Garrels, R.M. 1960. Mineral equilibria at low temperature and pressure. Harper & Brothers, New York, NY, 254p.

Gottschalk, G. 1986. Bacterial Metabolism (2nd ed.) Springer-Verlag, New York, NY. 359p.

Gould, B  chard and Lortie. 1994. Chapter 7: The nature and role of microorganisms in the tailings environment. *In* Short course handbook on environmental geochemistry of sulfide mine-wastes. J.L. Jambor and D.W. Blowes (eds.). Mineralogical Association of Canada, Waterloo, Ontario, pp. 185-200.

Graves, M.C. and Zentilli, M. 1988. The lithochemistry of metal-enriched coticles in the Goldenville-Halifax transition zone of the Meguma Group, Nova Scotia. *In* Current research, part B. Geological Survey of Canada, Paper 88-1B, pp. 251-261.

Hennigar, T.W., and Gibb, J.E. 1987. Surface and groundwater impacts of acid mine drainage from the Meguma slates of Nova Scotia. *In* Proceedings, Acid Mine Drainage Seminar/Workshop, Halifax, Nova Scotia, March 23-26, 1987. Environment Canada, pp. 165-187.

Holt, J.G., Krieg, N.R., Sneath, P.H.A., Staley, J.T., and Williams, S.T. (eds.). 1994. Bergey's manual of determinative bacteriology, 9th ed. Williams and Wilkins, Baltimore, Maryland. 787p.

Jacques, Whitford and Associates Ltd. 1990. Acidic slate assessment, Highway 107 construction, Petpeswick Lake, Halifax County. Unpublished Consult Study for Nova Scotia Department of Environment, March, 1990, 63p.

- Jambor, J.L. and D.W. Blowes (eds.). 1994. Short course handbook on environmental geochemistry of sulfide mine-wastes. Mineralogical Association of Canada, Waterloo, Ontario. 438p.
- Keppie, J.D. 1979. Geological Map of Nova Scotia. Nova Scotia Department of Mines and Energy.
- Keppie, J.D. and Muecke, G.K. 1979. Metamorphic map of Nova Scotia, 1:1000 000 scale.
- Kerekes, J., Freedman, B., Howell, G., and Clifford, P. 1984. Comparison of the characteristics of an acidic eutrophic, and an acidic oligotrophic lake near Halifax, Nova Scotia. *Water Pollution Res. J. Canada*, **19**(1): 1-9.
- King, M., and Hart, W. 1987. Contribution of acidity and heavy metals to surface and groundwater by pyritiferous drainage from the Halifax Formation in Nova Scotia. *Canadian Water Resources Journal*, **15**(4): 357-365.
- Kleinman, R.L.P. and Crerar, D.A. 1979. *Thiobacillus ferrooxidans* and the formation of acidity in simulated coal mine environments. *Geomicrobiology Journal*, **1**(4): 373-388.
- Kwong, E.C.M., Scharer, J.M., Byerley, J.J., and Nicholson, R.V. 1995. Prediction and control of bacterial activity in acid mine drainage. *In Proceedings, Conference on Mining and the Environment, Sudbury, Ontario, Canada, May 28-June 1, 1995. Edited by T.P. Hynes and M.C. Blanchette. CANMET, Ottawa, Vol. 1, pp. 211-216.*
- Kwong, Y.T.J. 1995. Influence of galvanic sulfide oxidation on mine water chemistry. *In Proceedings, Conference on Mining and the Environment, Sudbury, Ontario, Canada, May 28-June 1, 1995. Edited by T.P. Hynes and M.C. Blanchette. CANMET, Ottawa, Vol. 2, pp. 477-483.*
- Kwong, Y.T.J., and Lawrence, J.R. 1994. Mineralogical controls of sulfide oxidation. National Hydrology Research Institute, Contribution No. 94010, 87p.
- Leduc, L.G., and Ferroni, G.D. 1993. The need for *Thiobacillus ferrooxidans* strain selection in applications of bioleaching. *In Proceedings of the tenth annual general meeting of Biominet, SP94-1, October 28, 1993. Natural Resources Canada, pp. 25-42.*
- Lund, O.P. 1987. Acid drainage from mineralized slate at the Halifax International Airport. *In Proceedings, Acid Mine Drainage Seminar/Workshop, Halifax, Nova Scotia, March 23-26, 1987. Environment Canada, pp. 137-165.*
- Lund, O.P., Vaughan, J., and Thirumurthi, D. 1987. Impact of acid drainage pollution from mineralized slate at Halifax airport. *Water Pollution Resources Journal of Canada*, **2**(2): 308-325.

- Lundgren, D.G. and Dean, W. 1979. Biogeochemistry of iron. *In* Biogeochemical cycling of mineral-forming elements. *Edited by* P.A. Trudinger and D.J. Swaine. Elsevier Scientific Publishing Company, New York, NY, pp.211-251.
- MacInnis, I.N. 1986. Lithogeochemistry of the Goldenville-Halifax transition (GHT) of the Meguma Group in the manganiferous zinc-lead deposit at Eastville, Nova Scotia. B.Sc. Honours thesis, Dalhousie University, Halifax, Nova Scotia, 138p.
- MacInnis, I.N., Silver, S.R., Pašava, J., Graves, M.C., and Zentilli, M. 1994. Experimental evaluation of the relative acid drainage potential of pyrite and pyrrhotite. *Atlantic Geology*, **30**(1): 75.
- Mine Environment Neutral Drainage (MEND) Program. 1991. New methods for determination of key mineral species in acid generation prediction by acid-base accounting. Department of Energy, Mines and Resources Canada, Canada Centre for Mineral and Energy Technology, MEND Project 1.16.1c.
- McCready, R.G.L. 1987. A review of the physical, chemical and biological measures to prevent acid mine drainage: an application to the pyritic Halifax shales. *In* Proceedings, Acid Mine Drainage Seminar/Workshop, Halifax, Nova Scotia, March 23-26, 1987. Minister of Supply and Services Canada, Ottawa, Ontario. pp. 333-355.
- McGrath, P.H. 1969. Aeromagnetic interpretation Appalachia, New Brunswick and Nova Scotia. *In* Report of Activities, Part A, Geological Survey of Canada, Paper 70-1A, pp. 79-82.
- Natarajan, K.A. 1990. Electrochemical aspects of bioleaching of base-metal sulfides. *In* Microbial mineral recovery. *Edited by* H.L. Ehrlich and C.L. Brierley. McGraw-Hill Publishing Co., New York, NY, pp.79-106.
- Nordstrom, D.K. 1982. Aqueous pyrite oxidation and the consequent formation of secondary iron minerals. *In* Acid sulfate weathering, SSSA Special Publication Number 10, Proceedings of a symposium sponsored by Divisions S-9, S-2, S-5, and S-6 of the Soil Science Society of America, August 5-10, 1982. *Edited by* J.A. Kittrick, D.S. Fanning and L.R. Hossner. Soil Science Society of America, Madison, Wisconsin, pp. 37-56.
- O'Brien, B.H. 1985. Preliminary report on the geology of the Lahave River area, Nova Scotia. *In* Current Research, Part A, Geological Survey of Canada, Paper 85-1A, pp. 784-794.
- O'Brien, B.H. 1986. Preliminary report on the geology of the Mahone Bay area, Nova Scotia. *In* Current Research, Part A, Geological Survey of Canada, Paper 86-1A, pp. 439-444.

Paine, P.J. 1987. Historic and geographic overview of acid mine drainage. *In Proceedings, Acid Mine Drainage Seminar/Workshop, Halifax, Nova Scotia, March 23-26, 1987.* Minister of Supply and Services Canada, Ottawa, Ontario. pp. 1-45.

Pašava, J., Graves, M.C., MacInnis, I.N., and Zentilli, M. 1995. Black slates - A source of acid drainage at the Halifax International Airport, Nova Scotia, Canada. *In Mineral Deposits: From their origin to their environmental impacts. Proceedings of the Third Biennial SGA Meeting, Prague, Czech Republic, August 28-31, 1995, pp. 785-788.*

Pettipas, B. 1979. A statistical evaluation of the effect of acid leachate on water quality, in Union Square, Lunenburg County. Nova Scotia Department of Environment Report, June, 1979, 56p.

Pratt, A.R., Muir, I.J., and Nesbitt, H.W. 1994. X-ray photoelectron and Auger electron spectroscopic studies of pyrrhotite and mechanism of air oxidation. *Geochimica et Cosmochimica Acta*, **58**(2): 827-841.

Prescott, L.M., Harley, J.P. and Klein, D.A. 1996. *Microbiology*, 3rd ed. Times Mirror Higher Education Group, Inc., Dubuque, Iowa, 543p.

Pronk, J.T., and Johnson, D.B. 1992. Oxidation and reduction of iron by acidophilic bacteria. *Geomicrobiology Journal*, **10**: 153-171.

Ralph, B.J. 1979. Oxidative reactions in the sulfur cycle. *In Biogeochemical cycling of mineral-forming elements. Edited by P.A. Trudinger and D.J. Swaine.* Elsevier Scientific Publishing Company, New York, NY, pp. 369-400.

Raven, P.H. and Johnson, G.B. 1992. *Biology* (3rd ed.). Mosby-Year Book, Inc. St. Louis, Missouri, 1217p.

Ritchie, A.I.M. 1994. Sulfide oxidation mechanisms: controls and rates of oxygen transport. *In Short course handbook on environmental geochemistry of sulfide mine-wastes.* J.L. Jambor and D.W. Blowes (eds.). Mineralogical Association of Canada, Waterloo, Ontario, pp. 133-161.

Roberts, J.D. 1986. The viability of peat as a treatment medium for acid mine drainage. Masters of Environmental Studies (MES) thesis, Dalhousie University, Halifax, NS, 137p.

Robinson, C. 1996. Pyrrhotite composition and its relationship to acid drainage potential in the Halifax Formation, Meguma Group, Nova Scotia. B.Sc. Honours thesis, Dalhousie University, Halifax, Nova Scotia, 72p.

Robinson, C. and Fox, D. 1996. Pyrrhotite composition and its relationship to acid drainage from the Halifax Formation, Meguma Group, Nova Scotia. *Atlantic Geology*, **32**(1): p.85.

- Ryan, R.J., Fox, D., Horne, R.J., Corey, M.C., and Smith, P.K. 1995. Preliminary stratigraphy of the Meguma Group in central Nova Scotia. *In* Report of Activities, Nova Scotia Department of Natural Resources, Report 96-1, pp. 27-34.
- Sadler, C. 1991. Bayers Lake paving caps spoiled soil. *The Sunday Daily News*, September 22, 1991. p.3.
- Sanmugasunderam, V., Gould, W.D., McCready, R.G.L., Rajan, S., Beaulne, M., and Mainwaring, P. 1987. Bacterial and chemical leaching of complex sulphide ores. *In* Proceedings of the fourth annual general meeting of Biominet, Sudbury, Canada, November 5, 1987. CANMET Special Publication SP87-10, pp. 103-116.
- Schenk, P.E. 1970. Regional variation of the flysch-like Meguma Group (Lower Paleozoic) of Nova Scotia, compared to recent sedimentation off the scotian shelf. *In* The Geological Association of Canada, Special Paper Number 7, pp. 127-153.
- Schenk, P.E. 1995. Meguma Zone (Chapter 3). *In* Geology of the Appalachian-Caledonian Orogen in Canada and Greenland. *Edited by* H. Williams. Geological Survey of Canada, Geology of Canada, no. 6, pp. 261-277.
- Schwarz, E.J. 1974. Magnetic properties of pyrrhotite and their use in applied geology and geophysics. Department of Energy, Mines and Resources Canada, Geological Survey, Paper 74-59, 24p.
- Schwarz, E.J. and Broome, J. 1994. Magnetic anomalies due to pyrrhotite in Paleozoic metasediments in Nova Scotia, Eastern Canada. *Journal of Applied Geophysics*, **32**: 1-10.
- Silver, M. 1988. Construction of a wetland vegetated system designed to decrease acid and toxic metal loadings from quarry effluents. Marvin Silver Scientific Ltd., July, 1988, 16p.
- Silver, M., Ehrlich, H.L., and Ivarson, K.C. 1986. Soil mineral transformation mediated by soil microbes. *In* Interactions of soil minerals with natural organics and microbes, Soil Science Society of America Special Publication no. 17, pp. 497-519.
- Singer, P.C. and Strumm, W. 1970. Acidic mine drainage: the rate-determining step. *Science*, **167**: 1121-1123.
- Steger, H.F. 1982. Oxidation of sulfide minerals VII. Effect of temperature and relative humidity on the oxidation of pyrrhotite. *Chemical Geology*, **35**: 281-295.
- Steger, H.F., and Desjardins, L.E. 1978. Oxidation of sulfide minerals, 4. Pyrite, chalcopyrite and pyrrhotite. *Chemical Geology*, **23**: 225-237.

Strumm, W. and Morgan, J.J. 1970. Aquatic chemistry: an introduction emphasizing chemical equilibria in natural waters. John Wiley & Sons, Inc. New York, NY, 583p.

Thompson, B.D. 1978. An investigation of Meguma bedrock leaching in the Shubenacadie-Stewiacke river basin, Technical Report #8. Prepared for the Shubenacadie-Stewiacke River Basin Board, 48p.

Waldron, J.W.F. 1992. The Goldenville-Halifax transition, Mahone Bay, Nova Scotia: relative sea-level rise in the Meguma source terrane. *Canadian Journal of Earth Sciences*, **29**: 1091-1105.

Walsh, F. and Mitchell, R. 1972. A pH-dependent succession of iron bacteria. *Environmental Science and Technology*, **6**(9): 809-812.

Worgan, J. (1987) Acid mine drainage in reactive slates, "The Halifax International Airport Case" Transport Canada perspective. Proceedings Acid Mine Drainage seminar/workshop, Halifax, Nova Scotia.

Zentilli, M., Graves, M.C., Mulja, T., and MacInnis, I. 1986. Geochemical characterization of the Goldenville-Halifax transition of the Meguma Group of Nova Scotia: preliminary report. *In* Current research, part A. Geological Survey of Canada, Paper 86-1A: pp. 423-428.



**APPENDIX A: MICROPROBE DATA**

**Figure A-1:** CR-95-16 Strongly etched and less-etched subgrains of pyrrhotite from the microbial treatment. Note differences in trace metal content. Atomic %, normalized.

Etched	Spot#	Cu	Fe	As	S	Total
less	28	1.32%	42.23%	0.25%	56.20%	100.00%
less	29	1.32%	42.60%	0.36%	55.72%	100.00%
more	30	2.34%	41.92%	0.13%	55.61%	100.00%
more	31	2.53%	42.10%	0.00%	55.37%	100.00%

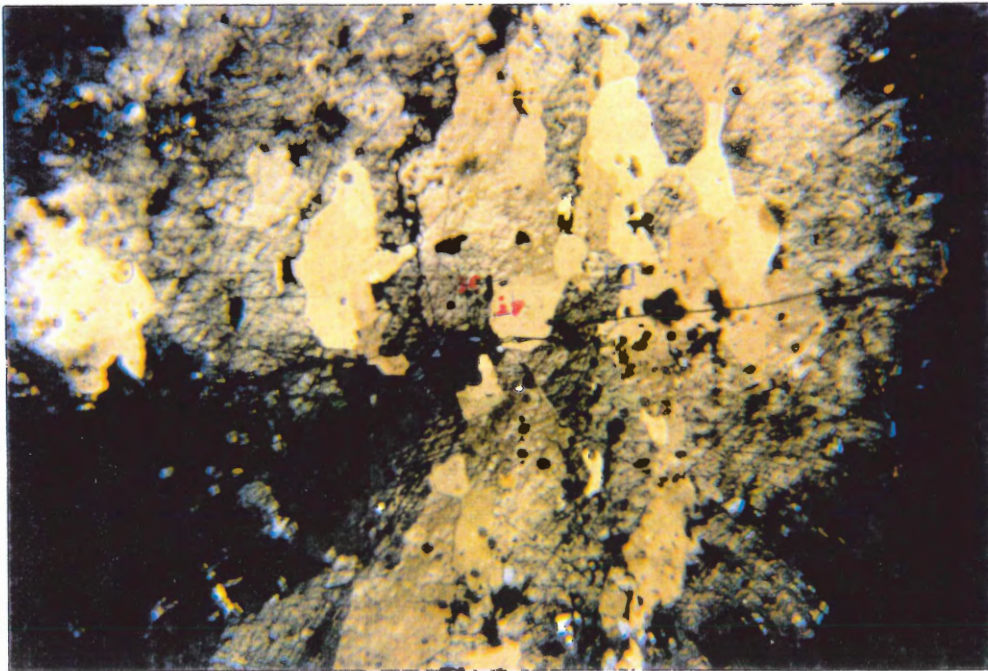


**Figure A-2:** Sample CR-95-16, microprobe points measured after oxidation. Differing S concentrations between the grains with blue tarnish and those with orange tarnish may be due to element loss or interference by the tarnish. A spot without tarnish had intermediate sulphur content. Repolishing would be necessary to study the composition of the starting material.

## Atomic %

colour	Spot#	Cu	Fe	As	S	Total
blue	17	2.75%	46.47%	0.10%	50.36%	99.68%
blue	18	3.14%	46.47%	0.10%	50.29%	100.00%
blue	19	1.96%	45.54%		52.50%	100.00%
blue	20	2.03%	45.41%	0.13%	52.43%	100.00%
blue	21	1.69%	45.65%	0.12%	52.54%	100.00%
blue	22	2.04%	45.13%		52.48%	99.65%
blue	23	2.41%	45.22%		52.37%	100.00%
clear	24	1.72%	46.66%	0.11%	51.50%	99.99%
orange	25	2.45%	46.86%		50.69%	100.00%
orange	26	2.72%	46.58%	0.10%	50.60%	100.00%
orange	27	3.24%	46.16%		50.60%	100.00%

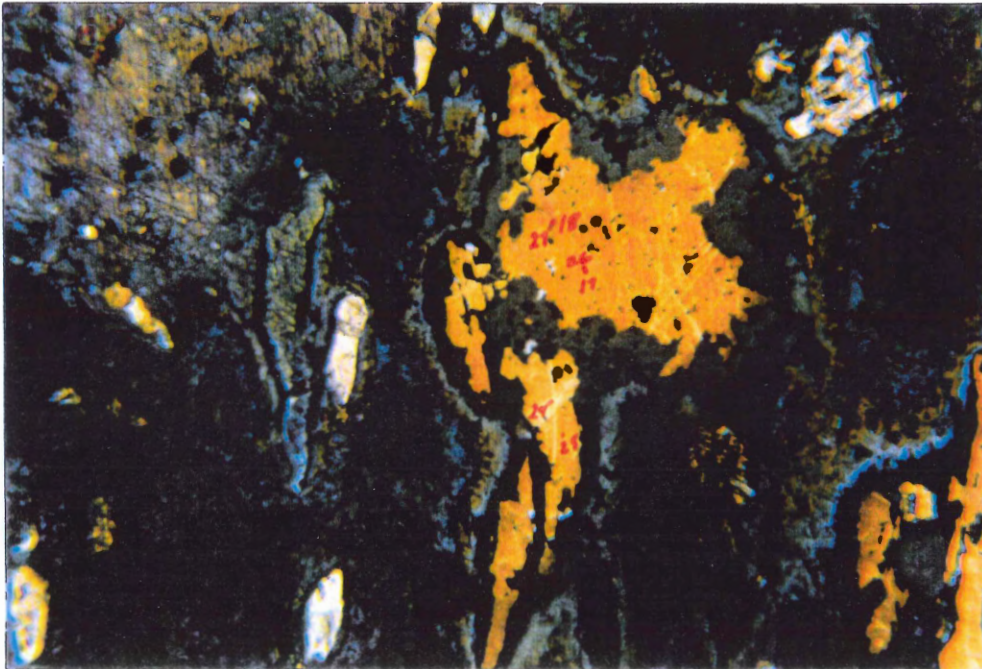
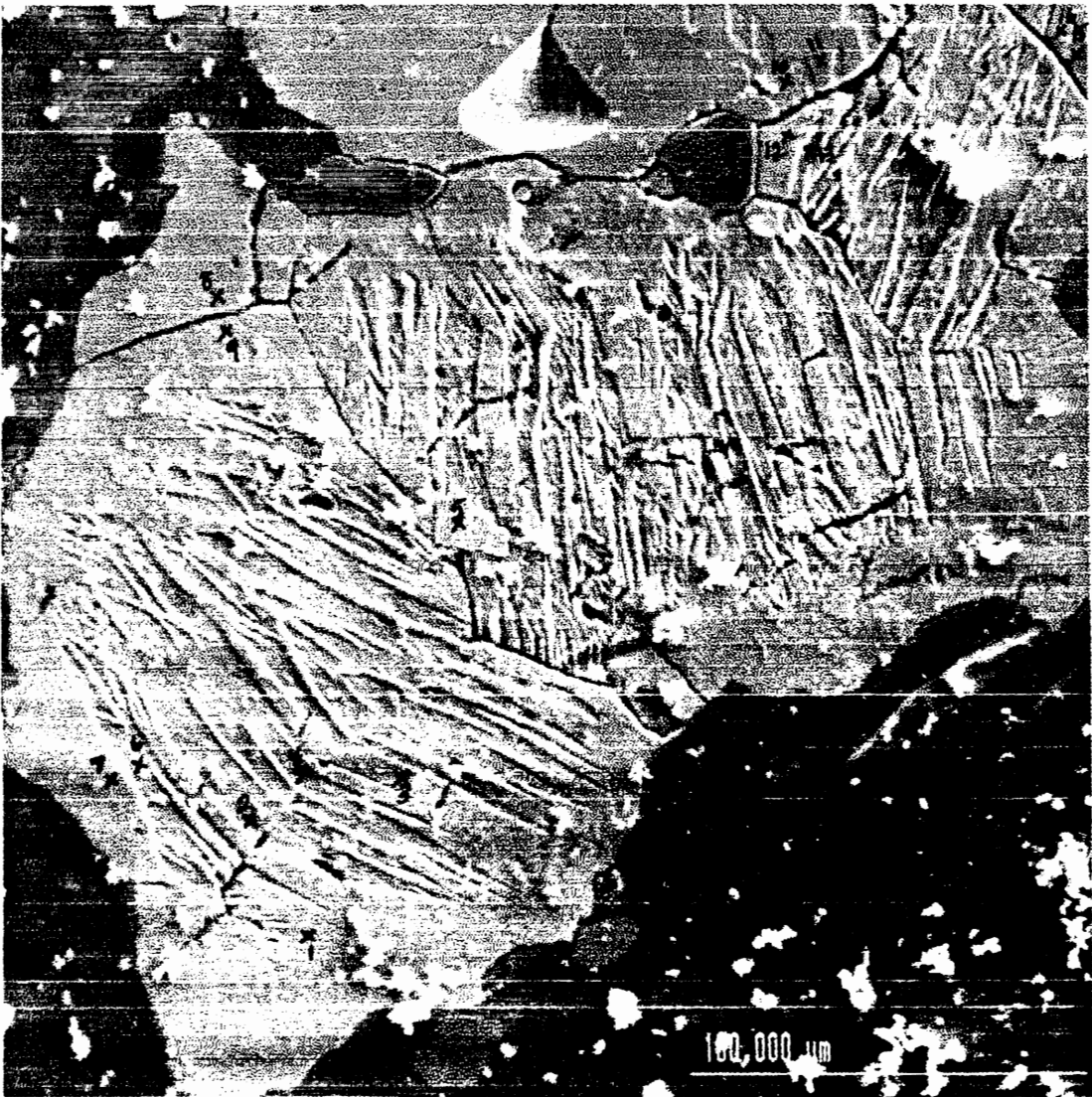


**Figure A-3:** Sample CR-95-002. Preferentially oxidized lamellae within pyrrhotites of sample CR-95-002 are compositionally indistinguishable from their host, eliminating the possibility that compositional variations were the reason for stronger corrosion, unless trace elements below detection limit are involved.

mineral	Spot #	Cu	Fe	As	S	Total	detail
pyrrhotite	2	0.91%	46.67%	0.00%	52.42%	100.00%	lamina
pyrrhotite	3	0.89%	46.14%	0.12%	52.60%	99.75%	lamina
pyrrhotite	4	0.67%	46.56%	0.00%	52.50%	99.73%	lamina
pyrrhotite	6	1.21%	45.85%	0.00%	52.66%	99.72%	lamina
pyrrhotite	10	0.42%	46.80%	0.10%	52.19%	99.51%	lamina
pyrrhotite	13	0.82%	45.88%	0.00%	53.03%	99.73%	lamina
un-laminated rim		0.82%	46.32%	0.04%	52.57%	99.74%	n = 6
laminated centre		0.73%	46.40%	0.11%	52.57%	99.80%	n = 8
pyrrhotite	1	0.91%	46.20%	0.15%	52.44%	99.70%	rim
pyrrhotite	7	1.01%	46.59%	0.09%	52.30%	99.99%	rim
pyrrhotite	8	0.59%	46.31%	0.15%	52.59%	99.64%	rim
pyrrhotite	9	0.78%	46.27%	0.09%	52.52%	99.66%	rim
pyrrhotite	11	0.35%	46.99%	0.17%	52.37%	99.88%	rim
pyrrhotite	12	0.70%	45.94%	0.00%	52.91%	99.55%	rim
pyrrhotite	15	0.62%	46.59%	0.09%	52.70%	100.00%	rim
pyrrhotite	16	0.89%	46.27%	0.12%	52.71%	99.99%	rim
cobaltite	5	0.00%	7.64%	0.34	31.63%	73.32%	incl.
chalcopyrite	14	25.30%	25.63%	0.00%	49.07%	100.00%	incl.

CR-95-002: probe points for the data on page A-3.



**APPENDIX B: WATER CHEMISTRY OF ARD SAMPLE: BEFORE OXIDATION,  
AFTER OXIDATION IN THE MICROBIAL TREATMENT, AND  
AFTER OXIDATION IN THE STERILE TREATMENT**

**MDS ENVIRONMENTAL SERVICES LIMITED**

**Sample : 97-H002961**  
**Client ID : RAJ-001**

<b>RCap 30 Analytes</b>	<b>Value</b>	<b>Units</b>	<b>LOQ</b>	<b>Method</b>
Sodium	65.0	mg/L	0.1	ICP-OES
Potassium	1.0	mg/L	0.1	ICP-OES
Calcium	14.6	mg/L	0.1	ICP-OES
Magnesium	6.7	mg/L	0.1	ICP-OES
Alkalinity (as CaCO3)	< 1	mg/L	1.	COBAS
Sulfate	146.	mg/L	2.	COBAS
Chloride	97.0	mg/L	1.0	COBAS
Reactive Silica (as SiO2)	23.2	mg/L	0.5	COBAS
Ortho Phosphorus (as P)	< 0.01	mg/L	0.01	COBAS
Nitrate + Nitrite (as N)	< 0.05	mg/L	0.05	COBAS
Ammonia (as N)	< 0.05	mg/L	0.05	COBAS
Iron	2.99	mg/L	0.02	ICP-OES
Manganese	1.36	mg/L	0.01	ICP-OES
Copper	0.06	mg/L	0.01	ICP-OES
Zinc	0.11	mg/L	0.01	ICP-OES
Color	< 5	TCU	5.	COBAS
Turbidity	0.1	NTU	0.1	NEPH.
Specific Conductance	850.	umhos/cm	1.00	ELECTRODE
pH	3.4	Units	0.1	ELECTRODE
Dissolved Organic Carbon	0.8	mg/L	0.5	U.V. -ox
<b>RCap 30 Computed Analytes</b>				
Hardness (as CaCO3)	64.0	mg/L	0.1	CALCULATED
Bicarbonate (as CaCO3)	< 1	mg/L	1.0	CALCULATED
Carbonate (as CaCO3)	< 1	mg/L	1.0	CALCULATED
TDS Calculated	354.	mg/L	1.	
<b>RCap 30 Computed Indexes</b>				
Cation Sum	4.53	meq/L		CALCULATED
Anion Sum	5.80	meq/L		CALCULATED
Ion Balance	12.2	%		CALCULATED
Langlier Index @ 4C	-7.31			CALCULATED
Langlier Index @20C	-6.91			CALCULATED
Saturation pH @ 4C	10.7	Units		Calculated
Saturation pH @ 20C	10.3	Units		Calculated

**Report To:**  
**Don Fox**  
 Dalhousie University  
 Dept. of Earth Sciences  
 Halifax, NS,

**Date Received: Feb 11, 1997**  
**Date Reported: Feb 19, 1997**

**Inorganics Manager**

*[Signature]*  
**Jerry Arenovich** *AS*

BEFORE OXIDATION

---

MDS ENVIRONMENTAL SERVICES LIMITED

Sample : 97-H002961  
Client ID : RAJ-001

---

Comments : Cation sum does not include contribution from metals.

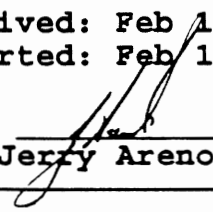
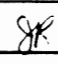
Inorganic Analytes	Value	Units	LOQ	Method
Aluminum	8700	ug/L	10.	ICP-MS

---

Report To:  
Don Fox  
Dalhousie University  
Dept. of Earth Sciences  
Halifax, NS,

Date Received: Feb 11, 1997  
Date Reported: Feb 19, 1997

Inorganics Manager

  
Jerry Arenovich 

---



**MDS ENVIRONMENTAL SERVICES LIMITED**

**Sample : 97-H002962**  
**Client ID : RAJ-002**

<b>RCap 30 Analytes</b>	<b>Value</b>	<b>Units</b>	<b>LOQ</b>	<b>Method</b>
Sodium	95.0	mg/L	0.1	ICP-OES
Potassium	12.4	mg/L	0.1	ICP-OES
Calcium	102.	mg/L	0.1	ICP-OES
Magnesium	10.8	mg/L	0.1	ICP-OES
Alkalinity (as CaCO3)	< 1	mg/L	1.	COBAS
Sulfate	297.	mg/L	2.	COBAS
Chloride	184.	mg/L	1.0	COBAS
Reactive Silica (as SiO2)	22.2	mg/L	0.5	COBAS
Ortho Phosphorus (as P)	< 0.01	mg/L	0.01	COBAS
Nitrate + Nitrite (as N)	< 0.05	mg/L	0.05	COBAS
Ammonia (as N)	< 0.05	mg/L	0.05	COBAS
Iron	< 0.02	mg/L	0.02	ICP-OES
Manganese	6.40	mg/L	0.01	ICP-OES
Copper	< 0.01	mg/L	0.01	ICP-OES
Zinc	0.10	mg/L	0.01	ICP-OES
Color	< 5	TCU	5.	COBAS
Turbidity	0.2	NTU	0.1	NEPH.
Specific Conductance	1350	umhos/cm	1.00	ELECTRODE
pH	4.7	Units	0.1	ELECTRODE
Dissolved Organic Carbon	3.8	mg/L	0.5	U.V.-ox
<b>RCap 30 Computed Analytes</b>				
Hardness (as CaCO3)	299.	mg/L	0.1	CALCULATED
Bicarbonate (as CaCO3)	< 1	mg/L	1.0	CALCULATED
Carbonate (as CaCO3)	< 1	mg/L	1.0	CALCULATED
TDS Calculated	724.	mg/L	1.	
<b>RCap 30 Computed Indexes</b>				
Cation Sum	10.5	meq/L		CALCULATED
Anion Sum	11.4	meq/L		CALCULATED
Ion Balance	4.29	%		CALCULATED
Langlier Index @ 4C	-5.20			CALCULATED
Langlier Index @20C	-4.80			CALCULATED
Saturation pH @ 4C	9.90	Units		Calculated
Saturation pH @ 20C	9.50	Units		Calculated

**Report To:**  
**Don Fox**  
 Dalhousie University  
 Dept. of Earth Sciences  
 Halifax, NS,

**Date Received: Feb 11, 1997**  
**Date Reported: Feb 18, 1997**

**Inorganics Manager**

*[Signature]*  
**Jerry Arenovich** *af*

. AFTER OXIDATION IN THE MICROBIAL TREATMENT

---

MDS ENVIRONMENTAL SERVICES LIMITED

Sample : 97-H002962  
Client ID : RAJ-002

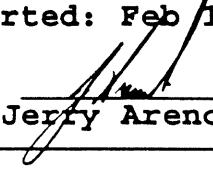
---

Inorganic Analytes	Value	Units	LOQ	Method
Aluminum	450	ug/L	10.	ICP-MS

---

Report To:  
Don Fox  
Dalhousie University  
Dept. of Earth Sciences  
Halifax, NS,

Date Received: Feb 11, 1997  
Date Reported: Feb 18, 1997

Inorganics Manager   
Jerry Arenovich

**MDS ENVIRONMENTAL SERVICES LIMITED**

**Sample : 97-H002963**  
**Client ID : RAJ-003**

<b>RCap 30 Analytes</b>	<b>Value</b>	<b>Units</b>	<b>LOQ</b>	<b>Method</b>
Sodium	112.	mg/L	0.1	ICP-OES
Potassium	1.7	mg/L	0.1	ICP-OES
Calcium	79.6	mg/L	0.1	ICP-OES
Magnesium	14.9	mg/L	0.1	ICP-OES
Alkalinity (as CaCO3)	< 1	mg/L	1.	COBAS
Sulfate	260.	mg/L	2.	COBAS
Chloride	191.	mg/L	1.0	COBAS
Reactive Silica (as SiO2)	36.6	mg/L	0.5	COBAS
Ortho Phosphorus (as P)	< 0.01	mg/L	0.01	COBAS
Nitrate + Nitrite (as N)	< 0.05	mg/L	0.05	COBAS
Ammonia (as N)	0.19	mg/L	0.05	COBAS
Iron	1.60	mg/L	0.02	ICP-OES
Manganese	6.00	mg/L	0.01	ICP-OES
Copper	< 0.01	mg/L	0.01	ICP-OES
Zinc	0.22	mg/L	0.01	ICP-OES
Color	7.	TCU	5.	COBAS
Turbidity	2.3	NTU	0.1	NEPH.
Specific Conductance	1370	umhos/cm	1.00	ELECTRODE
pH	4.5	Units	0.1	ELECTRODE
Dissolved Organic Carbon	6.9	mg/L	0.5	U.V. - ox
<b>RCap 30 Computed Analytes</b>				
Hardness (as CaCO3)	260.	mg/L	0.1	CALCULATED
Bicarbonate (as CaCO3)	< 1	mg/L	1.0	CALCULATED
Carbonate (as CaCO3)	< 1	mg/L	1.0	CALCULATED
TDS Calculated	697.	mg/L	1.	
<b>RCap 30 Computed Indexes</b>				
Cation Sum	10.2	meq/L		CALCULATED
Anion Sum	10.8	meq/L		CALCULATED
Ion Balance	3.14	%		CALCULATED
Langlier Index @ 4C	-5.51			CALCULATED
Langlier Index @20C	-5.11			CALCULATED
Saturation pH @ 4C	10.0	Units		Calculated
Saturation pH @ 20C	9.61	Units		Calculated

**Report To:**  
**Don Fox**  
 Dalhousie University  
 Dept. of Earth Sciences  
 Halifax, NS,

**Date Received: Feb 11, 1997**  
**Date Reported: Feb 18, 1997**

**Inorganics Manager**

*[Signature]*  
**Jerry Arenovich** *AB*

**AFTER OXIDATION IN THE STERILE TREATMENT**

---

MDS ENVIRONMENTAL SERVICES LIMITED

Sample : 97-H002963  
Client ID : RAJ-003

---

Inorganic Analytes	Value	Units	LOQ	Method
Aluminum	7400	ug/L	10.	ICP-MS

---

Report To:  
Don Fox  
Dalhousie University  
Dept. of Earth Sciences  
Halifax, NS,

Date Received: Feb 11, 1997  
Date Reported: Feb 18, 1997

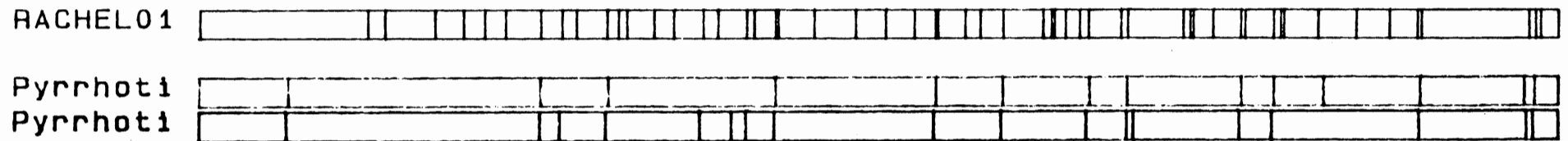
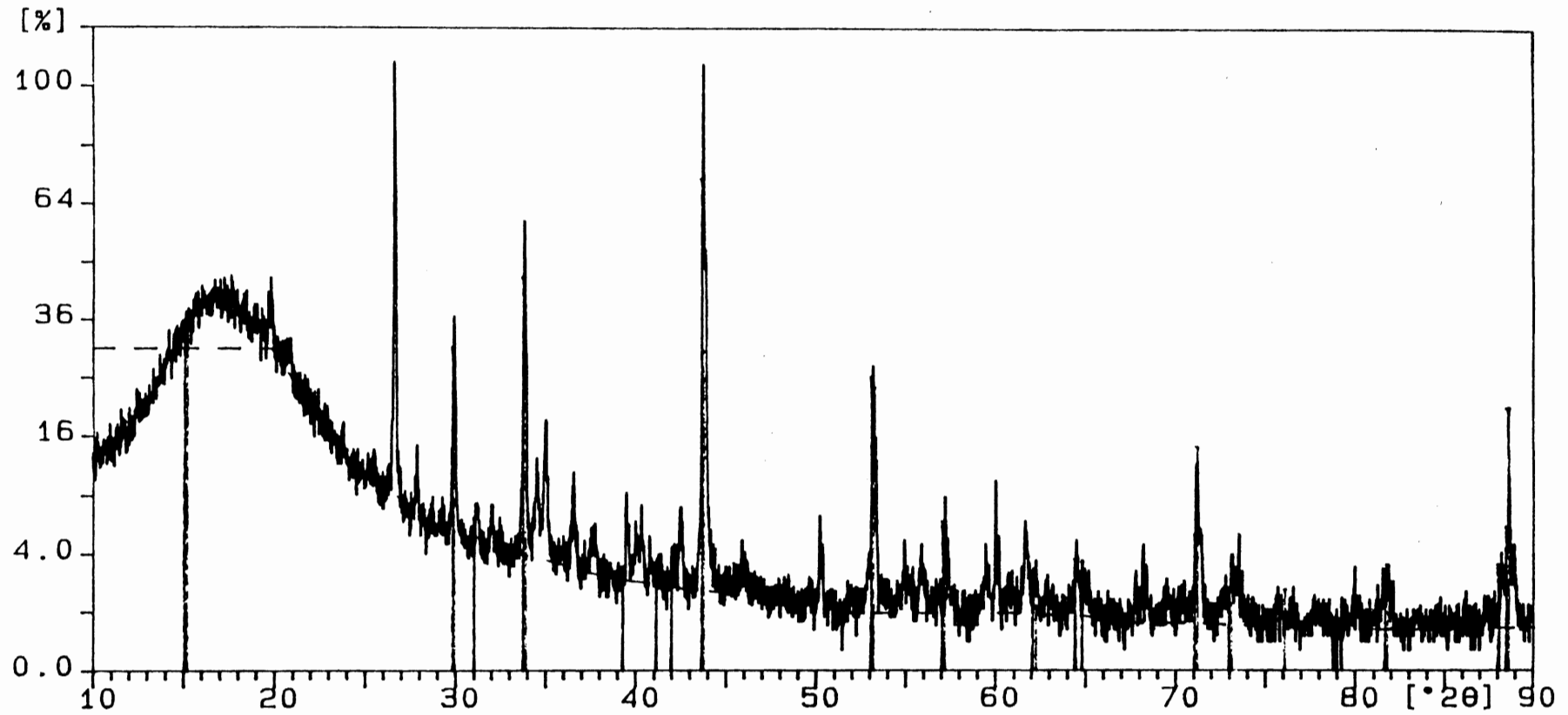
Inorganics Manager

  
Jerry Arenovich

**APPENDIX C: HEXAGONAL PYRRHOTITE XRD ANALYSIS**

Sample ident.: rachel01

7-Mar-1997 15:55



Thin section XRD analysis of RJ-96-003. Matches are both patterns for hexagonal pyrrhotite.